Journal of CO2 Utilization 82 (2024) 102756

Contents lists available at ScienceDirect

Journal of CO2 Utilization

journal homepage: www.elsevier.com/locate/jcou

Review Article

A comparative study on carbon neutral hydrogen carrier production: Formic acid from CO_2 vs. ammonia

Arti Mishra [a], Donghyun Kim [b], Talal Altahtamouni [c], Peter Kasak [a], Anton Popelka [a], Hyunwoong Park [d], Dong Suk Han [a,b,*]

[a] Center for Advanced Materials, Qatar University, PO BOX 2713, Doha, Qatar
[b] Department of Chemical Engineering, College of Engineering, Qatar University, PO BOX 2713, Doha, Qatar
[c] Research Planning and Development, VP Office of Research & Graduate Studies, Qatar University, PO BOX 2713, Doha, Qatar
[d] School of Energy Engineering, Kyungpook National University, Daegu 41566, Republic of Korea

ARTICLE INFO

Keywords:
Carbon neutrality
Hydrogen
Ammonia
Formic acid
Carbon dioxide conversion

ABSTRACT

Hydrogen (H_2) is increasingly recognized as a key player in the journey towards carbon neutrality, with ammonia (NH_3) and formic acid (FA) emerging as significant hydrogen vectors. This review highlights advancements in catalyst efficiency for FA synthesis from CO_2, particularly with bismuth (Bi) and tin (Sn) catalysts. It investigates diverse NH_3 and FA production methodologies, such as electrochemical, thermochemical, and photochemical processes, and underscores the integration of renewables to address their energy demands. The study also reviews novel materials like metal-organic frameworks (MOFs) and carbon-based catalysts that could enhance catalytic effectiveness. Transitioning from lab-scale models to industrial-scale applications requires addressing catalyst longevity and process enhancement, and it suggests investigating hybrid systems that might offer improved efficiency and yields. Concluding with a directive for future research, the study advocates for scalable, economically viable, and environmentally sustainable CO_2 conversion technologies, underscoring the essential roles of NH_3 and FA in a future with reduced carbon emissions.

1. Introduction

Human activities, particularly fossil fuel consumption and industrialization, have significantly disrupted the Earth's carbon cycle, posing a threat to various ecosystems. This disruption is mainly attributed to the increase in greenhouse gas emissions, especially carbon dioxide (CO_2), since the mid-1990 s [1,2]. The consumption of fossil fuels and biofuels such as ethanol, contributes to this issue, with over half of the energy being converted into CO_2. This has led to an increase in atmospheric CO_2 levels from 300 ppm before 1950 to a concerning 420 ppm today [3]. Projection indicate that global energy demand will push CO_2 emissions to over 40 gigatons by 2030 [4].

CO_2, while essential for the carbon cycle and supporting various industries, exacerbates the greenhouse effect when its concentration is too high [5], trapping more solar irradiation and leading to climate change [6]. Natural processes to mitigate these effects are limited, and simple sequestration techniques offer only temporary relief, with risks of environmental leakage [7]. A more sustainable approach involves utilizing CO_2, either by transforming it into useful products or by employing various capture technologies like chemical and physical absorption [8,9], adsorption [10,11], membrane separation [12,13], cryogenic separation [14,15], chemical looping [16,17], and mineral carbonation [18] (Fig. 1). Each method has its advantages and limitations, but their adoption faces challenges due to high costs [19], energy demands [20], lack of investment [21], and limited commercial interest [22], which hinder widespread implementation (Table 1). Direct CO_2 reduction is limited to niche applications, primarily in the oil and gas sector and specific industries, utilizing only a fraction of the available CO_2.

Indirect utilization of CO_2, converting it into valuable chemicals through electrocatalytic methods (including photochemical, thermochemical, and electrochemical processes)(Fig. 2) [23,24] and biological processes (such as microalgae-driven photosynthesis) [25], presents a promising approach (Table 2). These methods are currently at an intermediate level of technology readiness (TRL), mainly hindered by high electricity costs, which accounts for over 60% of operational expenses [26]. Integrating these processes with renewable energy sources, like solar and wind, could improve electrocatalytic process efficiency [27].

* Corresponding author at: Center for Advanced Materials, Qatar University, PO BOX 2713, Doha, Qatar.
E-mail address: dhan@qu.edu.qa (D.S. Han).

https://doi.org/10.1016/j.jcou.2024.102756
Received 24 December 2023; Received in revised form 26 March 2024; Accepted 29 March 2024
Available online 5 April 2024

CO_2 conversion offers a pathway to generate valuable chemicals like carbon monoxide (CO), methane (CH_4), ethylene (C_2H_4), acetic acid (CH_3COOH), methanol (CH_3OH), ethanol (CH_3CH_2OH), propanol ($CH_3CH_2CH_2OH$), and formic acid (HCOOH). Among these, formic acid (FA) presents intriguing possibilities as hydrogen (H_2) carrier, given its global NH_3 production exceeding 150 million metric tons (primarily for fertilizers) [28]. Beyond applications in animal feed, leather tanning, textiles, pharmaceuticals, and food preservation (E236) [29], FA's high H_2 storage capacity (580× greater than H_2 gas) [30] positions it as a promising fuel [31]. However, data on its commercial production remains limited. This review evaluates NH_3 and FA as a potential H_2 carriers, analyzing production costs, distribution channels, and market potential, assessing their suitability for H_2-based energy systems aligned with carbon neutrality goals.

2. Carbon neutrality and its challenges

Carbon, an essential element in Earth's ecosystems, forms the basis of CO_2, significantly impacting climate and weather patterns [40]. Present in living organisms, soils, rocks, and oceans, carbon circulates through a natural "carbon cycle", maintaining a delicate balance within ecosystems and influencing global temperatures [41]. This cycle involves processes like rock weathering, ocean sediment formation, and biological activity [42,43]. Achieving "carbon neutrality" means balancing the levels of CO_2 emissions with their removal from the atmosphere, essentially ensuring that activities do not contribute to an increase in atmospheric CO_2. Companies can strive for this by offsetting emissions through carbon capture and storage solutions. Transitioning to low-carbon energy systems an achieving true carbon neutrality require collaborative efforts across scales, involving stakeholders and potentially governmental mandates [44].

Regional energy availability extends beyond mere access and encompasses transparency about production, climate impacts, and progress towards decarbonization and carbon neutrality. Transitioning to a low-carbon future, with "City-Zen" initiatives like the EU's zero-emission cities program [45], is crucial. Studies show transportation's significant contribution to emissions, highlighted by cities like Helsinki [46] and Roeselare [47]. Circular economy principles and smart infrastructure can pave the way towards this goal, complemented by improved agricultural and forestry practices that benefit diverse sectors, reduce emissions, and protect carbon sinks. Similar approaches are vital for industries due to their high carbon footprint.

China's rapid growth necessitates its transition to carbon neutrality. Its strategy focuses on decarbonizing key sectors and adopting renewable energy, while balancing the need for stable energy supply. Measures like afforestation, CO_2 capture and storage (CCS), and potential carbon tax implementation aim to enhance energy security and reduce environmental impact. China's achievements, like a 48.4% reduction in carbon emissions by 2020 compared to 2005 [48], offer valuable insights for emerging economies undergoing rapid industrialization, potentially with support from developed nations [49].

Larger carbon footprints plague urban areas and wealthy nations due to consumption-heavy lifestyles. Tackling emissions from its source and rapid infrastructure development is complex [50]. Coal's cost-effectiveness makes it a mainstay for many countries, despite representing 40% of energy output. Balancing the shift away from fossil fuels with economic and energy security concerns, while awaiting advances in renewable and clean coal, is intricate [51]. Modernizing

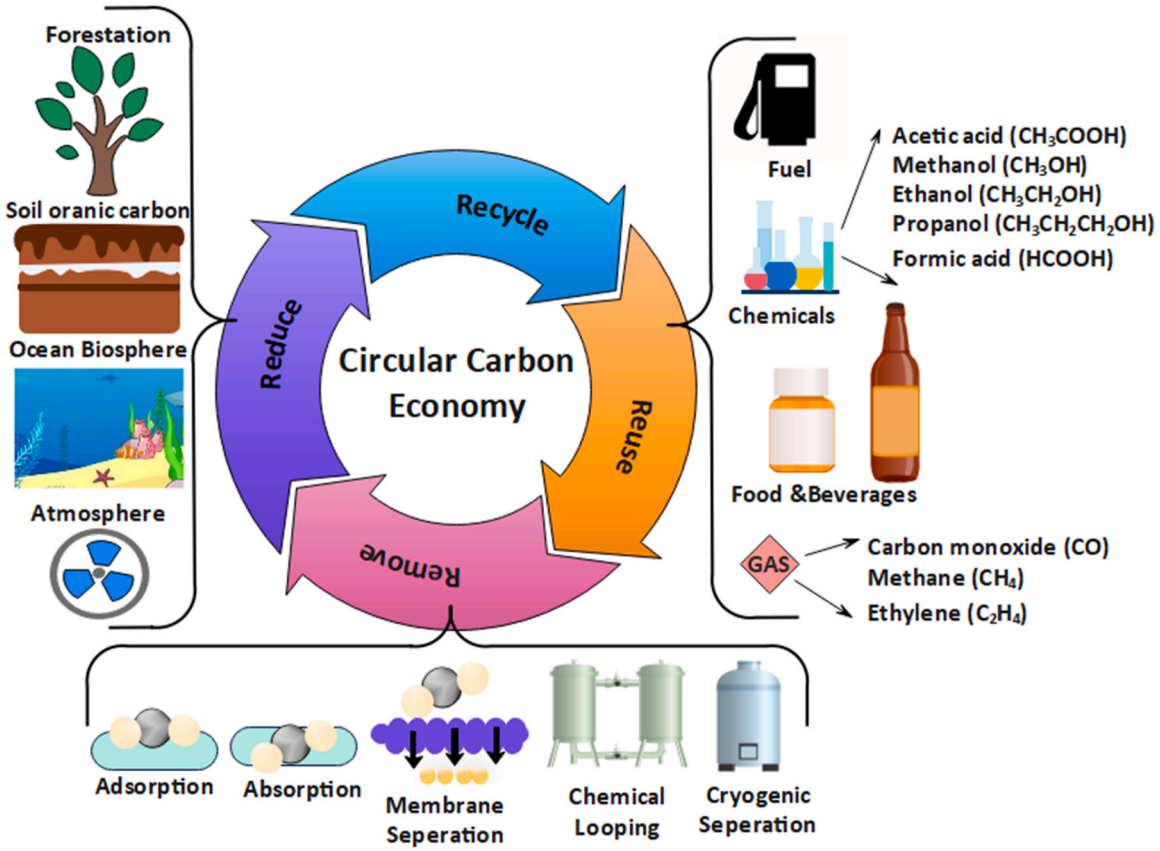

Fig. 1. Displays various methods targeting human-induced CO_2 capture, encompassing absorption, membrane separation, chemical looping, and cryogenic separation. Concurrently, it highlights nature's inherent mechanisms for CO_2 mitigation, encompassing the ambient air, terrestrial soil, vast oceans, dense forests, and organic biomass. Harnessing CO_2 offers multifaceted advantages, notably in synthesizing value-enhanced chemicals, generating diverse gases, formulating carbon-neutral fuels, and fostering innovations within the food and beverage sector.

Table 1
Advantages and disadvantages of manmade CO_2 capturing techniques.

Technique	description	Advantages	Disadvantages
Absorption [8,9]	Employs chemical and physical mechanisms using amine-based solvents and activators.	• Over 90% efficiency • Swift reaction rate • Regenerable sorbents • Cost-effective solvents • First commercialized post-combustion method	• High energy input for sorbent regeneration • Efficiency depends on CO_2 concentration. • Thermal degradation at high temperatures. • Environmental impact from solvent evaporation. • Oxidative degradation and system corrosion. • Additional processing for transport and storage.
Adsorption [10,11]	Categorized based on CO_2 and adsorbent interaction, uses materials like activated carbon, zeolites, and MOFs.	• More than 80% efficiency. • Less energy-intensive • Recyclable sorbents	• Selectivity depends on pressure and flow rate. • Frequent regeneration needed, non-continuous. • Lower efficiency than adsorption technologies.
Membrane separation [12,13]	Uses polymeric, metallic, ceramic, cellulose derivatives, and hybrid membranes.	• High selectivity with the right membrane. • Enhanced performance with temperature and pressure. • High flow rate gas capture. • Energy- and environment-friendly.	• Strict temperature and pressure requirements. • Pre-treatment of flue gases to prevent foaming and entrainment. • Fouling and low flux affect long-term operation. • Moisture affects polymeric and membrane performance. • Industrial applications often lead to membrane failure.
Cryogenic separation [14,15]	Exploits unique condensation points of gases at reduced temperatures for CO_2 condensation and isolation.	• Near-perfect gas purity • Ideal for large-scale applications • Fewer chemicals, less environmental impact. • Mature and reliable technology.	• High energy consumption. • Effective mainly for high CO_2 concentration gases. • Water condensation requires moisture removal. • Solidification of CO_2 can affect heat transfer.
Chemical looping [16,17]	Involves oxidation and reduction in separate reactors with metal oxide-based carriers.	• Unmixed CO_2 and N_2, avoids air separation. • Minimized NO_x formation. • Condenser separates CO_2 efficiently. • Heat utilization improves efficiency.	• System complexity due to separate reactors • Degradation of oxygen carrier over cycles. • pre-combustion sulfur removal required. • Oxygen carrier instability reduces efficiency.

industries in developing nations faces additional hurdles, including technological inertia. This underscores the need for global collaboration to develop negative-emission techniques [48].

Economic growth can coexist with environmental responsibility. Carbon-neutral energy transition strategies are crucial for CO_2 reduction. Photovoltaic, wind, hydro, bio, nuclear, geothermal, and H_2 emerge as sustainable alternatives. While H_2 has industrial uses for centuries, its energy potential is a recent realization. Demand has tripled since 1975 and is expected to exceed 10 million tons in the next decade. Zero-emission combustion make H_2 highly attractive [52], prompting many countries to explore a H_2-based economy for renewable grids, sector integration, and complete energy decarbonization [53].

3. Hydrogen economy

Since the early 1990 s, both EU and emerging economies have invested in building a H_2-based economy, aiming for net-zero CO_2 emissions by 2050 (Fig. 3) [54]. This interest is reflected in the surge of research, with over 3500 researchers contributing to studies on H_2 production, storage, transportation, and utilization in the past five years alone [55]. Four main methods dominate commercial H_2 production: steam methane reformation, oxidation, gasification (primarily using fossil fuels), and electrolysis powered by renewable sources. Notably, CO_2 itself can be use as a feedstock for H_2 production, paving the way for "green" H_2 with minimal carbon footprint. However, scaling up electrolytic H_2 production requires advancements in storage and transport solutions. Storing large quantities of H_2 poses economic and safety challenges, with various forms (gas, liquid, solid) each presenting difficulties [56]. Additionally, H_2 currently lags behind fossil fuels in terms of energy efficiency, demanding further innovation and infrastructure development [57]. Ensuring a reliable H_2 supply for end-users is crucial, and repurposing existing gas pipelines with regional adjustment shows promise [58].

Major automakers have showcased the viability of H_2-powered vehicles like the Mirai, Clarity, and Nexo. However, their higher price tag compared to traditional gasoline-powered vehicles highlights the need for cost reduction without compromising performance [59]. Standard H_2 storage uses pressures around 850 kPa, but the search for increased capacity has led to exploration of cryogenic tanks. These tanks, however, come with challenges like energy losses and reduced kinetic energy density [60]. Liquid organic H_2 carriers (LOHCs) offer a promising alternative for emission-free storage and transport, leveraging existing fuel infrastructure and stability. However, their widespread adoption is still in its early stages [61]. As an alternative to complex storage solutions, chemically containing H_2 through electrolysis is gaining traction. This involves processes like hydrogenation and dehydrogenation of specific molecules to facilitate liquid storage.

NH_3 and FA serve as examples of H_2 vectors, storing 17.8% and 4.5% H_2, respectively. Both utilize atmospheric gases (CO_2 or N_2) in their production, though these gases are eventually released. Interestingly, despite their low H_2 content, these molecules allow for H_2 recycling [62]. While NH_3 is well-researched, FA presents intriguing features with potential, which will be explored in subsequent sections.

3.1. Ammonia (NH_3)

Ammonia (NH_3) is emerging as a highly promising clean H_2 carrier, thanks to its unique properties. It offers a CO_2-free processes for hydrogenation and dehydrogenation, making it a key player in green energy solutions. Its low boiling point of 33.34 °C simplifies the liquefaction process, enhancing its suitability for efficient storage and transport. Additionally, NH_3's high H_2 storage density of 17.8 wt% facilitates effective H_2 packing [65], underscoring its potential as an energy carrier.

However, the primary method for NH_3 production, the Haber-Bosch process, has a significant environmental downside. Developed in the

early 20th century, this process was instrumental in mass-producing fertilizers, revolutionizing agriculture. Yet, it heavily relies on steam methane reforming (SMR) that uses fossil fuels such as natural gas, coal, and naphtha, resulting in substantial CO_2 emissions (1.6 kg CO_2/kg NH_3) [66]. This form of NH_3, often referred to as "Grey NH_3", represents a major source of CO_2 emissions, contributing approximately 235 million tons of CO_2 annually [67,68]. Despite its current market value of $71.98 billion, expected to rise to $110.93 billion by 2028, the environmental footprint of grey NH_3 is a significant concern. To mitigate these environmental impacts, it's crucial to rigorously manage emissions across the entire lifecycle of NH_3, including its production, transport, and use. Implementing robust emission control measures is essential to reduce its contribution to global CO_2 emissions and maximize its benefits as a clean energy carrier (Fig. 4).

3.1.1. *Blue NH_3*

NH_3 produced from fossil fuels with carbon capture technology, known as "Blue NH_3", presents a potential pathway for cleaner energy transitions. Two main methods exist for capturing CO_2 during its synthesis:

- Pre-combustion: Fuels like naphtha, coal, or natural gas are converted into a H_2-CO_2 mix using water gas shift reactors [70].
- Post-combustion: CO_2 is captured from flue gases after fuel burning, typically using alkanolamines (primary, secondary, or tertiary). These amines absorb CO_2 and release it for storage when heated [8].

Mixing different amines can improve CO_2 absorption, but research is needed to optimize their effectiveness, corrosion resistance, and ratios specifically for the NH_3 sector. Additionally, comprehensive evaluations of energy consumption, environmental impact, and corrosion potential are crucial for wider industrial adoption [71].

Beyond traditional capture methods, various materials like clays, zeolites, and activated alumina (Al_2O_3) offer CO_2 capture through adsorption. The NH_3 industry also utilizes synthetic polymers, like acylamine and styrene, in conjunction with membranes to selectively trap CO_2 under specific conditions. This shift towards membrane gas separation, encompassing polymers, palladium, and zeolites, allows for efficient CO_2 filtration. One such innovation, the membrane-assisted autothermal reforming (MA-ATR) reactor, stands out for its simplification of traditional NH_3 plant setups (Fig. 5a). Operating at cooler temperatures and consuming 20% less natural gas, this method achieves a remarkable 88.7% reduction in CO_2 emissions compared to conventional method [72]. Its economic viability is equally promising, boasting a 14.9% cost advatange over traditional CO_2 capture due to optimized heat exchange mechanisms, despite additional component costs. However, for MA-ATR ammonia to compete with liquified natural gas (LNG) in the energy sector, a CO_2 pricing mechanism of around €65/ton is necessary [73].

Chemical looping reforming (CLR), specifically the Calcium and Carbonate Looping (Ca-Cu) processes, offers a promising avenue for CO_2 capture in NH_3 synthesis. This method leverages calcium carbonate (limestone) and metal carbonates:

Table 2
Advantages and disadvantages of various catalytic CO_2 utilization methods.

	Advantages	Disadvantages
Photochemical [32,33]	• Utilizing solar power hence more sustainable • Reaction conditions can be controlled easily	● Efficiency is less than electrochemical methods ● Complex intermediate and final product separation ● Photocatalytic cell design is challenging
Electrochemical [34,35]	• Operates at room temperature and pressure • Highest stability has been achieved • The process can be made more cost-effective by utilizing renewable energy sources. • Reactions at low temperatures are possible.	• Energy-intensive processes result in high operating costs. • CO_2 reduction reaction required high potential • Low product selectivity is a result of an abundance of intermediate product.
Thermochemical [36,37]	• Lower energy requirement • Easier process through plasma splitting	• Operates at high pressure and temperature • Reversible operation • Thermodynamic instability • Lowest efficiency
Biological [38,39]	• Utilization of algae made the process more economical • Utilize photosynthesis phenomena	• Environmental condition dependent process • The energy-intensive harvesting and drying of microalgae for bioresource use are its main drawbacks.

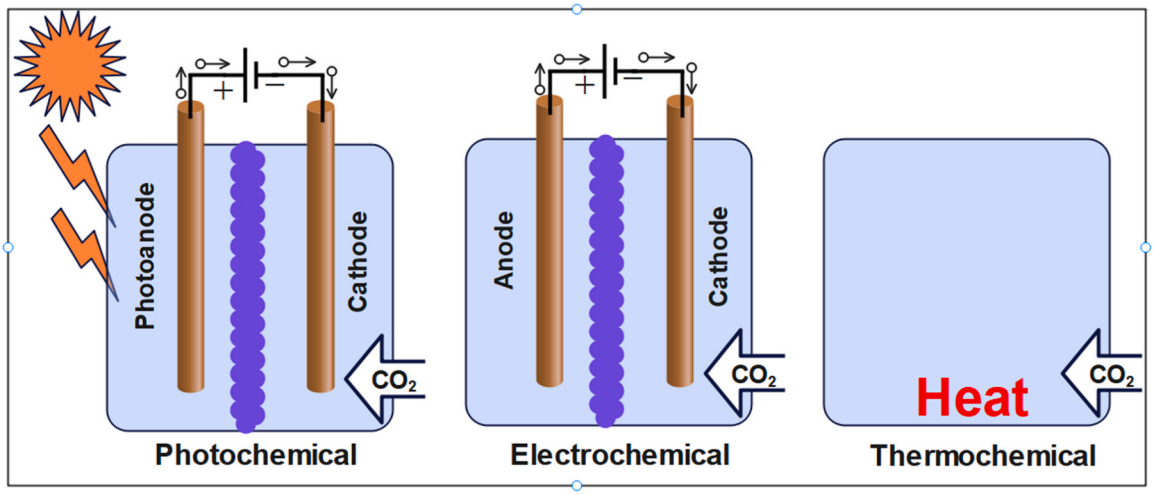

Fig. 2. Electrocatalytic processes for CO_2 utilization span photochemical, electrochemical, and thermochemical methods. Photochemical reactions use light energy, often sunlight, for CO_2 activation. Electrochemical approaches apply external electric potential to facilitate CO_2 reduction, while thermochemical methods employ heat, often alongside catalysts, to drive CO_2 transformations under specific conditions [23,24].

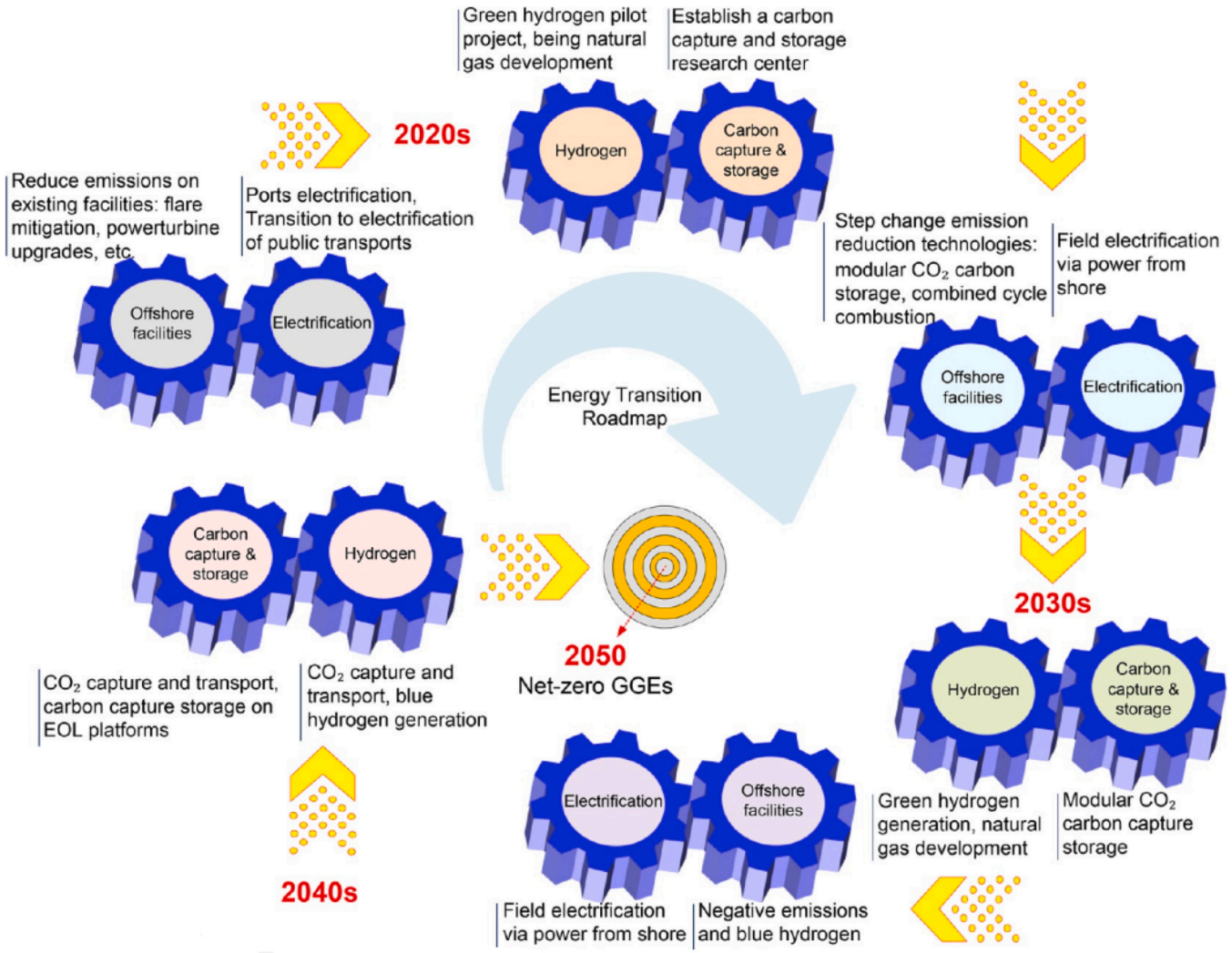

Fig. 3. Energy transition roadmap, derived from a report crafted by the NL oil and gas industry recovery task force [63]. This roadmap emphasizes harnessing wind energy resources and recuperating energy from diverse industrial sectors to generate clean energy. The integration of advanced carbon capture, utilization, and storage (CCUS) systems is paramount in this strategy, aiding the attainment of the overarching net-zero carbon objectives. Reprinted with permission [64].

- Releasing CO_2: These compounds release CO_2 when heated, converting limestone to quicklime (calcium oxide) and metal carbonates to metal oxides.
- Capturing CO_2: Reintroducing these oxides to flue gases enables them to absorb CO_2 and transform back into carbonates.

This cyclical process effectively provides heat for steam methane reforming while significantly reducing CO_2 emissions. Financially, CLR boasts a 19% decrease in capital costs, making production more affordable despite slightly higher operational expenses. This translates to a CO_2 avoidance cost of around \$5/ton_{CO2}, highlighting its potential for cost-effective capture [74]. The Ca-Cu-based CLR system captures a remarkable ~97% of CO_2, limiting emissions to 42.6 kg_{CO2}/ton_{NH3} [75]. Integrating pressure swing adsorption (PSA) refines the gas mixture by processing it through a dense adsorbent bed. However, managing interconnected pressurized fluidized beds with consistent solid circulation remains a technical challenge, hindering its development (Fig. 5**b** and **c**) [76]. One proposed solution involves a stationary oxygen carrier in a single vessel, exposed to different gas flows via gas-switching valves [77]. Notably, the dynamic packed-bed CLR approach merges ATR and SMR features, operating under high pressures and temperatures (600–900°C). Demonstrating its stability in extended tests, this method offers a promising alternative [78]. The gas-switching reforming (GSR) method offers another approach, avoiding the thermal limitations of packed-bed reactors. Yet, potential cross-mixing of reactor phase effluents could compromise CO_2 capture and overall product quality [79]. Finally, incorporating CLR with bio-oil from biomass pyrolysis allows for more efficient and water-independent H_2 generation at 650°C [80].

Leading NH_3 producers are increasingly adopting the blue NH_3 method, as highlighted in Table 3. KBR in the U.S. has employed CO_2 capture using the primary reformer flue gas stream, consuming 3.56 MJ/$kgCO_2$ of energy [82]. CF industries is set to produce blue NH_3 at their Donaldsonville and Yazoo City sites in the U.S., with a \$285 million investment, aiming for an annual production of 1.25 million tons by 2024. Navigator's Heartland Greenway project will enable OCI's Iowa Fertilizer Company plant to capture 500,000 tons of CO_2 and produce 300,000 tons of blue NH_3 by 2024 [83]. The Abu Dhabi National Oil Company (ADNOC) plans to establish a blue NH_3 facility in Ruwais, Abu Dhabi, with the TA'ZIZ industrial zone expecting to produce one million kilotons annually while capturing 800,000 tons of CO_2 [84]. Qatar Energy (QE) is also on track to launch a blue NH_3 facility in the GCC by 2026, with a goal of 1.2 million tons of NH_3 and capturing about 1.5 million tons of CO_2 annually [85].

In transportation, Saudi Arabian Oil Company (SABIC) Aramco, with support from the Japanese Ministry of Economy, Trade, and Industry, is developing cross-border transport infrastructure, marking the first

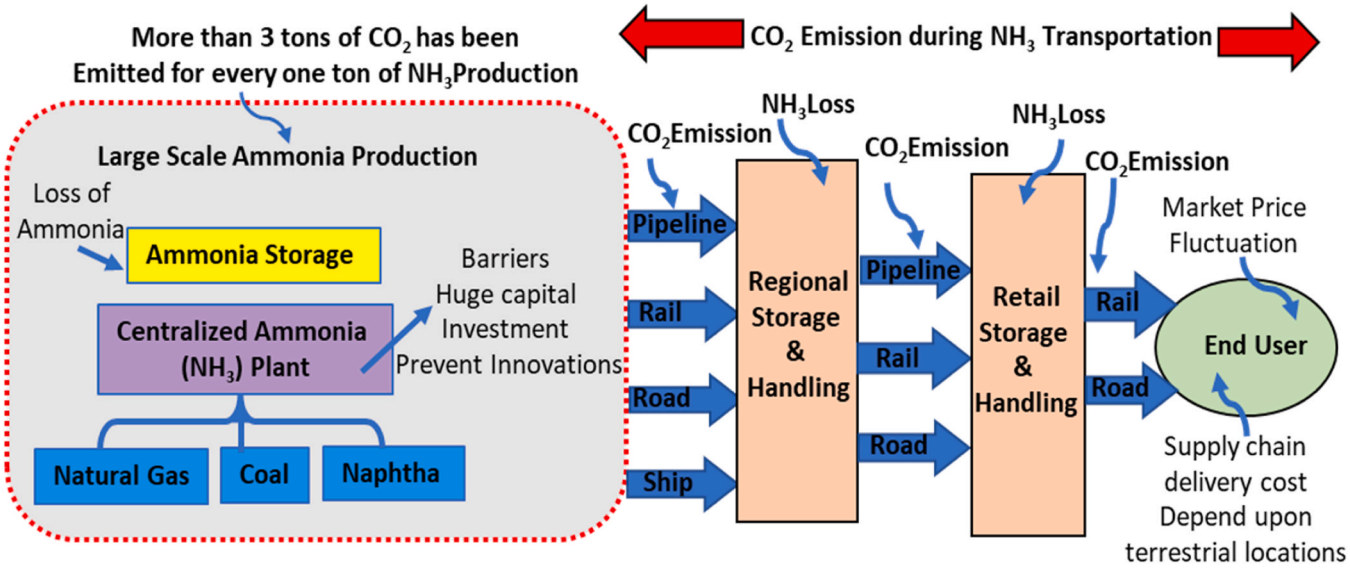

Fig. 4. The commercial lifecycle of grey NH_3 covers everything from its creation to its distribution to consumers. This process has multiple steps, and it's essential to understand each one. One of the most crucial aspects is closely monitoring and managing CO_2 emissions. Because of the environmental effects of CO_2, it's vital that throughout grey NH_3's journey, emissions are kept under control. redrawn from [69].

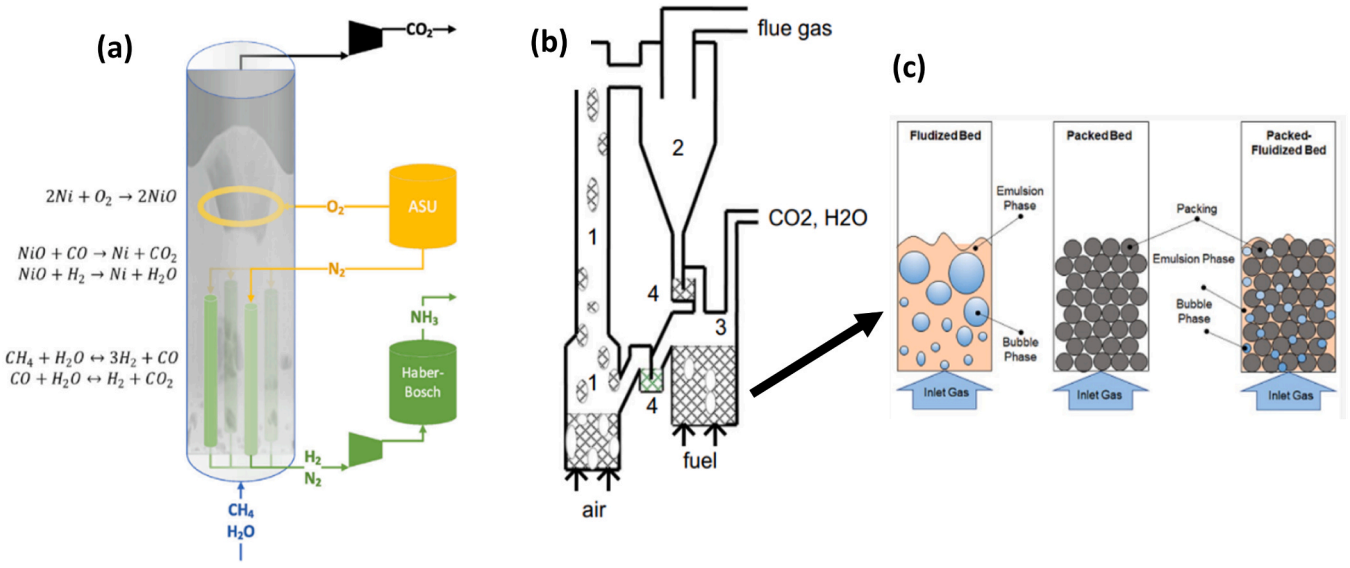

Fig. 5. (a) MA-ATR concept as illustrated: Reforming activities are localized near the membrane's lower regions, with the adjacent areas facilitating the reduction of the oxygen carrier using bypassed fuel. Concurrently, the top sections of the reactor witness the oxidation of the oxygen carrier, driven by a consistent oxygen supply from the air separation unit ASU [72]. (b) The design of the chemical looping reforming (CLR) emphasizes interconnected fluidized beds. This system comprises an air reactor (1) for intake, a cyclone (2) serving as a particulate separator, a fuel reactor (3) for fuel processing, and loop seals (4) ensuring operational coherence [75, 76]. (c) The packed fluidized bed reactor features solid particles, commonly catalysts or absorbents, being fluidized by specific mediums - be it gases like air or nitrogen or liquids like water or organic solvents. This structured fluidization optimizes gas-solid interactions, thereby augmenting reaction efficacy [81].

shipment of 40 tons of blue NH_3 to Japan in September 2020 [86]. Uniper and Novatek have committed to shipping up to 1.2 million tons of blue NH_3 annually from Siberia to Germany, aiming to transition Germany into an a H_2-centric hub with NH_3 import and processing facilities [87]. Saudi Aramco introduced Saudi Arabia's first H_2 refueling station in 2019, serving six Toyota Mirai fuel cell vehicles, while Novatek plans to start a blue NH_3 plant in Siberia's Yamal Peninsula by 2022, adjacent to the Yamal LNG facility. These developments highlight blue NH_3's role as a transitional strategy towards reducing carbon emissions with existing infrastructure, underscoring the ultimate goal of achieving carbon neutrality for enduring environmental sustainability.

3.1.2. *Green NH_3*

Recent advancements have paved the way for producing NH_3 without relying on fossil fuels or generating CO_2, a process known as green NH_3 production. H_2 for this method can be obtained from water electrolysis (WE), utilizing renewable energy sources. The three primary WE techniques include alkaline WE (AWE), polymer electrolyte membrane WE (PEM WE), and solid oxide electrolysis (SOE) cell. Additionally, N_2 gas can be produced via a cryogenic air separation units, also powered by renewable energy, as depicted in Fig. 6. Although WE is known for its high energy requirements, the use of renewable energy is crucial. The feasibility of deploying renewable energy for this purpose varies geographically, highlighting the importance of geographical and

Table 3
Top ten NH_3 producer countries.

Country	Annual NH_3 Production (kiloton)	Major Plants	Source	Reference
China	44000		Mostly coal	[88]
India	25000	Matix Fertilizers & Chemicals, Panagarh NH_3 Plant	coal-bed methane	[89]
		Jaypee Fertilizers & Industries, Kanpur NH_3 Plant	Naphtha	
		Yara International, Babrala NH_3 Plant	Natural gas	
Russia	20000	JSC EuroChem Northwest	Natural gas	[90]
United States	9470	CF Industries Inc. (Donaldsonville, LA) and (Port Neal, IA)	Natural gas	[91]
		Koch Industries (Enid, OK)	Natural gas	
Trinidad and Tobago	5500	Tringen I & II Point Lisas Industrial Estate	Natural gas	[92]
Indonesia	5100	Pupuk Kaltim, North Bontang,	Natural gas	[93]
Ukraine	4300	Odesa Portside Chemical Plant (OPP)	Natural gas	[94]
Canada	3900	Nutrien	Natural gas	
Egypt	3000	Egypt Basic Industries Corporation (EBIC), Ain Sukhna	Natural gas	[95]
Germany	2800	SKW Piesteritz	Coal and Natural gas	[96]

techno-economic assessments prior to initiating commercial green NH_3 production.

The commercial viability of green NH_3 production has sparked numerous simulation and modeling studies across different regions, assessing the potential based on available renewable energy resources, as detailed in Table 4. Studies by Ikaheimo et al. [97] in Northern Europe and subsequent research in Scotland demonstrated that production costs are influenced by the choice of WE technique and renewable energy sources such as solar, wind, hydro, and biomass [98]. Gomez et al. [99] analyzed various methods for generating H_2 and N_2 for NH_3 synthesis, finding the electrochemical reactor paired with cryogenic air separation for N_2 and WE for H_2 as the most efficient, though their assessment did not solely focus on renewable sources. In South America, studies in Chile and Argentina showed that a wind-solar hybrid

Table 4
Geographical location based Techno-economic studies for green NH_3 production.

Region	Renewable Energy	Water Electrolysis	Levelized Cost ($/ton)	Reference
Northern Europe	Solar, wind, biomass, hydro	Polymer electrolyte membrane (PEM)	450–470	[97]
Scotland	Solar, wind	PEM	719	[98]
South central US	-	PEM	951	[99]
Chile and Argentina	Solar and wind	PEM	500	[100]
Qatar	Wind	Alkaline and PEM	-	[101]
Europe	Wind Solar	SOE	1060	[102]
Toronto	Wind Solar hybrid	PEM	-	[103]
Toronto	Solar	PEM	-	[104]
Germany	Coastal wind	Alkaline	917	[105]
		PEM	1323	[105]
Turkey	Solar	PEM	-	[106]
Turkey	Solar and biomass hybrid	PEM	-	[107]
Portugal	Biomass	PEM	620–950	[108]
India	Solar, Coastal wind	Alkaline and PEM	811	[109]

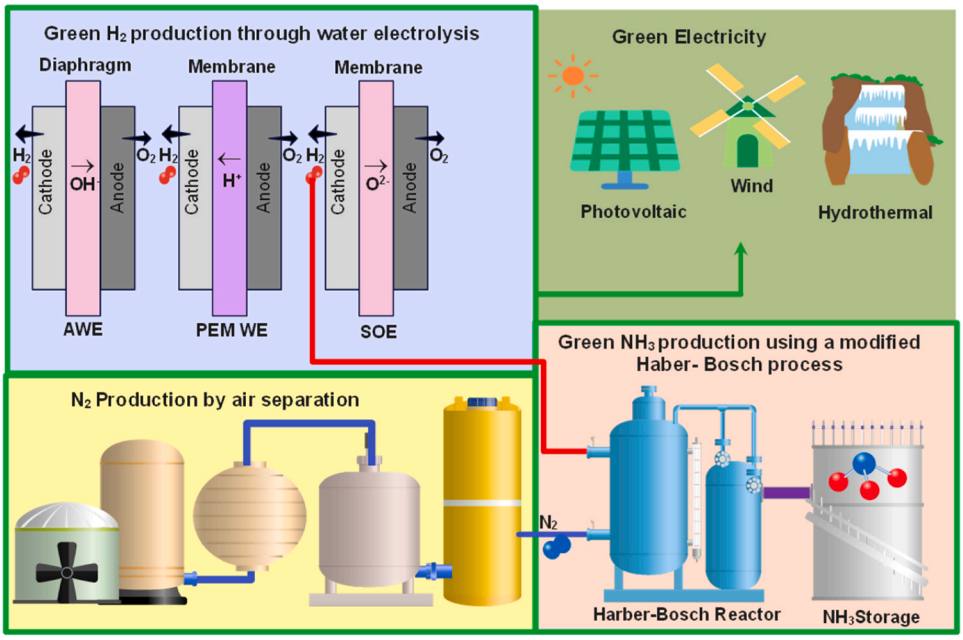

Fig. 6. Schematic of green NH_3 production showcases an integrated process. Electricity, derived from renewable energy fed air separation unit (ASU) and water electrolysis system. The ASU isolates nitrogen (N_2) from the atmosphere, while the water electrolysis unit splits water (H_2O) into hydrogen (H_2) and oxygen (O_2) through processes like Alkaline WE (AWE), Polymer Electrolyte Membrane (PEM) WE, or Solid Oxide Electrolysis Cell (SOEC). The extracted N_2 and the produced H_2 are then combined under pressure and temperature in the modified Haber-Bosch process to yield green NH_3, bypassing the traditional reliance on fossil fuels and associated CO_2 emissions. (reproduced from [65]).

system could lower the levelized cost of NH_3 (LCOA) production [100].

Further studies have investigated electrochemical NH_3 production using wind energy, with one study focusing on a molten salt electrolyte in Lusail, Qatar, underscoring the benefit of high summer wind speeds for energy generation - a finding relevant to similar arid regions [101]. Zhang et al.'s work on high-temperature SOE at 650°C highlighted the significant impact of electricity costs on NH_3 production. In the EU, scenarios like Germany's energy surplus have been shown to potentially reduce green NH_3 prices by up to 80% [102]. Research in Toronto by Ishaq and Dincer [103] demonstrated the efficiency of wind and solar PV-powered electrolysis, with April identified as the most productive month, and subsequent studies emphasized the role of solar radiation intensity on system efficiency [104].

Nosherwani et al. [105] examined Germany's coastal regions, utilizing onshore wind energy for green NH_3 production with both PEM WE and AWE techniques, suggesting that advancements in WE technology could transform the green NH_3 market. Istanbul-based research into solar-powered NH_3 production found a PEM electrolyzer's electrical demand to be 3410 kW with a 26.1% energy efficiency under average solar conditions [106]. Efficiency increased to 59% when combining biomass with solar parabolic dish collector technology for a 20 MW system, illustrating diverse strategies to enhance green NH_3 production's efficiency and sustainability across global contexts [107].

In Sines, Portugal, Silva et al. [108] assessed the economic viability of NH_3 production, revealing the plant to be profitable with a net present value (NPV) of 3714 k€, an internal rate of return (IRR) of 24.3%, a modified IRR (MIRR) of 14.9%, and a payback period (PBP) of 4.6 years. However, they also identified risks, especially the NPV's sensitivity to fluctuations in NH_3 production rates and market prices. Their recommendation for a biomass NH_3 plant in this scale serves as an model for integrating bioeconomy and circular economy concepts to enhance regional sustainability and environmental friendliness [108].

Power et al. [109] conducted a separate analysis on NH_3 production in various coastal Indian cities, utilizing onshore wind, ground-based photovoltaic panels, and batteries. They calculated the domestic NH_3 production cost at $780/ton, with the export price slightly higher at $830/ton. This study suggested that electrochemical NH_3 synthesis, while nascent, has the potential to outperform the conventional Haber-Bosch process in terms of energy efficiency [109]. In practical application, a pilot project in Porsgrunn, Norway, supported by Enova funding, is progressing with a 24 MW electrolyzer facility aimed at generating 20,000 tons of green NH_3 annually, which is expected to cut the region's carbon emissions by 5% [110]. Meanwhile, KAPSOM's commercial green NH_3 plant in western Jutland, Denmark, is poised to start operations by 2023, with a planned annual production of 5000 tons of NH_3 [111]. These initiatives in Norway and Denmark highlight the growing momentum behind green NH_3 production within Europe, demonstrating its feasibility and potential environmental benefits.

Commercial-scale NH_3 production is challenging, largely due to the higher energy input required for its exothermic reaction and complex thermal management. Achieving energy efficiency, especially for autothermal operation, is resource-intensive. Renewable energy sources such as solar or wind could mitigate this issue. Although the modified Haber-Bosch method for green NH_3 production is promising, its financial viability is mostly constrained to large-scale operations, hindering its uptake in less prosperous area [112]. A primary obstacle for employing NH_3 as H_2 storage medium is the lack of efficient NH_3 decomposition and H_2 purification techniques [111]. While transportation costs for liquified H_2 and NH_3 are similar, factors including economics, environmental impact, and safety must be considered. Pure H_2 boasts a mass-energy density of 120 MJ/kg compared to NH_3's 18.6 MJ/kg; however, considering energy losses in processes such as heating and refining, H_2 recovered from NH_3 can have energy yield comparable to that of directly obtained H_2, emphasizing the ongoing exploration for alternative H_2 carriers.

3.2. Formic acid (FA) (or formate)

FA, a liquid at room temperatures with a melting point of 8.3 °C, is recognized for its high H_2 capacity of 53 g H_2/L, offering a safe and efficient solution for H_2 storage and transportation due to its low toxicity and flammability [113]. Recent decades have seen notable advances in FA production, utilizing photochemical, electrochemical, and thermochemical methods, each offering distinct advantages such as high selectivity and yield, particularly when using specific transition metal catalysts.

Technical definitions relevant to FA production include:

- **Catalyst:**
  A substance that increases a chemical reaction's rate by providing a lower-energy pathway, thus enhancing efficiency without being consumed [114].
- **Electron doner:**
  A molecule that releases electrons upon light exposure, essential in photochemical reactions for converting light to chemical energy [115].
- **Irradiation time:**
  This is key in photochemical reactions, as it governs how long reactant molecules interact with light photons, leading to events like electron excitation and bond breaking. This period is vital for determining the reaction's progress and efficiency, influencing the amount of light absorbed and the speed of the reaction. Modifying this time can alter the reaction's yield and selectivity, thereby affecting the end result [116].
- **Turn over number (TON):**
  It quantifies the efficacy of a catalyst in a photochemical reaction by measuring how often a single catalyst molecule helps convert reactants to products. It is the ratio of the quantity of product formed to the number of catalyst molecules used. A larger TON signifies a more efficient catalyst [115].
- **Selectivity (%):**
  It measures the proportion of a specific desired product formed compared to other potential products. High selectivity signifies a dominant reaction pathway that efficiently yields the target product, minimizing undesired byproducts. Conversely, low selectivity indicates a higher likelihood of multiple products and side reactions [116].
- **Apparent quantum yield (%):**
  It represents the efficiency of a photochemical reaction, indicating the number of molecules transformed for each photon absorbed. This yield is calculated as the ratio of transformed molecules to absorbed photons and is affected by the light's wavelength and intensity, reactant concentration, and the use of sensitizers or catalysts [116].
- **Current density (mA/cm^2):**
  In electrochemical reaction, current density measures the amount of electrical current flowing through a unit area of the electrode surface. It reflects the rate of electron transfer, with higher values indicating faster reactions and lower values indicating slower ones [117].
- **Applied potential (V):**
  It acts as the externally controlled voltage driving electrochemical reactions. Measured in volts, it provides the energy to overcome activation barriers, facilitating the conversion of reactants into products. By adjusting this potential, we can selectively promote oxidation or reduction of specific species involved in the reaction [117].
- **Faradic efficiency FE (%):**
  It quantifies how effectively an electrochemical reaction converts consumed electricity into the desired product. It compares the actual amount of product formed or reactant consumed with the theoretical amount based on the passed electricity [116].

- **Catholyte/Anolyte:**
  Catholyte is the electrolyte in a cell's cathode compartment where reduction takes place, while anolyte refers to the electrolyte at the anode compartment, enabling oxidation by containing electron-donating species. These solutions assist ion and electron movement towards their respective electrodes [118].
- **Stability:**

It describes a system's capacity to preserve its chemical and physical properties under electrical stress over time, requiring selective materials, optimized design, and controlled operation to reduce degradation [118].

3.2.1. Photochemical

Photochemical system utilize molecular photocatalysts for their efficiency and selectivity in generating charge carriers that reduce CO_2 to FA. Studies have explored various semiconductor families including oxides, sulfides, and phosphides, with Yaashikaa et al. covering their characteristics [119]. Nguyen et al. emphasized the effectiveness and affordability of TiO_2 composites as photocatalysts [120]. Research by Yang et al. on diamond-based photocatalysts examined different configurations and enhancements to improve FA production efficiency [121].

Metal oxide frameworks (MOFs), known for their distinct structures, facilitate electron localization and minimize electron-hole recombination [122], making them particularly effective in photocatalysis. Innovations have combined MOFs with coordination polymers (CPs) for enhanced outcomes, with MOFs featuring Pb(II) achieving a 12.4% quantum yield under 365 nm light [123]. Zr-based MOFs, incorporating chromophore linkers like Zn, Mn, Fe, and Cu, have introduced new design approaches, notably with Fe-based nano MOFs showing high efficiency [124].

Liu and their team demonstrated the photocatalytic prowess of the amorphous NH_2-MIL-68 MOF, reaching a 94.1% FE in 12 hours, which underscores its abundant active sites and remarkable catalytic performance, achieving a current density of 34.2 mA/cm^2 at 2.05 V [125]. These developments highlight the potential of MOFs and their composites with CPs in setting new benchmarks for efficiency and innovation in photocatalytic applications.

Recent studies in photocatalysis have made notable progress with elements such as Ru, Ir, Cu, and Ni, achieving significant improvements in selectivity and turnover number (TON), as shown in Tables 5 and 6, along with Fig. 7**a**. The Mes-IrPCY2, a tetradentate PNNP-type Ir photocatalyst featured in Fig. 7**b**, is particularly remarkable for its 145 hours of stability and a TON of 2560 for converting CO_2 to FA without requiring an external photosensitizer [136]. Research comparing various half-metallocene Ir(III) complexes demonstrates diverse products and CO_2 reduction pathways, detailed in Fig. 7**d** across a 48-hr period [138]. Studies on iridium(III) terpyridine and 2, 2'-bipyridine complexes have shown significant structural adaptations, with FA emerging as a byproduct [128].

The Ru complex uniquely serves both as a photosensitizer and catalyst in CO_2 reduction, bringing innovation to photoredox catalysis [126]. The application of elevated synthesis temperatures on g-C_3N_4 has led to its improved performance in converting CO_2 to FA, particularly when used with a Ru(II) cocatalyst [129]. The layered perovskite structure of $Li_2LaTa_2O_6N$ stands out for its effectiveness in CO_2 to FA conversion under visible light [130], while Ta_3N_5-based hybrid photocatalyst showed enhanced selectivity for this reaction [132]. The Ru II complex, presented in Fig. 7**c**, introduces a novel approach by moving away from traditional a-diimine ligands, achieving 24-hour stability and 99% efficiency [131,135]. Additionally, the trans(Cl)-[Ru(6-X-bpy)$(CO)_2Cl_2$] complex, when subjected to photolysis, exhibited high FA selectivity, though at a lower yield [139] [140]. Research into Ru-based compounds highlights their capability to increase reactivity and directs further study towards ligand effects on various metals to optimize FA selectivity [145].

In advancing visible-light-driven CO_2 reduction, binuclear Co complexes displayed product selectivity influenced by the basicity of the reaction medium [133]. Organometallic compounds such as Re$(bpy)_2(CO)_2$ [134] and pentanuclear cobalt (Co5) complexes [141] opened new pathways for selectively converting CO_2 to FA [134,141]. Additionally, two unique Ni(II) complexes achieved near-perfect selectivity and an TON of 14000, highlighting their potential for eco-friendly applications [137].

Challenges in selectivity control for photochemical reduction stem from the reactivity of metal hydrides with CO_2. Schneck et al. identified N-H elimination as the crucial step affecting hydride displacement and underscored the combined effect of metal and ligand in the selectivity of nickel hydride complexes [146]. Theoretical analyses by Grill et al. of transition metals like Mn, Re, and Ru, highlighted the role of ionic liquid TEOA as both an electron donor and a hydrogen-bonding agent with

Table 5
Tabulated data for formate production using photochemical methods.

Catalyst	electron doner	Solvent	Irradiation time (hours)	Turn Over Number (TON)	Selectivity (%)	Reference
Ru complex	Triethanolamine (TEOA)	DMA/H_2O	4	14	99	[126]
Mo complex	TEA	MeCN	20	5	99	[127]
Ir complex	TEOA	MeCN	24	20	90	[128]
Ru complex	Ag-g-C_3N_4	DMA	5	650	99	[129]
Ru complex	TEOA	MeCN	15	110	99	[130]
Ru complex	TEOA	DMF	24	380	99	[131]
Ru complex	Ag-Ta_3N_5	MeCN	15	-	98	[132]
Co complex	MeCN	TEA	20	110	93	[133]
Co complex	MeCN	TEA+BIH	23	386	97	[133]
Re complex	TEOA	DMF	24	2750	99	[134]
Ru complex	TEOA/BI(OH)H	DMA	24	3296	83	[135]
Ru complex	TEOA/BI(OH)H	DMA	24	3792	86	[135]
Ir complex	BIH	DMA+H_2O	145	2080	87	[136]
Ni complex	TEOA	EtOH+H_2O	10	14000	99	[137]
Metallocene Ir(III) complex	(TEOA)	DMF	48	840	54	[138]
Monobipyridyl Ru(II) complex	Tetrabutylammonium Perchlorate (TBAP)	DMF	5	103	58	[139]
Ru complex	TEOA	MeCN	15	19	99	[140]
Co_5	BIH + $Ir(ppy)_3$	DMF	1	229		[141]
ClFDH/AgCNs/TiO_2/g-C_3N_4	EDTA	MES	4	10,000		[142]
FDH/CD	EDTA / dithiothreitol	$NaHCO_3$	1	3500	90	[143]
2D porphyrin nanoplates	Ru complex	Buffer Solution				[144]

Table 6
Tabulated data for formate production using photochemical methods.

Catalyst	Solvent/ED	pH	Irradiation time (hours)	λ (nm)	Apparent Quantum Yield (%)	Reference
Ru complex	CH_3CN		12	500		[145]
Pb (II) MOF complex	DMSO/BIH		5	400	2.6	[123]
Pb (II) MOF complex	DMSO/BIH		5	365	12.4	[123]
Zr MOF complex	CH_3CN/TEOA	9.3	4	>415	>99	[124]

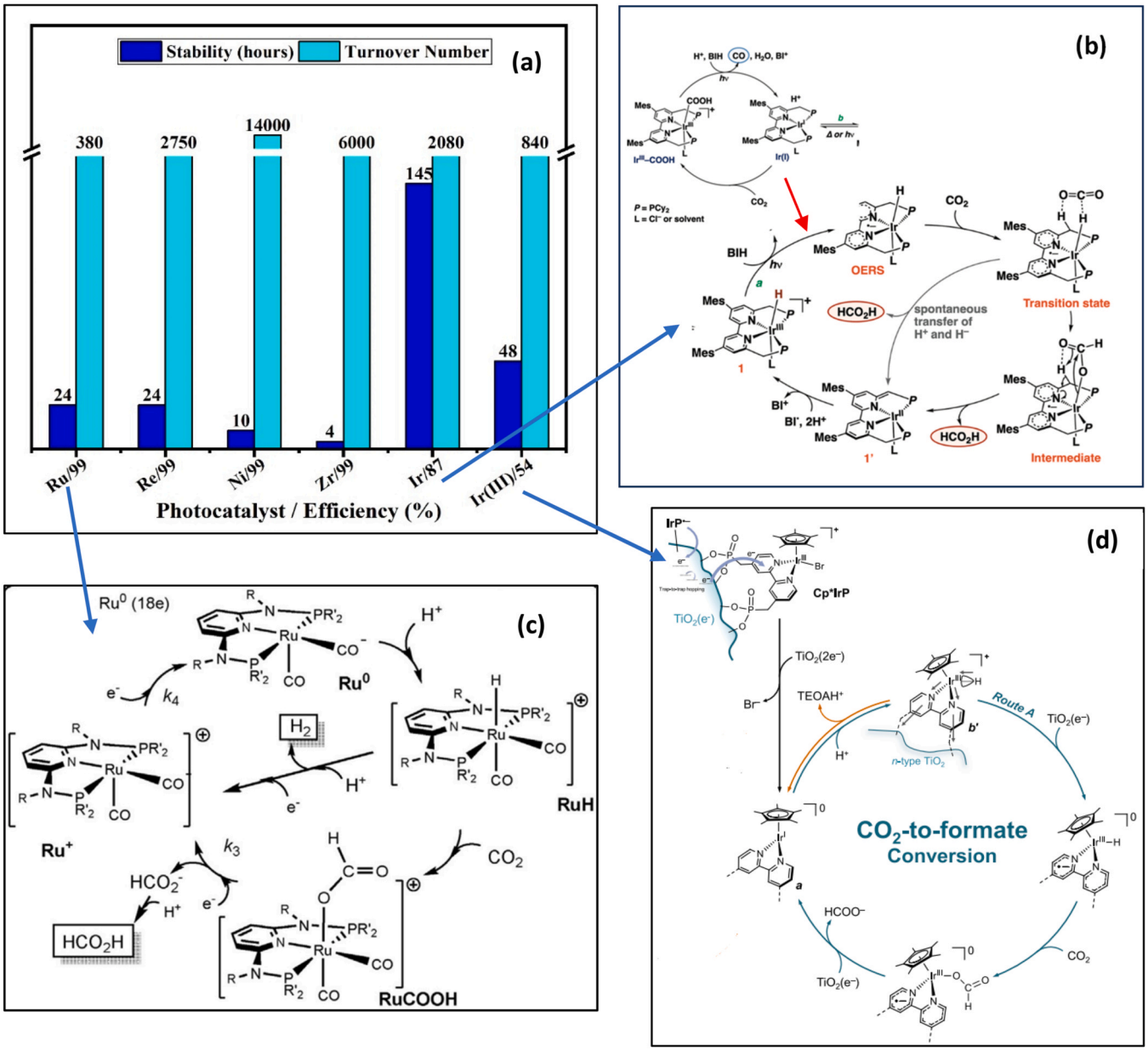

Fig. 7. (a) Comparative analysis of stability and turnover among various photocatalysts [124, 131, 134, 136–138]. (b) The tetradentate PNNP-type Ir photocatalyst, Mes-IrPCY2, is particularly notable. Demonstrating a stability of 145 hours, it achieved a turnover number of 2080 in converting CO_2 to FA. Notably, this performance was achieved without an external photosensitizer and boasted a Faradaic efficiency of 84% [136]. (c) The proposed mechanism for converting CO_2 to FA highlights the role of the Ru II complex. With its innovative molecular structure, these complex challenges the traditional preference for a-diimine ligands. It exhibits a stability of 24 hours and a turnover number (TON) of 380 [131]. (d) The schematic outlines electron transfer processes in the heteroternary hybrid system, emphasizing the TiO_2-immobilized Cp*IrP complex's mechanistic pathways. This complex, showing varied product outcomes and CO_2 reduction pathways under both homogeneous and heterogeneous conditions, exhibits a stability of 48 hours and a turnover number (TON) of 840 [138].

catalytic additives [147]. This research draws inspiration from natural photocatalysis seen in photosynthesis, prompting efforts to mimic these biological processes to refine photochemical strategies.

Mimicking photosynthesis, the use of formate dehydrogenase (FDH) for non-photosynthetic CO_2 conversion has gained attention. Catalysts imitating the molybdenum center in FDH, such as dithiolenes, have been synthesized [127]. Gao et al. achieved a TON of 10,000 in 4 hrs by combining FDH with silver nanoclusters, TiO_2, and g-C_3N_4, with the

silver clusters playing a critical role as depicted in Fig. 8**a** and **b** [142]. Integrating FDH with carbon nanotubes (CNTs) or amorphous carbon dots (CDs) achieved 90% FE at pH 6.7 [143]. Singh et al. employed 2D porphyrin nanoplates with FDH for an economical method, taking advantage of their efficient electron channels and enhancing catalyst durability [144]. Meanwhile, Wang et al. crafted a Cu_2O-Pt/SiC/IrOx MOF composite using a refined photo-deposition technique, forming an artificial photosynthetic system that effectively separates reduction and oxidation phases, yielding 896.7 μmol/g·hr as shown in Fig. 8**c** and **d**. [148].

However, the challenge lies in replicating the self-healing abilities of natural systems in artificial ones, and the limited durability of FDH enzymes hampers their broader application. Current research is exploring a combined photo-electrochemical (PEC) and enzymatic approach for CO2 conversion, aiming to improve electron transfer to FDH, align energy levels for optimal reduction, and ensure photo-stability in water [149]. The search for more efficient photocatalysts to convert CO2 into FA persists as a key area of research interest.

3.2.2. *Electrochemical*

The electrochemical CO_2 reduction relies on stratified catalytic materials at the electrode interface for effective CO_2 conversion. Various catalysts, including metal complexes and films, have been studied, with Cu [150], Sn [151,152], and Bi-based catalysts [153] proving particular effective, as presented in Table 7 and Fig. 9**a,** which summarize their stability and energy efficiency. The forthcoming sections will discuss electrochemical strategies that exhibit both high stability and potential for commercial application.

Catalysts, particularly based on Sn, Bi, Cu, and In, have been assessed for their durability, Faradaic efficiency (FE), and energy consumption, with those exceeding 100 hrs of stability showcased in Fig. 9a. The gas-diffusion electrode (GDE) was identified as a superior cathode configuration for continuous CO_2 reduction to formate, consisting of a carbon fibrous base, a microporous layer, and a catalytic surface, detailed in Fig. 9b.

The formate production cell, with its expected electrochemical reactions and ionic transfers, is illustrated in Fig. 9c. The microporous layer plays an essential role in dispersing reactants uniformly and enabling electron transfer [154]. Typically, CO_2 electroreduction employs aqueous electrolytes like $KHCO_{3(aq)}$ for ion conduction, which, however, results in a mix of liquid products and dissolved salts, demanding energy-intensive separations. A promising alternative, the solid-state electrolyte (SSE) approach depicted in Fig. 9d, uses solid electrolytes to produce pure liquid fuels, merging electrochemically formed cations (e.g., H^+) and anions (e.g., $HCOO^-$) directly. Hence, GDE and SSE are prevalent in high-efficiency electrocatalytic systems under investigation for their operational prowess [155].

3.2.2.1. Tin (Sn)-based electrocatalysts. Sn composites are gaining attention for their effectiveness in converting CO_2 to FA via electrochemical methods. Yang et al. developed a Sn nanoparticle GDE cathode through thermal evaporation, capable of yielding FA in 5 – 20 wt% concentrations. This system, integrating a Sustainion™ anion exchange membrane (AEM) and an imidazole ionomer. demonstrated over 500 hrs of stable operation at 140 mA/cm^2 and 3.5 V (Fig. 9**b**). Ongoing studies are focused on enhancing the cell's dimensions and performance with

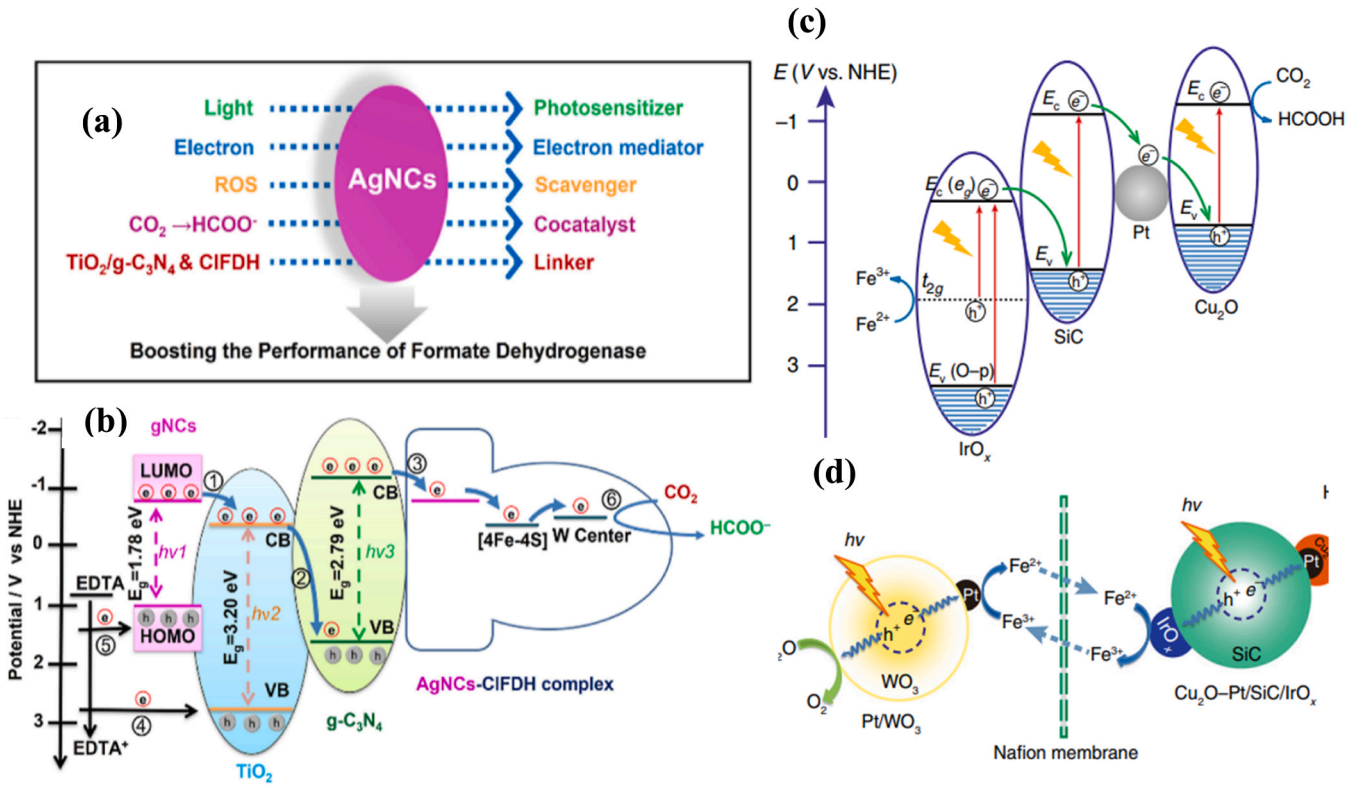

Fig. 8. (a) AgNCs serve multiple roles: they act as a photosensitizer for semiconductors by capturing light, function as a linker by wiring enzymes to material surfaces, operate as a cocatalyst by activating enzymes and enhancing catalytic reactions, mediate electron transfer between enzymes and material interfaces or electrodes, and protect enzymes by scavenging ROS generated during photocatalysis. (b) Energy-Level Diagram delineating approximate redox potentials pertinent to the photochemical formation of FA. In diagram VB represents the valence band, while CB signifies the conduction band. Upon light absorption, the AgNCs hybrid in conjunction with the TiO_2/g-C_3N_4 heterostructure undergoes electron transference to the AgNCs−ClFDH complex, culminating in the reduction of CO_2 to FA. Concurrently, photoexcited holes are effectively quenched by EDTA present in the buffer mixture [142]. Depiction of Electronic Structure and Photocatalytic Mechanism across Cu_2O-Pt/SiC/IrOx MOF composite. (c) Illustrates the electron transfer dynamics in the Cu_2O–Pt/SiC/IrOx when exposed to light. (d) Suggests an artificial photosynthetic setup mechanism for the decoupled system, emphasizing enhanced FA production through CO_2 reduction [148].

Table 7
Tabulated data for FA production using electrochemical methods.

Catalyst	Current Density (mA/cm^2)	Applied potential (V)	FE (%)	Catholyte	Anolyte	Catholyte pH	Stability (hours)	Reference
Sn nanoparticles	140	3.5	94	DI		7–11	500	[154]
Bi nanosheet	30	1.5	100	0.5 M $NaHCO_3$	0.5 M $NaHCO_3$	7–8.5	10	[156]
2D-Bi	200	1.1	83	DI	0.5 M H_2SO_4		100	[155]
Bi	1.5	0.75	> 99	0.1 M $KHCO_3$	0.1 M $KHCO_3$	6.8	2	[157]
Cu_2O nanoparticles	5.2	-0.64	98	0.5 M $KHCO_3$	2 M KOH + 0.8 M H_3BO_3	7.6	20	[158]
SnO_2	500	0.5	90	0.4 M K_2SO_4	1 M KOH	7	11	[159]
Mesoporous Sn/SnO_x	13	-1.2	~90	0.1 M $KHCO_3$	0.1 M $KHCO_3$	6.8	12	[160]
Bi dendrites on Pb substrate	18.8	-0.82	92	0.5 M $KHCO_3$	0.5 M $KHCO_3$	7.3	15	[161]
In/In_2O_{3-x}	-1.8	-0.82	~ 90	0.5 M $NaHCO_3$	.5 M NaOH +2 mM octylamine	7.3	10	[162]
Bi nanoparticles	14.4	-1.5	92	0.1 M $KHCO_3$	0.1 M $KHCO_3$	7.2	20	[163]
n-BuLi-Bi	500	-1.1	97				100	[164]
Bi dendrites	10	2.7	> 99	1 M $KHCO_3$ + 0.1 M CsCl	1 M $KHCO_3$		360	[165]
Bi_2O_3	200	3.5	91.3	Humidified CO_2	DI		1000	[166]
Pb^1Cu	100		96	0.5 M $KHCO_3$	0.5 M $KHCO_3$		180	[167]
Bi-ene-NW	88	-1.17	92	0.5 M $KHCO_3$	0.5 M $KHCO_3$	7.4	500	[168]
Dental amalgam on Cu foam	250		> 99	K_2SO_4			900	[169]
BiO_x	37.8	-1.7	~ 90	1 M $KHCO_3$	1 M $KHCO_3$	-	-	[170]
$Sn-Bi/SnO_2$	100	-0.65	95	Humidified CO_2	0.1 M $KHCO_3$		2400	[171]
Ag-In-S	19.6	-1.0	91.7	0.5 M $KHCO_3$	0.5 M $KHCO_3$	7.2	10	[172]
Bi-GDE	870			1 M CsOH	1 M CsOH			[173]
$SnO_2/Bi_2O_2CO_3$ heterojunction on N,Scodoped-carbon	200	-0.8	85	1 M KOH	1 M KOH		5	[174]
Nano porous SnTe	23	-1.0	98	0.1 M $KHCO_3$	0.1 M $KHCO_3$	6.8	60	[175]
Bi nanosheets	62	-0.95	93	0.5 M $KHCO_3$	0.5 M $KHCO_3$	-	10	[176]
Bimetallic Bi/Sn electrode	34	-1.0	94.8	0.1 M $KHCO_3$	0.1 M $KHCO_3$	6.8	20	[177]
Bi nanosheet with trimethoxy silane	-94	-1.2	98.1	0.5 M $KHCO_3$	0.5 M $KHCO_3$	7.4	26	[178]
MOF Bi	-6.2	-2.8	99	0.45 M $KHCO_3$ + 0.5 M KCl	1.0 M KOH	8.4	4	[179]
s-mesoPdCu	8.1	-0.5	>99	0.1 M $KHCO_3$	0.1 M $KHCO_3$	6.8	250	[180]
In doped $Bi_2O_2CO_3$ nanosheet	17.2	-0.9	100	0.5 M $KHCO_3$	0.5 M $KHCO_3$	7.4	22	[181]
$BaBiO_3$ perovskite	21.0	-1.2	>99	0.1 M $KHCO_3$	0.1 M $KHCO_3$	-	60	[182]
Surface O_2 rich Bi@C nanoparticle	10.5	-0.99	91	0.5 M $KHCO_3$	0.5 M $KHCO_3$	7.4	18	[183]
indium cyanamide nanoparticles (InNCN)	400	-0.72	99	0.1 M $KHCO_3$	0.1 M $KHCO_3$		160	[184]
Bi nanoparticles	150		100	0.45 M $KHCO_3$ + 0.5 M KCl	1 M KOH		5	[185]

specialized electrocatalysts and membranes [154].

A SnO_2-reinforced GDE, supported by carbon, attained up to 90% FE at a current density of 500 mA/cm^2 [159]. Additionally, a mesoporous Sn/SnO_x-based electrocatalyst achieved 89.6% FE at −1.2 V vs. RHE [160]. Despite their efficacy, Sn composites sometimes encounter challenges such as energy-intensive barriers and sluggish kinetics, affecting selectivity at specific voltages. To counter this, multi-component Sn-Te alloys have been engineered by Yang et al. to refine the surface and electronic characteristics of the metal catalyst, moving beyond traditional scaling limitations and improving catalytic actions [175]. The custom-designed nanoporous SnTe attains 98% FE and sustains over 93% performance across 60 hrs [175].

3.2.2.2. Copper (Cu)-based electrocatalysts. Cu-based catalysts have been enhanced with Cu_2O nanoparticle on a (111) facet cathode, combined with a NiFe hydroxide carbonate anode to reduce CO_2 at high pressures of 45 and 60 atm. Through square wave redox cycling, a Cu foil coated with 99% Cu_2O nanoparticles achieved over 98% FE [158]. Despite Cu's common use in catalysis, it typically produces a mix of reaction products. Zheng et al. improved specificity by integrating single-atom Pb, Bi, and In with Cu, where the Pb_1Cu reached 96% FE, with the main activity on the Cu rather than the Pb sites. Computational models suggest these activated Cu sites are crucial for steering the reaction toward FA production while suppressing side-products, sustaining pure FA output for 180 hrs at 200 mA/cm^2 in a MEA-SSE reactor (Fig. 10a and b) [167].

Further progress has been made with single-crystalline Pd nanocubes from a Pd-Cu alloy, offering high surface area and mesoporous channels for catalysis (Fig. 10**c** and **d**). These structures maintained over 99% selectivity at various potentials and demonstrated exceptional stability, persisting at 0.5 V vs. RHE for 250 hrs. These developments represent a leap in the precision and durability of Cu-based catalysts for CO_2 reduction (Fig. 10e) [180].

3.2.2.3. Bismuth (Bi)-based electrocatalysts. Bi-based nanosheets, particularly those sourced from bismuth oxyiodide, have gained recognition for their electrocatalytic properties and durability. These ultrathin sheets, with their single-crystal structure and expanded surface areas, demonstrate near-perfect selectivity for FA at 30 mA/cm^2 and remain stable beyond 10 hrs, a performance supported by DFT analysis. When used alongside an iridium catalyst, they bolster full-cell electrolysis, even with the low power input from two AA batteries [156]. Xia et al. introduced a method for continuous electrocatalytic CO_2 to FA conversion using SSD electrolytes, which can achieve over 90% FE and produce high-quality FA up to 12 M concentration (Fig. 9**d**)). Remarkably, this setup sustained a 0.1 M FA output for 100 hrs with consistent selectivity and activity, demonstrating the practicality of SSD electrolytes in electrocatalysis [155,157].

Bi-based porous electrodes, known as "Biden", were synthesized using the dynamic H_2 bubbling templates technique. TEM analysis reveal their defect-rich sites and high-index facets, contributing to a 98% FE at –0.82 V vs RHE, only a 600 mV overpotential [161]. Bi's integration with nitrogen-doped porous carbon (Bi@NPC) has led to catalysts that harness synergy between Bi and carbon, achieving 92% FE

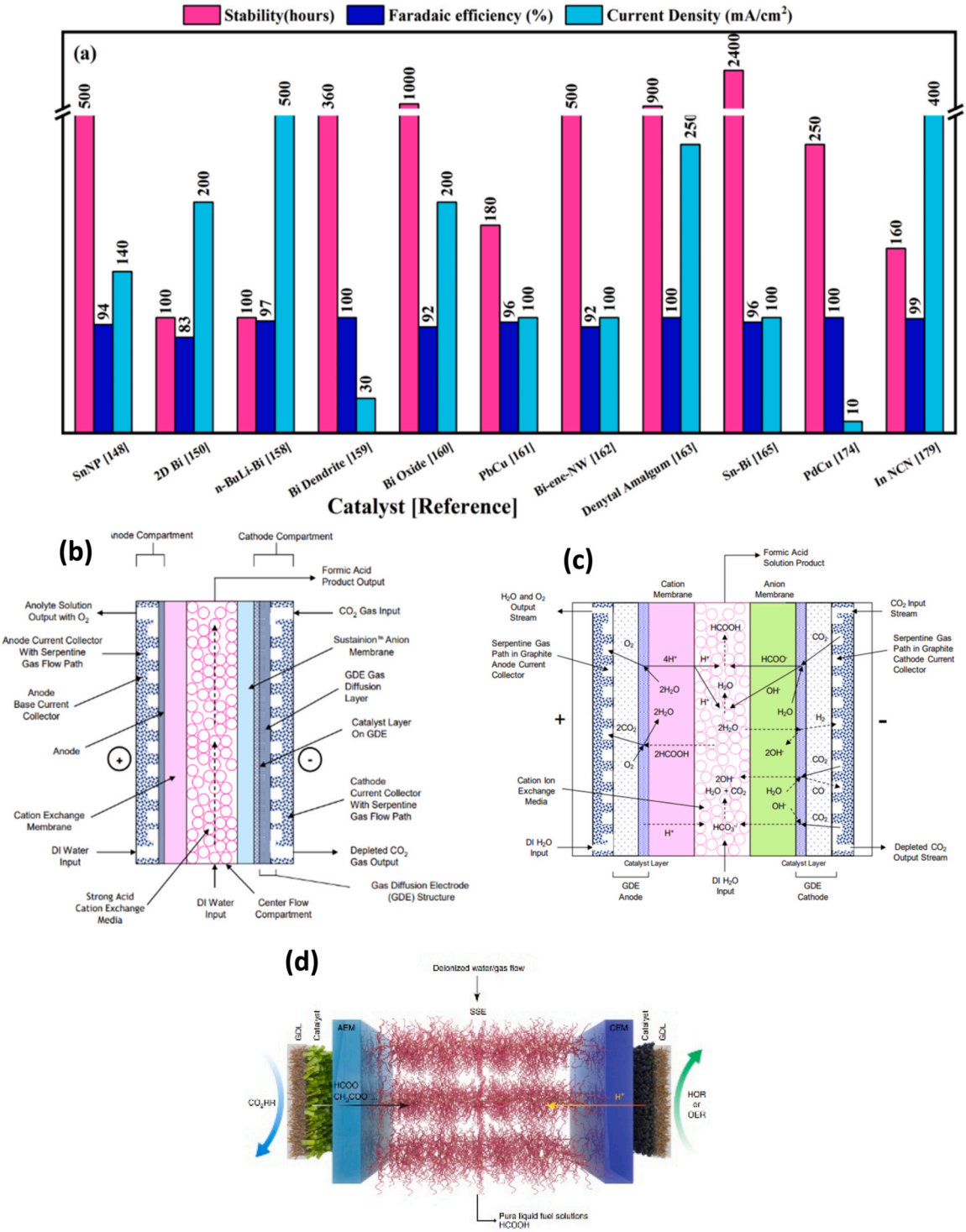

Fig. 9. (a) Examination of different catalysts focusing on stability, faradic efficiency and energy consumption metrics. [154, 155, 164–169, 171, 180, 184]. (b) An illustrative configuration for a 3-compartment GDE cell. The CO_2 reduction is enhanced by the inclusion of an imidazolium ionomer within the nanoparticle catalysts at the GDE cathode (here Sn). (c) Detailed depiction of the FA cell, demonstrating the projected electrochemical reactions and ion transferences. This setup manifests peak stability metrics of 500 hours, maintaining a current density at 140 mA/cm^2 and a Faradaic efficiency of 94% [154]. (d) A schematic outline of the CO_2 reduction cell incorporating a solid-state electrolyte (SSE). This SSE can function as either an anion or cation conduit. Depending on the specific solid ion-conducting electrolyte interposed, the FA (HCOOH) product might be generated vIa ionic recombination of intersecting ions either at the left (in cases of H^+ conductors) or the right (in instances of $HCOO^-$ conductors) interface. This interaction is seen between the central conduit and the membrane, followed by its diffusion through the liquid phase, achieving a stability measure of 100 hours [155].

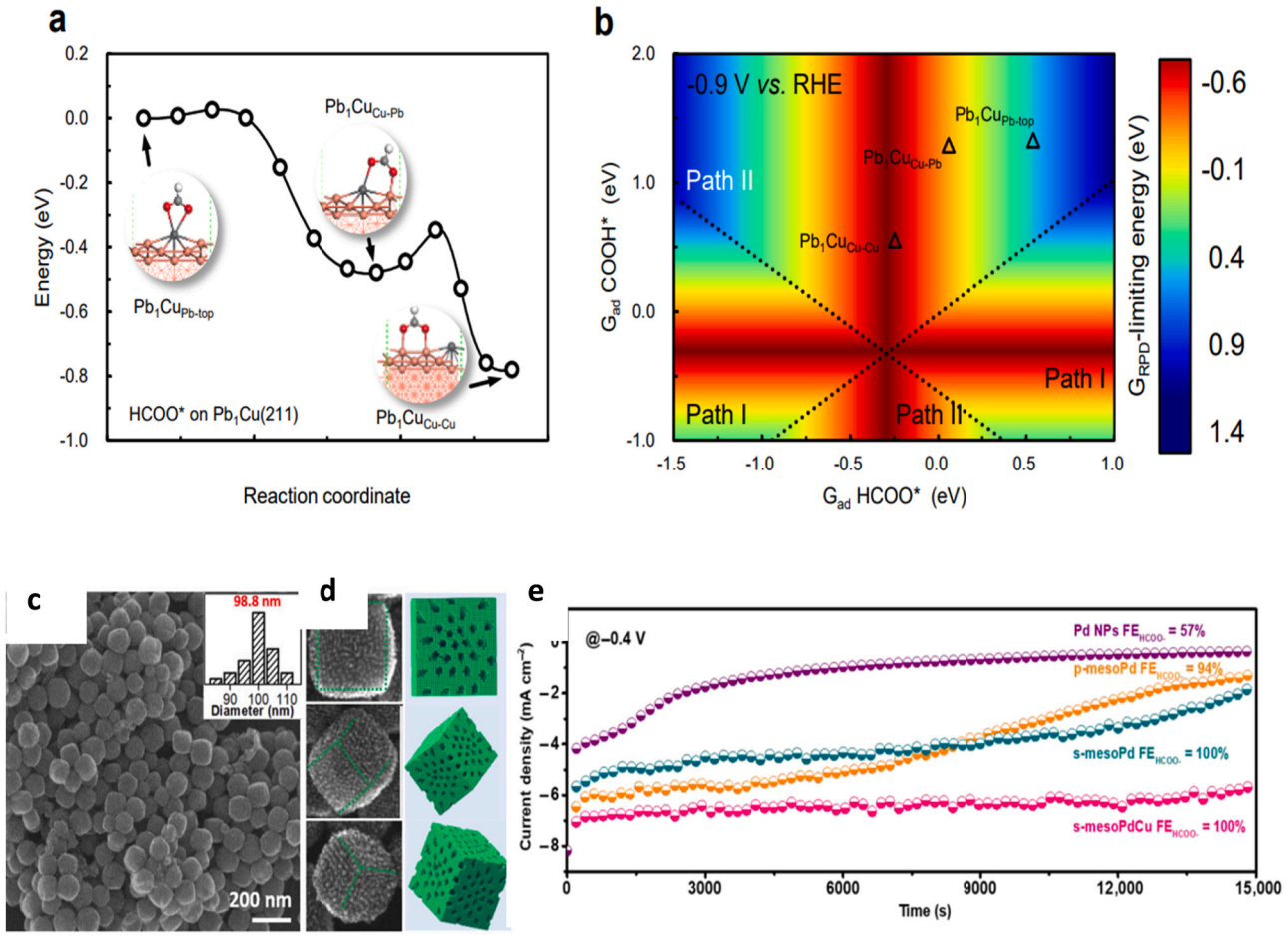

Fig. 10. Comparative analysis of diverse sites on single atom Pb based catalyst Pb^1Cu is presented. (a) The energy variation during the transfer process of HCOO* from the Pb-top site to both Pb-Cu and Cu-Cu sites on Pb^1Cu is delineated. (b) The two-dimensional (2D) reaction phase diagram elucidates the activity of CO_2 reduction in FA production across various active sites on Pb^1Cu. demonstrate the catalyst's capability by continuously producing pure FA for 180 hours @ 100 mA/cm^2 using a specialized membrane electrode assembly (MEA) SSE reactor. [167] (c) Scanning Electron Microscope (SEM) depictions of s-mesoPdCu with an inset in (d) detailing the distribution scale of the nanocubes. (e) Chronoamperometric 250 hours stability analysis for variants such as s-mesoPdCu, s-mesoPd, p-mesoPd, and Pd NPs when set at −0.4 V has shown highest stability and current density for s-mesoPdCu catalyst. [180].

[163]. Fan et al. developed a system for continuous production of high-purity FA, available as vapor or liquid. It uses a porous solid electrolyte (PSE) to separate cathode and anode, allowing formate and protons to combine into FA, which can be vaporized via an inert gas stream through the PSE. A nBuLi-treated Bi catalyst, abundant in grain boundaries, yielded impressive results: 450 mA/cm^2 current densities, 97% FE, and over 100 hrs of stability. This setup also enabled the creation of extremely concentrated FA solutions, almost 100 wt% [164]. Porous dendritic Bi electrodes, synthesized by Piao et al., achieved 100% FE (Fig. 11a). The presence of specific halides and cations was found to significantly influence the partial current density for formate production (JFM), with DFT calculations indicating a dominant reaction pathway through the *OCOH species, enhanced by Cs^+ and Cl^-. Linked with a photovoltaic cell, these electrodes produced FA with nearly 95% FE (J_{FM} ≈10 mA/cm^2) and an overall solar-to-fuel efficiency of around 8.5%, maintaining stability for 360 hrs and retaining their structural integrity (Fig. 11b and **c**) [165].

Studies have investigated three-compartment reactor designs incorporating a GDE, situated between an Anion Exchange Membrane (AEM) on the cathode side and a Cation Exchange Membrane (CEM) on the anode side. This arrangement forms a middle chamber for FA synthesis (Fig. 9b). The Sustainion™ membrane is a favored AEM choice, as demonstrated by Yang et al. in conjunction with a Bi-based catalyst, enabling continuous operation for 1000 hrs and generating FA concentrations over 10 wt% at a current density of 200 mA/cm^2 [166].

Zhang et al. crafted an innovative, self-standing, three-dimensional bismuthene network (Bi-ene-NW) that acts as a highly effective electrocatalytic membrane. Its single-atom-thick layers and edge-site defects make it an efficient catalytic cathode. When integrated into a GDE flow cell, it achieved current densities of 560 mA/cm^2 and maintained stability for over 500 hrs. The exceptional performance of Bi-ene-NW is due to its multitude of active sites, complex channels for mass transport, and excellent conductivity, facilitating both mass and electron movement. ATR-IR data and subsequent analyses also point to the edge defects of Bi-ene as crucial for stabilizing the reaction intermediates [168]. Along similar lines, a unique BiOx catalyst derived from a Bi MOF has been synthesized, characterized by a carbon layer and a high density of oxygen vacancies [170].

Sn- and Bi-based catalysts are favored in research for their efficiency, cost-effectiveness, and eco-friendliness. Strategies to improve these catalysts include structural modifications like shaping, defect introduction, grain boundary creation, and compositional adjustments. This enhancement process entails investigating binary systems, oxides, sulfides, dopants, and composites [186]. A schematic in Fig. 11d displays the $Bi_{0.1}Sn/SnO_2$ interface during electrochemical reactions, where a redox-tuned surface preserves activity and protects the $Bi_{0.1}Sn$ from corrosion over extended periods. SEM images in Fig. 11e show the $Bi_{0.1}Sn$ crystals before and after a 100-hr reaction, with consistent grain boundaries. DFT results in Fig. 11f indicate that the active sites with stabilized binding energies favor the formation of formate at 0 eV

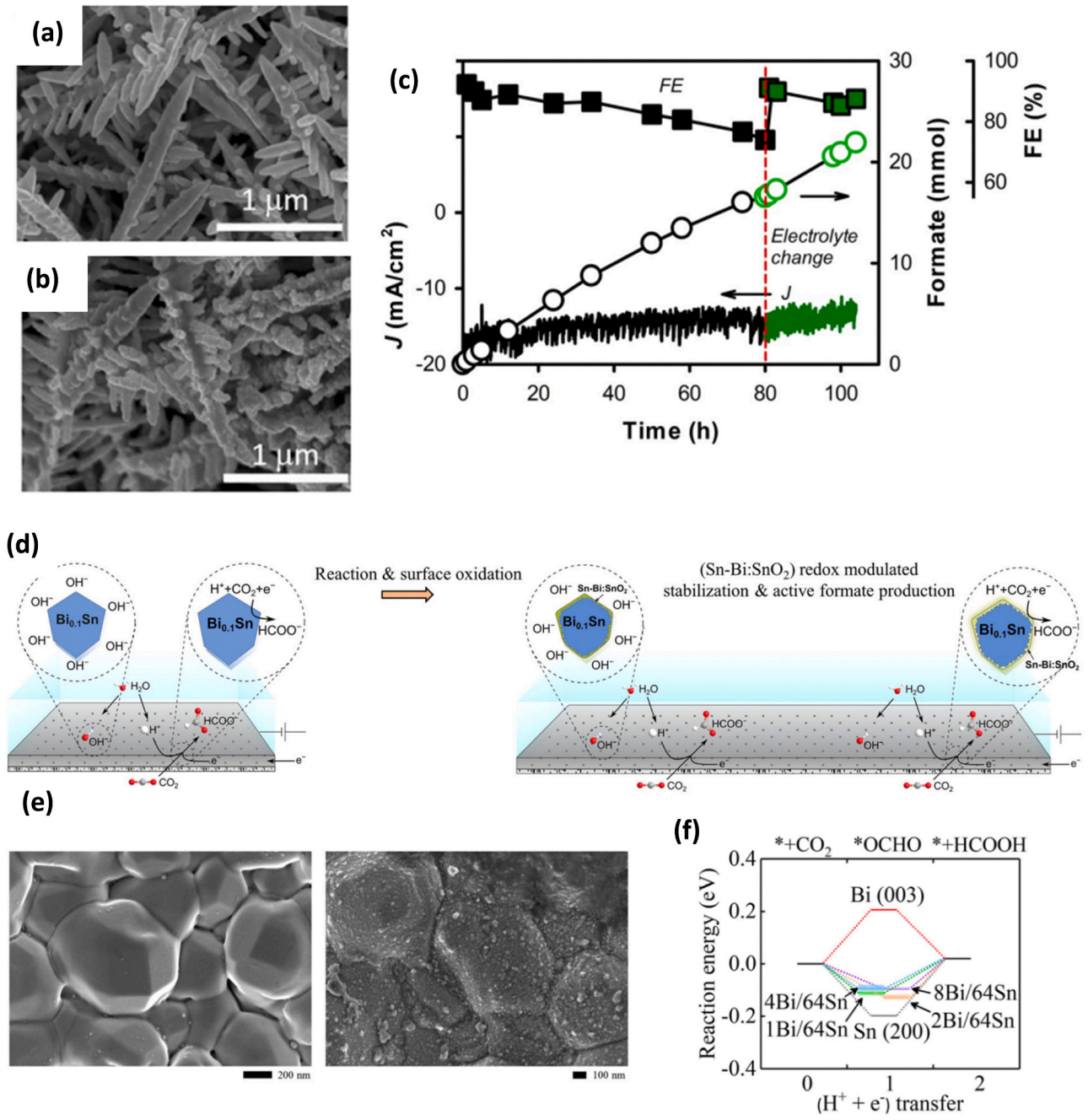

Fig. 11. (a) Scanning Electron Microscope (SEM) images showcasing the structure as formed via electrodeposition of porous Bi cathode for a duration of 5 seconds and (b) after a prolonged use of 360 hours. (c) Chronoamperometry results of 360 hours durability test using an IrO_2 anode paired with a porous Bi cathode. The setup was maintained at a consistent DC voltage of 2.87 V. Notably, after every 72 hours of electrolysis, the employed electrolyte (1 m KBC + 0.1 m CsCl) was replenished, while persisting with the same IrO_2 and Bi pairing [165]. (d) Schematic showcases a $Bi_{0.1}Sn/SnO_2$ surface during the electrochemical reaction. The redox-modulated Sn-Bi/SnO_2 surfaces maintain activity and shield the $Bi_{0.1}Sn$ catalysts from corrosion during prolonged CO_2 reduction reaction. (e) SEM images of as-prepared $Bi_{0.1}Sn$ crystals and $(Bi_{0.1}Sn/SnO_2)/Bi_{0.1}Sn$ particles after 100 hours of reaction. (f) Density Function Theory (DFT) calculations suggest that stabilized active sites enhance *OCHO binding energy, optimizing the $HCOO^-$ formation on various surfaces at 0 eV potential. Bi_ySn_{64}, with varied Bi ratios, presents a multitude of adsorption sites. The catalysts demonstrate a mix of high activity and stability, achieving over 2400 hours (100 days) of continuous CO_2 to FA reduction [171].

potential. Variations in Bi content in Bi_ySn_{64} alloys provide multiple adsorption sites, which are instrumental in enhancing the binding energy for *OCHO.

Li et al. employed a GDE fabricated from Sn and Bi on PTFE, demonstrating stability at 60 mA/cm^2 for 100 hrs. Using humidified CO_2 in a two-chamber reactor, they achieved formate concentrations of 153 g/L over the same duration. A liquid cathode feed system yielded above 90% FE at 100 mA/cm^2, remarkably sustained for 2400 hrs [171].

Furthering Sn-Bi alloy applications, the $SnO_2/Bi_2O_2CO_3$ on nitrogen and scandium-doped carbon (SnO_2/BOC@NSC) catalyst achieved 86.7 mA/cm^2 at −1.2 V vs. RHE with a 90.75% FE. In flow cells, this catalyst reaches up to 200 mA/cm^2 at −0.8 V vs. RHE, aligning with industrial benchmarks. Performance assessments and sophisticated X-ray studies reveal the efficacy stems from the synergistic actions of SnO_2/BOC, which enhance CO_2 activation and facilitate electron transport [174].

Alloying Bi with Cu has enabled ambient temperature synthesis methods [176]. Controlled electrodeposition crafted a Bi/Sn dendrite catalyst on a copper mesh, yielding pine needle-shaped Bi_5Sn_{60} dendrites that exhibited 95% FE and maintained stability for 20 hrs at −1 V vs. RHE due to their large active sites and metal oxide contact [177]. Bi deposited on Cu foam, enhanced with a fluorinated organosilane, leveraged three-phase interface engineering to achieve 98% FE and over 90% stability for 26 hrs in an H-cell setup [178]. Improving upon this, carbonized Bi-based MOFs reached 99% FE [179]. Indium-doped Bi nanosheets obtained a full 100% FE with 22 hrs of stability over a 450 mV range [181]. Modified $BaBiO_3$ perovskites support conversion through dual-site catalysis, with BBO undergoing atomic rearrangement under catalysis-relevant voltages, forming eBBO. This restructuring also encourages Ba^{2+} ion release into the electrolyte, securing 60 hours of stability at 21 mA/cm^2 with 99% FE [182].

Bi nanoparticles synthesized with carbon nanotubes via pyrolysis method attained 91% FE for 18 hours [183]. Adjusting SnBi catalyst molar ratios revealed that a Sn^{2+}/Bi^{3+} ratio of 1.0 achieved 96.4% FE and a FA yield of 684.7 μmol/cm^2·h at −1.06 V vs. RHE. A lower ratio, $Sn_{0.5}Bi$, increased the yield to 733.2 μmol/cm^2·h but slightly reduced FE to 96% [187]. Exploring anodes, Sainz et al. [185] developed hand-crafted NiO-based anodes which, compared to previous DSA/O_2 anodes, produced 100% FE with remarkably low energy usage of 200 kWh/kmol. The introduction of Sustainion® as a binder in anode fabrication significantly enhanced longevity without compromising performance [185].

3.2.2.4. Indium (In)-based electrocatalysts. Advancements in In-based catalysis materials (In_2O_3) led to great FE improvement in CO_2 reduction [162]. Zhang et al. [172] strategically synthesized indium, sulfur, and silver composites that deliver 94% FE with 560 mA/cm^2 at −0.951 vs RHE in the flow cell. Research indicates that the Ag-In-S interface strain is instrumental in boosting CO_2 reduction by reducing the energy barriers of intermediates and expediting charge transfer [172]. Jia et al. investigated indium cyanamide nanoparticles (InNCN), characterized by their highly electron-donating $[NCN]^{2-}$ ligands and the dynamic equilibrium between $[N{=}C{=}N]^{2-}$ and $[N{\equiv}C{-}N]^{2-}$ [184]. These nanoparticles are lauded for their 96% FE at 250 mA/cm^2. Furthermore, they require just −0.72 V vs. RHE in bulk electrolysis to achieve a current of 400 mA/cm^2, and they maintain stability for an impressive 160 hrs at 125 mA/cm^2 [184].

3.2.2.5. Other electrocatalysts. Park and Shin [169] developed a new dental amalgam-based catalyst applied to a copper foam electrode, achieving CO_2-to-FA conversion efficiencies of 80–100% across current densities from 50 to 250 mA/cm^2 in a specially designed flow-through electrochemical cell (Fig. 12). This configuration attained a peak FA concentration of 18 wt% (2.4 M). The design features a central cathode flanked by dual anodes in adjacent chambers, separated by CEMs (Nafion 117), optimizing the flow of cation (K^+) and protons (H^+) for enhanced electron generation at both anodes. Incorporating interconnected DSA mesh anodes, this system sustained continuous activity for 900 hrs at 50 mA/cm^2 [169].

3.2.2.6. Simulation Studies. Atomic-scale simulations have been pivotal in understanding the reaction mechanisms on various catalyst facets, shedding light on the structure-activity relationships to refine catalyst performance before empirical testing. Zhang et al. [188] explored a CuZn binary metal on a superstructured aerogel (CuZn@KCA), derived from N-doped konjac glucomannan (KGM) aerogel integrated with CuZn metal organic frameworks (CuZn-MOF), through comprehensive Multiphysics simulations. This catalyst, CuZn@KCA, achieved a 75% FE at 1.0 V vs. RHE, with its mass transfer rate significantly outperforming that of CuZn-MOF alone by 16-fold, attributed to its enhanced mass transfer features [188].

In another study, Zheng et al. [189] utilized DFT to analyze a Pd_3Au alloy, focusing on how work function changes and the catalyst's *d*-band center affect overpotential, revealing the influence of surface roughness and electronic structure on CO_2-to-FA conversion. A direct relationship was found between surface charge and hydrogen evolution reaction (HER) activity. The investigation also underscored the critical role of dynamic hydrogen bonding in water during the reaction, stressing the relevance of water molecules in catalysis and the need for explicit solvent models to capture accurate solvation effects in simulations [189].

3.2.2.7. Membrane-based capacitive deionization (MCDI). Advancements in CO_2 reduction have led to improvements in capture efficiency, operational flexibility, versatile electrode materials, and durability. However, challenges such as system complexity, higher energy consumption, electrode degradation, and limited selectivity remain. A promising solution is membrane-based capacitive deionization (MCDI), a cutting-edge technique for CO_2 capture based on capacitive adsorption. MCDI efficiently captures ionic CO_2 forms (HCO_3 and CO_3^{2-}) within the electrical double layer of an anode, while protons move towards the

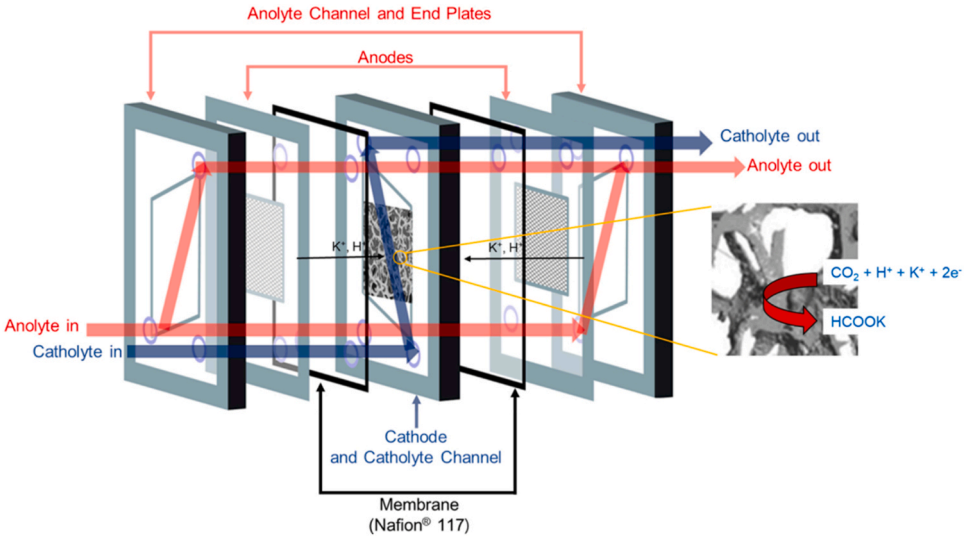

Fig. 12. A distilled depiction of the flow-through electrochemical cell configuration. Utilizing a dental amalgam composite on a copper foam electrode, the system showcases its capability to CO_2 into FA within this tailor-made electrochemical setup [169].

cathode to preserve charge balance. The adsorbed ions are then released by short-circuiting or reversing electrode polarity, enhancing adsorption efficiency and reducing energy consumption [190]. Yet, MCDI faces obstacles like elevated ohmic resistances and the high costs associated with ion exchange membranes, which significantly contribute to the overall expenses [191].

Efficient CO_2 to FA conversion faces significant hurdles, including high energy requirements and CO_2's limited solubility in aqueous electrolytes, which poses a challenge for cost-effective methodologies. Achieving the commercial success of advanced electrochemical systems necessitates optimizing the interaction among gaseous CO_2, liquid electrolytes, and solid electrocatalysts. This involves improvements in CO_2 reduction at the cathode, oxygen evolution at the anode, the materials used for electrodes, and the choice of electrolytes. The use of environmentally detrimental and costly heavy metals like cadmium and mercury, as well as the high cost of scarce metals such as indium and palladium, further complicate development. While Sn-based catalysts are a potential alternative, they struggle with selectivity and require high overpotentials. Bi-based catalysts, noted for their low toxicity and abundance, emerge as a viable option for CO_2 reduction, yet they too encounter issues like carbonate salt accumulation during extended operation at high currents, which can degrade reactor performance over time [186]. Strategies to address these challenges include the periodic replacement of electrolytes or augmenting water supply to reduce salt buildup [174]. Additionally, some research suggests using bipolar membranes to revert carbonate ions to CO_2 by introducing protons to the cathode area, although this approach might lead to increased ohmic resistance and higher cell potentials compared to using slimmer monopolar membranes [192].

3.2.3. Thermochemical

Thermochemical FA production employs heat to drive chemical reactions, often through the decomposition or combination of compounds. This process is divided into three main methods: biothermal, which uses biocatalysts and heat; hydrothermal, which applies pressure and heat; and thermocatalytic, which involves heating chemical catalysts.

3.2.3.1. Biothermal. Microalgae emerges as a sustainable and promising source for chemical production, boasting rapid, all-year growth, efficient CO_2 capture, low water requirements, and the ability to thrive in wastewater, particularly within hydrothermal reactions. The significance of microalgae lies in its carbohydrate and lipid compositions, which are crucial for fermentation-based FA (fatty acid) production and vary according to species and environmental conditions (Fig. 13**a**). Notable research by Park et al. [194] and Jin et al. [196] has shown the potential of thermochemical FA generation from microalgae, utilizing Glucosamine in methane sulfonic acid (MSA) and Spirulina and Chlorella in a bicarbonate medium, respectively. These studies highlight the use of catalysts from renewable aquatic sources, considered to be environmentally friendly [196].

The process of converting glucosamine to FA, achieving a yield of about 50% at 200°C (Fig. 13b), involves hydrothermal conversion using MSA, with specific reaction conditions of 50 g/L glucosamine and 0.37 M MSA at 188.7°C for 48.5 min [194] [196]. Further, research by

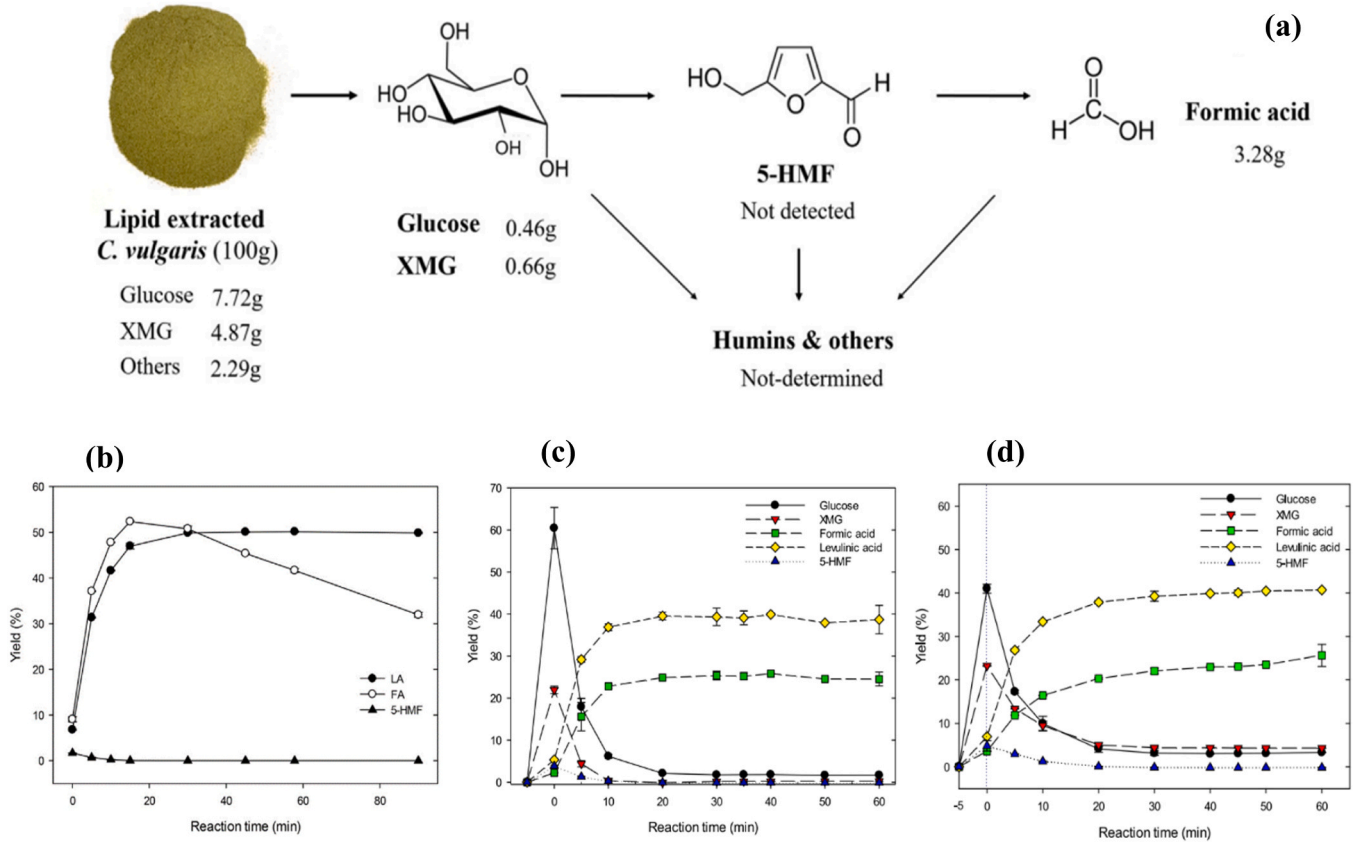

Fig. 13. (a) A streamlined representation of FA (FA) production from the lipid-extracted residue of C. vulgaris. Initially, the polymeric carbohydrates in the lipid-extracted residue (LER) of microalgae are broken down into monomeric sugars. These sugars are then dehydrated to form 5-hydroxymethylfurfural (5-HMF), which subsequently rehydrates to produce FA. However, this conversion mechanism inadvertently leads to the formation of undesired byproducts like humic substances. Under the 5% LER and 0.95 M HCl at 170°C for 60 minutes, from 100 g of LER 3.28 g FA (or 22.06% of the original sugar) were obtained. Notably, 5-HMF was absent under these conditions, while residual glucose and XMG measured at roughly 0.46 g (3.16%) and 0.66 g (4.39%), respectively [193]. The study examined how the reaction time influences the yields of 5-HMF, and FA (b) glucosamine is subjected to 190 °C and 2 M HCl [194] (c) Scenedesmus obliquus is subjected to 180 °C and 0.85 M H_2SO_4 [195] and (d) *C. vulgaris.* is subjected to 170 °C and 0.95 M HCl [193].

Jeong et al. on thermochemical conversion with the Scenedesmus obliquus (green microalgae) [195] and Chlorella vulgaris [193], using H_2SO_4 and HCl respectively, showcased FA yields of 25.8% and 22.06% under optimized conditions. These yields were obtained by processing 5 wt% concentration of Scenedesmus obliquus with 0.8 M H_2SO_4 at 180°C for 40 min (Fig. 13c), and lipid-extracted residue from C. vulgaris with 0.95 M HCl at 170°C for 60 min (Fig. 13d). The optimization of reaction conditions through a Box–Behnken design, evaluating the combined severity factor (CSF), indicated that FA yields could be marginally increased with higher CSF levels. The yield patterns were modeled using non-linear sigmoidal and Gaussian equations, showing that higher CSF conditions significantly enhance FA production, suggesting the potential of defatted S. obliquus and LER as renewable sources for bio-based compound synthesis [193,195].

3.2.3.2. Hydrothermal. Hydrothermal methods allow for the conversion of CO_2 into FA using organic compounds such as alcohols, thanks to specific reaction pathways that include CO_2 reduction and glucose breakdown. The CO_2 is introduced in the form of sodium bicarbonate and ammonium carbamate, with glucose serving as the primary reducing agent. Various catalysts, such as metals, metal oxides, and activated carbon (C), are utilized to enable these reactions, resulting in the predominant production of FA, as illustrated in Fig. 14 [197].

3.2.3.3. Thermocatalytic. Recent advancements in the hydrogenation of CO_2 using metal catalysts have led to the creation of effective processes for formate production. These processes often operate under high pressures (20–80 bar) and involve the use of additives (acidic or basic) to address the thermodynamic challenges posed by the standard free energy change (ΔG°) of 7.6 kcal/mol at 298 K, which makes the reaction typically unfavorable. The addition of bases has been a key strategy to favorably shift the equilibrium towards formate [198].

Innovative catalysts such as Cu [199], MoS_2 [200], Fe_3O_4 [201], Pd–Ni [202], and single atom Ru [203] have been introduced, enhancing CO_2 reduction capabilities. Notably, the CuO_x-TiO_2 catalyst, in combination with bases, achieved TON of 6.62 for FA at 40 bar and 200 °C [199]. The MoS_2/f-DSAC catalyst also stood out, delivering a TON of 510 per hour at 200°C over 15 hrs at 20 bar, with a relatively low activation energy of 12 kJ/mol [200]. FA yields of 53% and 52% were reported using C and Fe_3O_4 catalysts with sodium bicarbonate, respectively. Using ammonium carbamate was with Fe_3O_4, the FA yield peaked at 25%.

For tracking the carbon source in FA, $NaH^{13}CO_3$ has been utilized [201], indicating the effectiveness of these catalytic processes. Bimetallic systems, specifically Pd–Ag and Pd–Ni, were explored for their ability to covert CO_2 into FA, with the Pd–Ni system showing a conversion rate nearly four times higher than that of the Pd–Ag system. This efficiency was attributed to the electron-deficient nature of Ni, which enhances charge polarization and thus CO_2 conversion [202].

A study on a single atom Ru catalyst supported on N-doped TiO_2 highlighted the importance of N-dopant sites in creating a strong binding environment for Ru, leading to improved catalytic stability and performance, The Ru/MN-TiO_2 catalyst demonstrated a TON of 3180, maintaining 42% of its original activity after five recycle tests, showcasing the beneficial effects of both substitutional Ns and interstitial Ni dopants. This contrasts with the performance of Ru/N-TiO_2 and Ru/TiO_2, emphasizing the role of strong binding sites in enhancing stability and efficiency in hydrogenation processes [203].

3.2.3.4. Simulation studies. Sengupta et al. [204] conducted gradient-corrected DFT analysis to investigate the production of FA from CO_2 hydrogenation using Ti_6Se_8 clusters, both bare and ligand-enhanced. They found that adding PMe_3 and CO ligands turned the metal-chalcogenide cluster into an efficient donor/acceptor system, enhancing its catalytic function. Modifying ligand proportions on the cluster was shown to influence the barrier heights of the CO_2 hydrogenation reaction, thus dictating the conversion rate. The investigation covered reaction pathways for the ground state Ti_6Se_8 and its ligand form, analyzing relative energies for various magnetic moments in $[Ti_6Se_8(PMe_3)_{3-m}(CO)_m]$ clusters (where m = 1,2), as depicted in Fig. 15a and Ti_6Se_8 cluster in Fig. 15b-d. These modifications by the ligands affect the cluster's electronic spectrum without changing the order or filling of electronic levels, indicating a consistent shift in reactivity. Computational analysis identified two electronic factors affecting barrier heights. Donor ligands elevate the cluster's electronic levels, lowering its ionization energy and facilitating charge transfer. This elevation also weakens the cluster's hydrogen atom binding, benefiting the hydrogen transfer process. Although the research emphasized Ti_6Se_8 clusters, these findings could extend to other metal chalcogenide clusters [204].

3.2.3.5. Hybrid systems. Achieving sustainable FA production requires a multifaceted approach, combining techniques like photocatalytic, hydrothermal, thermocatalytic, and biothermal processes for synergistic

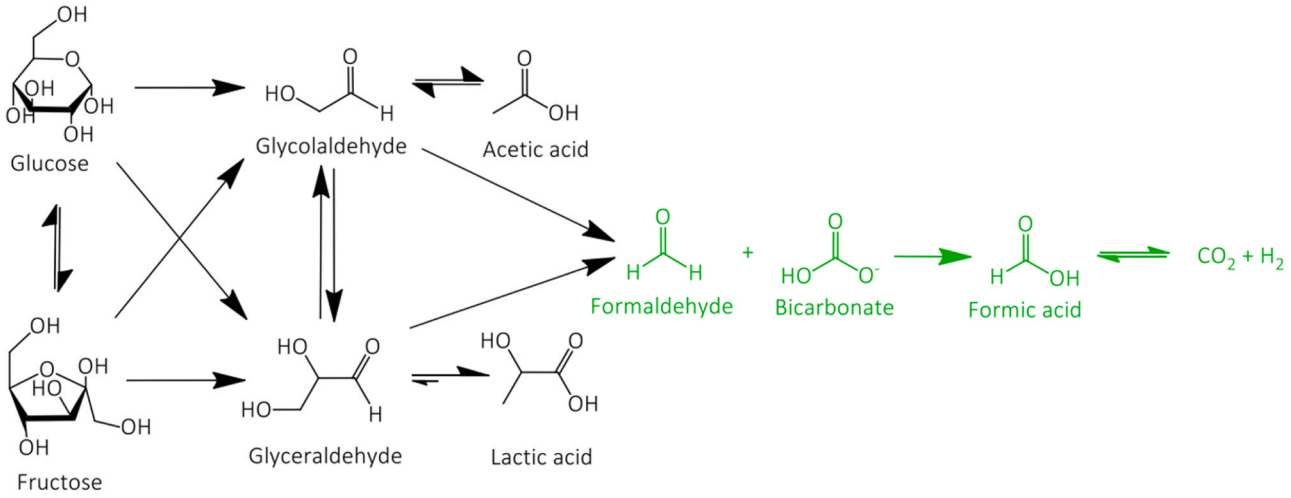

Fig. 14. Illustration of the dual pathways of glucose transformation. The first pathway, depicted in black, shows glucose undergoing isomerization to become fructose, which can further degrade into compounds such as glycolaldehyde and glyceraldehyde. Glyceraldehyde is also capable of further fragmentation into various other molecules. The second pathway, highlighted in green, represents the production of formic acid (FA) through the conversion of CO_2 and glucose or its derivatives under hydrothermal conditions. This diagram encapsulates the potential of glucose to serve as a precursor for FA in specific environmental setting [197].

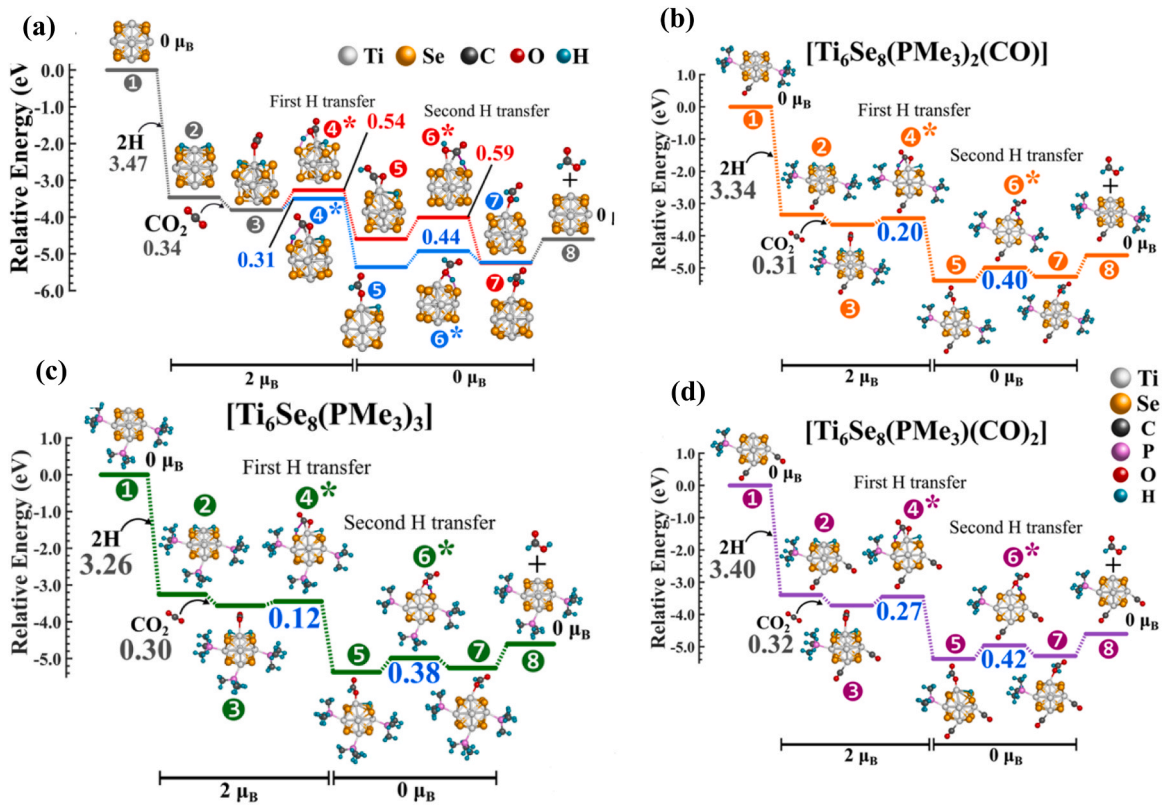

Fig. 15. (a) The reaction pathways for ground state Ti6Se8 cluster. (b, c and d) The reaction pathway's relative energies were analyzed for different magnetic moments of [Ti6Se8(PMe3)3-m(CO)m] clusters (where m = 1,2). When evaluating the barrier heights of both hydrogenation steps for all four ligated clusters, i.e., [Ti6Se8(PMe3)3-m(CO)m] (m = 0–3), it's clear that by methodically adjusting the ratio of PMe3 to CO ligands, the hydrogenation barriers can be systematically modified. The variations in the first and second barriers with each adjustment are between 0.07–0.13 eV and 0.02–0.10 eV, respectively. Binding energies for H and CO_2 are displayed in grey, while barrier heights for pathways A and B are illustrated in red and blue, respectively. Transition states are indicated with an asterisk (*) [204].

effects [205]. Singh et al. [206] showcased the integration of photocatalytic and biothermal strategies using microalgae such as *Chlamydomonas reinhardtii* and *Spirulina*, where the application of potassium-doped graphitic carbon nitride (K-g-C_3N_4) led to notable increases in formate production by 59% and 13%, respectively [206]. Meanwhile, Pie et al. [207] employed a dual hydrothermal and thermocatalytic approach with a Sn foil electrode (Fig. 16a), which facilitated a a continuous $Sn^{\delta+}$/Sn redox cycle (Fig. 16b) enhancing bicarbonate reduction to formate, demonstrated by impressive current density (121 mA/cm^2) and 83% FE in 3 mol/L $KHCO_3$ at 100 °C [207]. Schwarz et al. [208] introduced a combination of hydrothermal and biothermal methods using *Acetobacterium woodie* (Fig. 16c), enabling efficient CO_2 hydrogenation to FA over extended periods, effectively acting as a "biobattery" for energy storage without producing acetic acid [208].

The development of thermally stable catalysts, such as single atom catalysts (SACs), face challenges due to low loading capacities, highlighting the need for solutions like utilizing MOFs for enhanced performance [209]. Despite the potential of microalgae and biomass for FA production, they face limitations in productivity compared to electrochemical methods. Additionally, challenges in large-scale biomass production and the economic feasibility of processing hinder the broader commercial application of microalgae for bioenergy.

4. Formic acid (FA) vs. ammonia (NH_3)

The utilization of FA and NH_3 spans across various industrial domains, as illustrated in Fig. 17a and b, highlighting their widespread applications. FA plays a critical role in industries, with its application breakdown showing 30% in agriculture, 35% in leather and textile industries, 25% in rubber production, and 7% in the pharmaceutical sector. NH_3, on the other hand, finds its largest use in agriculture, constituting 80% of its total market, followed by smaller shares in leather and textiles (3%), rubber production (5%), and pharmaceuticals (10%). The data further highlights the pivotal role of NH_3 in urea production for agriculture, while FA's distribution across similar market segments like rubber, leather, and textiles underlines its significant economic impact, as inferred from financial studies [29,69]. For a in-depth comparison, Table 8 presents a side-by-side analysis of FA and NH_3, exploring their properties, advantages, and challenges. Table 9 focuses particularly on economic viability, scalability, and long-term sustainability of fuels.

4.1. Hydrogen production from NH_3 and HCOOH

The thermal decomposition of NH_3 ($2NH_3 \rightarrow N_2 + 3\,H_2$) is an endothermic process with an enthalpy change (ΔH) of 92 kJ/mol, necessitating elevated temperatures to drive efficient hydrogen production. Over recent decades, significant research has been dedicated to studying this reaction, focusing on producing high-quality H_2 [217].

In NH_3 synthesis, N_2 adsorption is typically the rate-limiting step, whereas the rate-determining step for NH_3 decomposition varies. Noble metal catalysts, such as Ru, Rh, Ir, Pt, or Pd, usually involve N–H cleavage as the rate-determining step, achieving conversion around 500 °C. Among them, Ru-based catalysts have exhibited the highest activity in catalyzing NH_3 decomposition. The properties of Ru-based catalysts, like Ru/CNT, have been enhanced by utilizing supports such as graphene nanocomposites, high surface area graphite, and carbon

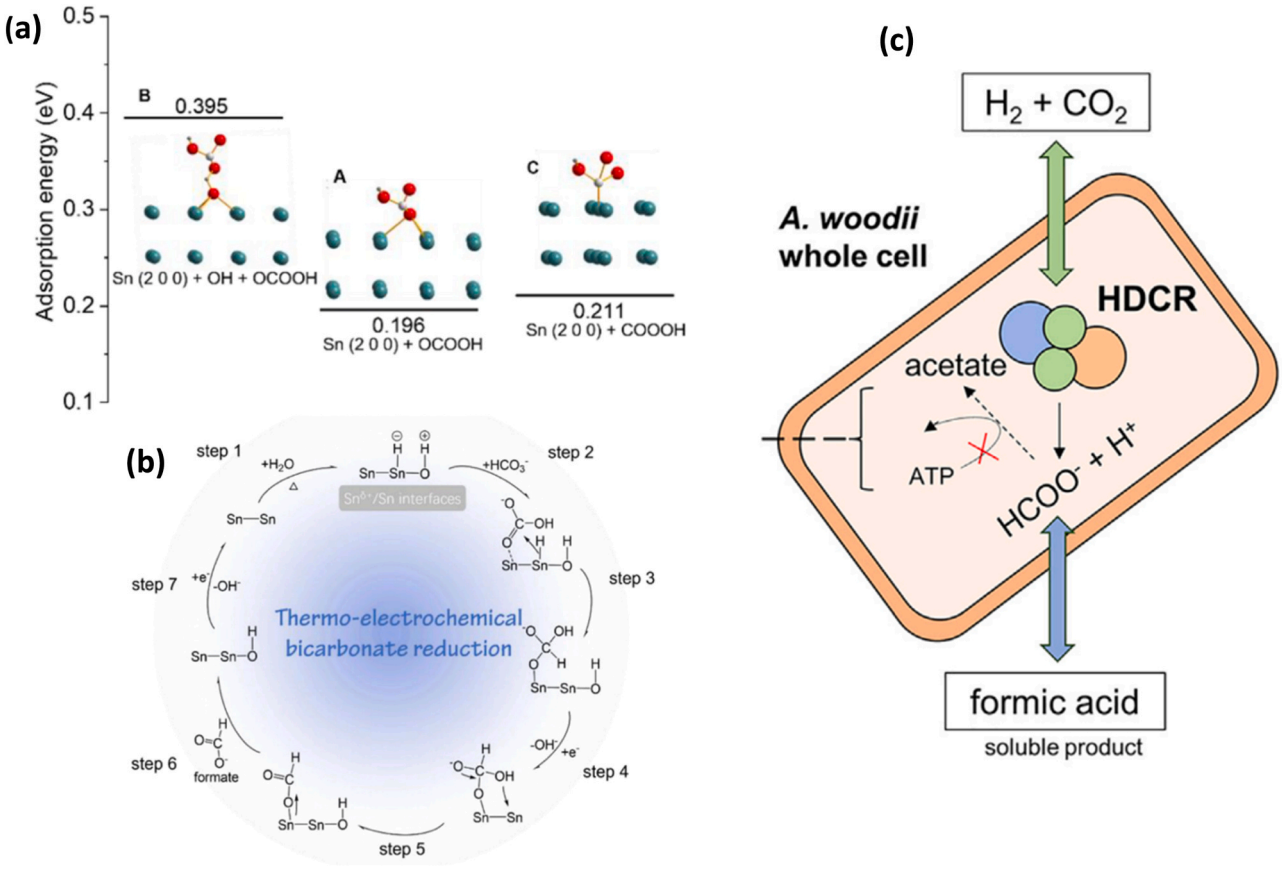

Fig. 16. (a) DFT analysis of adsorption mechanisms on the Sn(2 0 0) facet. (b) Suggested reaction pathways for thermo-electrocatalytic bicarbonate reduction (TEBR) at 100°C in water [207]. (c) The gaseous substrates, H_2 and CO_2, readily permeate the cell membrane, at which point the *Acetobacterium woodii* enzyme facilitates the hydrogenation of CO_2, converting it to FA. This system allows multiple cycles of CO_2 hydrogenation to FA within a single bioreactor [208].

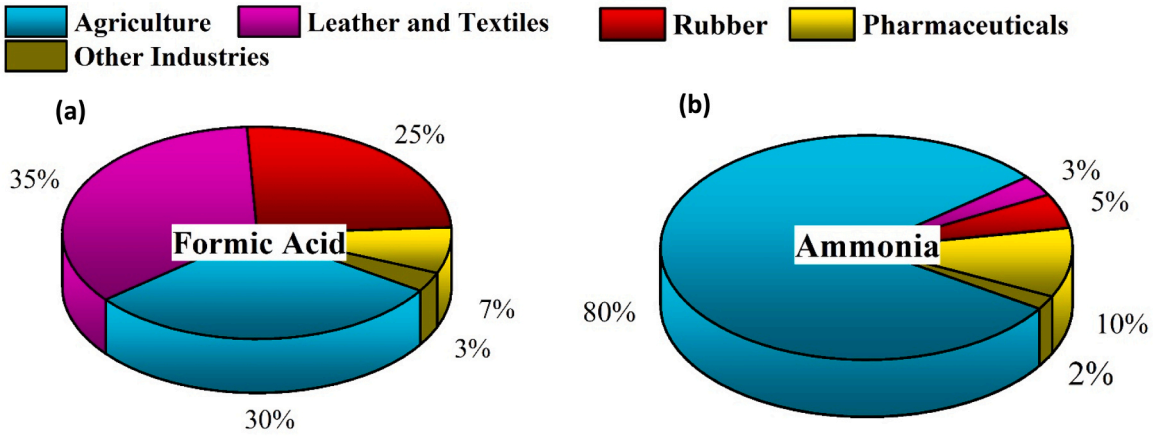

Fig. 17. The sectoral distribution of global market for FA and NH_3: (a) For FA, the agricultural sector accounts for 30%, leather and textile industries for 35%, rubber processing for 25%, pharmaceuticals for 7%, with the remaining 3% spread across various other sectors. (b) NH_3 is predominantly used in agriculture, with an 80% share, leather and textiles at 3%, rubber-related industries at 5%, pharmaceuticals at 10%, and 3% in miscellaneous applications. These percentages are approximate, with a potential variance of ±2% owing to data source discrepancies and fluctuating market trends [29,69].

nanofibers [218]. The most effective Ru catalyst involves doping 12 wt % potassium onto Ru and supporting it on MgO and CNT. By utilizing KOH-modified Ru, complete conversion is achieved at temperatures around 500 °C. However, their high cost and limited availability pose challenges for widespread adoption [219]. Conversely, non-noble metal catalysts, including Fe, Co, Ni, etc., typically feature N_2 desorption as the rate-determining step, albeit at higher temperatures exceeding 600 °C [220]. These catalysts are attractive due to their cost-effectiveness, abundance, and good catalytic activity. To reduce operating temperatures, bimetallic catalysts [221] and metal carbide/nitride catalysts [222] have been favored. The structure of the catalyst, particularly the size and dispersion of metal across nanoclusters, plays a critical role in its catalytic performance [223].

Formic acid decomposition ($HCOOH \rightarrow H_2 + CO_2$) is also an endothermic process but requires lower temperatures, typically between 50 and 100 °C, and various catalysts including both noble (Pt, Pd, Ru, Au)

Table 8
Characteristics comparison of NH_3 and FA as fuel [210–214].

Properties	Formic Acid (FA)	Ammonia (NH_3)
Physical state	Nontoxic, colorless liquid with a pungent odor; environmentally friendly under ambient conditions.	Highly toxic, strong odor gas at room temperature.
Melting and boiling point	Melting point at 8.3 °C; boiling point at 100.8 °C hence a liquid at room temperature.	Melting point at −77.73 °C; boiling point at −33.4 °C, thus liquified and typically stored at about −30°C.
Vapor pressure	4.6 KPa at 20 °C, less than gasoline (100.1 KPa), suggesting that existing gasoline infrastructure could be adapted for FA.	858 KPa at 20 °C, requiring specialized cryogenic tankers with refrigeration for trasnport.
Auto-ignition temperature	520 °C, which is lower than NH_3	650 °C higher than FA.
H_2 release	Catalytic decomposition into H_2 generally requires a temperature of 100 – 150 °C, but can occur at ambient temperature with noble metal-based catalysts.	Catalytic decomposition into H_2 requires a temperature of 200 – 250 °C
Fuel cell operation temperature	Direct FA fuel cells operate at around 180 °C.	Solid oxide fuel cells use NH_3 and operate at very high temperatures, over 700 °C.
Critical density	1.3 g/ml.	0.24 g/ml.
Combustion	Heat of combustion at 7.6 MJ/l (254.6 KJ/mol), with high adiabatic flame temperature of 2200 °C and a maximum laminar burning velocity of 25 cm/s at 100 °C, indicating superior fuel properties [215].	11.2 MJ/l (382.8 KJ/mol) heat of combustion, with an adiabatic flame temperature of 1800 °C, less effective heat transfer through radiation, and a lower combustion rate, making it unsuitable as a jet fuel [216].
Infrastructure	Less widespread industrial scale production and infrastructure compared to NH_3.	Well-established infrastructure for production, transportation, and storage, especially in the agricultural sector for urea.
Carbon Emissions	Decomposition yields H_2 and CO_2, with the potential for CO_2 to be captured and used to regenerate FA.	Decomposition yields H_2 and N_2, with no direct carbon emissions.

Table 9
Comparison of NH_3 and FA in terms of economic viability, scalability, and long-term sustainability.

Properties	**Formic Acid (FA)**	**Ammonia (NH_3)**
Economic Viability		
Transportability	Less volatile, thus safer for transport.	Well-established in its transportation infrastructure due to widespread use in the fertilizer industry.
Market demand	Emerging market with versatility for use in chemical synthesis, energy storage, and as a potential carrier for hydrogen.	Diverse applications beyond fertilizers, including industrial chemicals, refrigerants, and as a potential clean fuel.
Production costs	Influenced by the efficiency of catalysts, availability of CO_2 (often a byproduct), and the cost of CO_2 capture methods.	Influenced by the cost of natural gas (a primary feedstock), renewable energy costs for green NH_3, and carbon capture and utilization costs for blue NH_3.
Scalability		
Scalability	Mostly small-scale but potential for growth with advancements in catalyst technology and renewable energy integration.	Large-scale operations exist but expansion faces logistical and operational challenges.
Transition challenges	Relatively easier to integrate into existing infrastructure and adapt to renewable energy advancements.	Transition to green production reliant on improvements in renewable energy technology and storage solutions
Advantages	Can be stored and transported more easily compared to NH_3, offering greater flexibility.	High production volume but facing challenges in storage and transportation for energy applications.
Long-term Sustainability		
Renewable pathway	CO_2 reduction offers a renewable method for FA synthesis when combined with electrolysis and hydrogenation processes.	Offers potential for carbon neutrality when coupled with renewable energy sources and carbon capture technologies.
Sustainability challenges	Lower toxicity and safer handling reduce potential environmental risks compared to NH_3.	Faces significant challenges due to its potential for nitrogen pollution and broader environmental impacts.
Research focus	Directed towards enhancing catalyst efficiency, minimizing environmental impacts, utilizing renewable resources, and establishing FA as a hydrogen carrier.	Concentrates on improving production efficiency, reducing environmental impact, and realizing NH_3's potential as a renewable fuel.

and non-noble metals (Ni, and Co) [224–226].

Furthermore, the decomposition reactor is a vital device responsible for breaking down NH_3 and FA molecules into hydrogen and other gases, providing an efficient and precisely controllable means for hydrogen production. Moreover, it offers a reliable platform for the effective utilization of catalysts in decomposition processes. Despite extensive research conducted on the decomposition of NH3 and FA catalysts in the past decade, comprehension of how catalyst structure influences activity remains incomplete. Optimization and innovation in the design of these reactors are essential for enhancing efficiency and advancing hydrogen production technologies [227].

5. Commercialization stage: challenges and market expectations

The surge in natural gas prices in Europe, influenced by the Russia-Ukraine conflict [228], has posed significant economic hurdles for NH_3 production facilities in the region. BASF, a leading chemical producer globally, has reduced NH_3 production at its Antwerp and Ludwigshafen sites [229] due to these challenges. To navigate the fluctuating natural gas prices, BASF has adjusted its production strategies to maintain profitability. Similarly, Yara, a top NH_3 manufacturer in Germany, has seen a notable reduction in its production, with a decrease of over 27% [230]. These industry adjustments are contextualized by the broader market trends for FA and NH_3, as shown in global market analyses (Fig. 17). FA's production was reported at 870 kt, with a value of around $943 per ton, and is expected to see a strong growth rate of 3.87% a cumulative annual growth rate (CAGR) through 2027. In contrast, NH_3's production stood at 178,330 kt, priced at $400 per ton, with a more modest growth forecast of 1.88% CAGR [29,69]. This comparison underscores a growing interest in FA, potentially as an alternative H_2 fuel, given its more dynamic market growth compared to NH_3.

Electrochemical methods stand out in FA production for their scalability, achieving efficiency up to 1 A/cm^2 [167], nearly 100% FA yield, and operational stability beyond 2400 hours [165], with the selection of electrolytes and electrode potentials playing crucial role. Putten et al. [231] demonstrated the use of FA as a LOHC in a system with the capacity to power city buses or act as an independent, carbon-neutral power source, highlighting its practical viability [231]. The U.S. Department of Energy (US DOE) backs a project at the University of Delaware focused on developing a 5-liter reactor using MCDI technology, which is currently at technology readiness level (TRL) of 3–5, with selectivity between 94% and 100%. Cost analysis for electrochemically produced FA estimates it between $0.46/kg to $1.16/kg, influenced primarily by electricity costs; to reach production costs below $0.2/kg, electricity prices must fall under the $0.02 per kWh [23], This

underscores the importance of accessible, eco-friendly energy sources in meeting rising FA demand. Despite ongoing research on the economics of FA production, detailed techno-economic assessments (TEA) for its large-scale manufacture remain scarce. Additionally, solving the challenge of electrode exfoliation at high potentials necessitates innovative approaches.

Rumayor et al. [232] and Proietto et al. [233] conducted significant studies on the technical and economic aspects of electrochemical processes, focusing particularly on the use of gas diffusion electrodes (GDE) cathodes enhanced with carbon-supported Sn nanoparticles. Rumayor et al. detailed optimal operational parameters, including a 200 mA/cm^2 current density, a cell potential of 4.3 V, and aiming for a 42.3% Faradaic efficiency. They evaluated a Sn/C-GDE cathode projected to last 4.45 years, used alongside a Nafion 117 membrane with a 60,000-hour lifespan and a dimensionally stable anode anticipated to operate for ten years. Their findings underscored the necessity of extending the cathode's lifespan beyond 4.45 years to maintain consumable costs below 10% of total production expenses, a crucial factor for competitiveness against conventional fossil fuel processes [232].

Proietto et al. examined diverse electrochemical configurations, including a divided filter press cell with a Nafion® 117 membrane and single solution pass; a micro-structured divided flow cell also with a Nafion® 117 membrane; a three-compartment cell with Sustanion™ AEM and Nafion 324 CEM; an undivided pressurized cell facilitating continuous solution recirculation without a membrane; and a divided pressurized cell with continuous recirculation and a bipolar membrane. Their studies, focusing on both GDE and high-pressure (HP) techniques, underscored the goal of achieving a minimum of 30 wt% FA concentration from electrolysis, maintaining current densities over 120 mA/cm^2, and operating at voltages between 2.5–3 V. The research on GDE aimed at enhancing its durability and economic feasibility, whereas HP strategies focused on improving FA production yields through cathodes of greater selectivity and larger active areas [233]. The research by both teams underscored the critical need for advancements in cell architecture, process optimization, and anode development to mitigate FA degradation, recommending strategies such as minimizing electrode distances, employing electrodes with low overpotentials, and choosing energy-efficient electrolytes.

Norouzi et al. [234] undertook techno-economic evaluations of various anolyte materials, including KOH, IrO_2, DAS/O_2, and Amberlite IR120, pinpointing IrO_2 as the top performer. The profitability of these processes hinges on advantageous market scenarios, affordable renewable energy sources, and significant CO_2 pricing mechanisms like those found in the EU ETS. Sensitivity analyses emphasized the pivotal role of electricity usage in the electrochemical reduction of CO_2 to FA, suggesting that with enhancements in cathode longevity and leveraging excess renewable energy, such processes could attain economic feasibility in the foreseeable future [232,233]. Yang et al. [235] reported that using off-peak power from wind and solar sources for CO_2-to-FA reduction makes both electrochemical and thermochemical approaches more practical [235]. Additionally, Ai et al. [236] showcased the environmental advantages of integrating hydropower with electrochemical reduction, resulting in a notable decrease (24%) in dependence on petrochemical resources [236].

The viability of FA as a LOHC has been explored in various studies [237] [64] [238]. Systems encompassing production, transportation, dehydrogenation, and CO_2 recycling have been individually assessed through techno-economic analysis (TEA) and life cycle assessment (LCA). Kim et al. found that while a LOHC system based on thermocatalytic CO_2 hydrogenation to produce FA is initially more expensive than liquefied H_2 distribution, it becomes more cost-effective with a 12% cost reduction when switching to electrochemical CO_2 hydrogenation for FA synthesis. Moreover, using different dehydrogenation methods can lead to a further 23–32% cost decrease [237]. Additionally, when wind-generated electricity is the primary energy source, the environmental impact of electrochemical FA production is significantly reduced, by up to 39% compared to liquefied H_2 distribution [238].

Ghorbani's study integrated post-combustion CO_2 capture with a copper-chlorine thermochemical process and FA production cycles, presenting a novel mix of electro-thermochemical processing utilizing both industrial flue gas thermal energy and wind energy. The results indicates the production of 833.3 kg/h of FA, with substantial energy and exergy efficiencies. Despite notable exergy losses occurring within the electro-thermochemical process, comprehensive analyses and multi-objective optimizations using neural networks and genetic algorithms have identified an optimal operational point. This point demonstrates that harnessing power from wind turbines to the tune of 9.90 MW can achieve high energy and exergy efficiencies, underscoring the system's effectiveness [64]. These insights underscore the potential for CO_2-to-FA conversion to become economically viable in the medium term, particularly with improvements in cathode durability and increased use of renewable energy sources (Fig. 18).

6. Summary and future perspective

Hydrogen is increasingly recognized as a crucial fuel in achieving carbon neutrality, with NH_3 (ammonia) and FA (formic acid) emerging as notable H_2 vectors. Current studies actively explores CO_2 utilization techniques to produce carbon-neutral NH_3 and FA fuels, with the promise of reducing annual annual CO_2 emissions by up to 10%, or 3.7 gigatons, and the prospect of further expansion. Our comprehensive review examines recent progress in blue NH_3, green NH_3, and FA production methods, alongside tackling the inherent obstacles within the H_2 economy and CO_2 mitigation efforts. While blue and green NH_3, derived from captured CO_2 and renewable energy sources, are still nascent compared to the widely used gray variant in fertilizers, the shift to using NH_3 as a H_2 carrier is complex, given its physical properties and potential toxicity.

The effectiveness of NH_3 and FA production is closely linked to the efficiency of the catalysts used. Bismuth (Bi) and tin (Sn) based catalysts are renowned for their stability, maintaining performance for over 2000 hrs with 1 A/cm^2 current density. The helical pyramid-shaped structure of Sn-Bi catalysts, with its broad surface area, active sites, and screw dislocation defects, facilitates electron transfer critical for CO_2

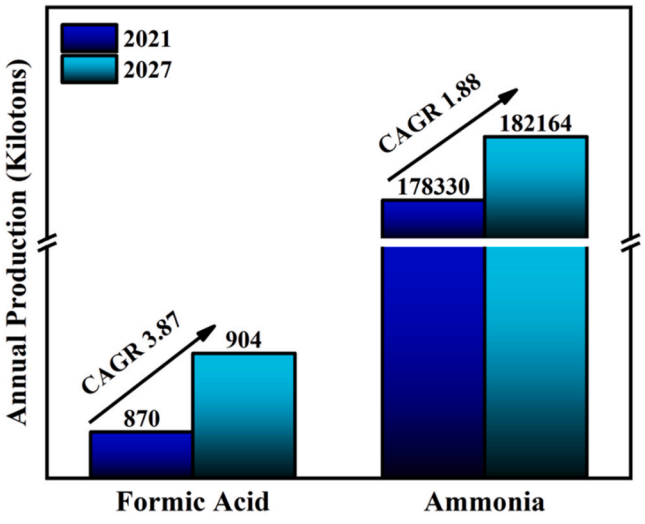

Fig. 18. The 2021 global market dynamics for FA and NH_3, analyzing production capacities, valuation, and growth forecasts through 2027. FA's production was recorded at 870 kilotons, with a market valuation averaging $943 per ton, and is expected to expand at a compound annual growth rate (CAGR) of 3.87% until 2027. In comparison, NH_3's production capacity stood substantially higher at 178,330 kilotons, with its price at approximately $400 per ton. NH_3's market is predicted to grow at a CAGR of 1.88%, which is significantly lower than that of FA, indicating a more modest expansion in the NH_3 sector [29,69].

intermediate formation. The synergy of Sn metal oxide with Bi metal oxide enhances CO_2 stabilization, pivotal for FA synthesis via the OCHO intermediate. For long-term commercial use, however, these catalysts require further refinement. Their complex structures can introduce impediments like defects that affect catalytic efficiency. The catalyst's electronic properties, such as conductivity and active site configuration, can be improved through doping and integration with other materials, leading to performance gains. Maintaining catalyst activity over time is crucial, highlighting the ongoing need for research to extend their lifespan. Advances in electrocatalyst technology depend on a deep understanding of their mechanics, where combining in-situ characterizations with theoretical models is advantageous. Single atom Cctalysts (SACs), known for their unique properties in heterogeneous catalysis, face challenges in reaction complexity and system design that affect maintaining precise FA concentrations, necessitating more sophisticated catalytic environments. Therefore, while significant progress has been made in delineating the impact of these factors on FA and green NH_3 production, the discovery of an ideal parameter set remains an ongoing endeavor.

In FA production, the choice of electrolyte, current density, and electrode potential are critical factors. Commonly used electrolytes are alkaline aqueous solutions, especially bicarbonate solutions, which maintain a stable pH between 6 and 7 and dissolve CO_2 effectively. Despite the advantage of acid electrolytes, they can lead to challenges such as electrode degradation at high potentials. The cost of ion exchange membranes, vital for segregating cathodic and anodic liquids, is a significant factor, driving the need for cost-effective membrane solutions in cell design. In contrast, photocatalytic and thermocatalytic methods for CO_2 conversions can suffer from low selectivity due to harsh conditions required and are hindered by a lack of clarity in reaction understanding, with complex pathways and kinetics resulting in ambiguous reaction mechanisms. Electrochemical method for FA production are energy-intensive and thus require the integration of renewable energy, the availability of which can vary greatly with local weather patterns, necessitating flexible energy integration from sources such as solar or wind.

Advancements in materials science are vital for the development of catalysts that are both effective and selective for the electrochemical, thermochemical, and photochemical conversion of CO_2 to FA. This includes exploring novel materials such as metal-organic frameworks (MOFs), carbon-based catalysts, and heteroatom-doped materials, which show promise in enhancing catalytic performance and longevity. Moreover, the refinement of CO_2 reduction processes is key, requiring the optimization of electrodes, electrolytes, and operational parameters to enhance reaction rates, elevate current densities, and suppress byproduct formation, thereby improving yield and efficiency.

For photochemical CO_2 reduction, the focus should shift to pioneering methods that effectively utilize solar energy, which may involve designing photocatalysts with specific band structures for optimal light capture and electron transfer. Introducing sophisticated light-harvesting constructs could further improve photon use. A deeper molecular-level understanding of CO_2 to FA reaction mechanisms is also critical, necessitating the analysis of intermediates and pathways across varying conditions through advanced spectroscopy and simulations.

Translating lab-scale experiments to industrial applicability entails ensuring long-term catalyst stability, the potential for rejuvenation in actual production environment, and scaling to meet industrial current densities benchmark. The transition of promising CO_2 reduction techniques to industrial scale and their thorough techno-economic evaluation to ascertain viability and market competitiveness is fundamental. It involves pinpointing cost factors, fine-tuning process variables, and considering how these systems could integrate with existing industrial setups.

Investigating hybrid systems that merge different CO_2 conversion technologies or pair CO_2 reduction with other processes may boost efficiency and product yield due to synergistic effects. The development of cost-effective separation and purification methods for extracting high-purity FA is also crucial, and could include novel solvent systems, membrane technologies, or adsorption techniques tailored to FA's unique properties and those of its byproducts.

The exploration of biological avenues, such as microbial or enzymatic systems for CO_2 into FA conversion, offers potential. Probing into microorganisms with efficient formate production and optimizing bioreactor conditions can enhance productivity while conserving energy. Pursuing carbon-neutral or negative FA production by combining CO_2 reduction with renewable energy use or bio-sourced CO_2 sources is another area for research.

As we progress, it is imperative to maintain the quality of both green NH_3 and FA, even when scaling up for mass production. Future efforts should include setting up pilot plants for real world testing of these technologies, addressing scalability challenges. Identifying and developing new applications for FA as a renewable source, whether as a chemical feedstock, fuel additive, energy carrier, or industrial intermediate, is crucial. Exploring potential synergies with existing markets and supply chains can help integrate FA-based solutions. By pursuing these research paths, the scientific and engineering communities can propel sustainable CO_2 utilization technologies forward and hasten the transition to a low-carbon future.

CRediT authorship contribution statement

Dong Suk Han: Writing – review & editing, Writing – original draft, Supervision, Funding acquisition. **Hyunwoong Park:** Writing – review & editing. **Talal Altahtamouni:** Writing – review & editing. **Donghyun Kim:** Writing – review & editing. **Peter Kasak:** Writing – review & editing. **Anton Popelka:** Writing – review & editing. **Arti Mishra:** Writing – original draft.

Declaration of Competing Interest

The authors declare the following financial interests/personal relationships which may be considered as potential competing interests: Dong Suk han reports financial support was provided by Qatar National Research Fund. If there are other authors, they declare that they have no known competing financial interests or personal relationships that could have appeared to influence the work reported in this paper.

Data availability

Data will be made available on request.

Acknowledgements

This study is made possible by the Qatar National Research Fund (QNRF) under National Priorities Research Program (NPRP) grant (#NPRP13S-0202-200228). Open Access funding is provided by the Qatar National Library (QNL). H.P. is grateful to the National Research Foundation of Korea for financial support (RS-2023-00254645).

References

[1] P.J. Gleckler, P.J. Durack, R.J. Stouffer, G.C. Johnson, C.E. Forest, Industrial-era global ocean heat uptake doubles in recent decades, Nat. Clim. Change 6 (4) (2016) 394–398, https://doi.org/10.1038/nclimate2915.
[2] R. Cassia, M. Nocioni, N. Correa-Aragunde, L. Lamattina, Climate change and the impact of greenhouse gasses: CO_2 and NO, friends and foes of plant oxidative stress, Front. Plant Sci. 9 (2018) 273, https://doi.org/10.3389/fpls.2018.00273.
[3] X. Lan, P. Tans, K.W. Thoning, Trends in Atmospheric Carbon Dioxide, 2022. ⟨https://doi.org/10.15138/9N0H-ZH07⟩. (Accessed 15 October 2022).
[4] G. Adams, F. Aloulou, L. Aniti, E. Boedecker, W. Brown, N. Chase, et al., International Energy Outlook 2016, U.S. Energy Information Administration, 2016, pp. 139–148.
[5] J.R. Petit, J. Jouzel, D. Raynaud, N.I. Barkov, J.M. Barnola, I. Basile, et al., Climate and atmospheric history of the past 420,000 years from the Vostok ice

core, Antarctica, Nature 399 (6735) (1999) 429–436, https://doi.org/10.1038/20859.
[6] P. Friedlingstein, M.W. Jones, M. O'Sullivan, R.M. Andrew, D.C.E. Bakker, J. Hauck, et al., Global carbon budget 2021, Earth Syst. Sci. Data 14 (4) (2022) 1917–2005, https://doi.org/10.5194/essd-14-1917-2022.
[7] A.S. Agarwal, Y. Zhai, D. Hill, N. Sridhar, The electrochemical reduction of carbon dioxide to formate/formic acid: engineering and economic feasibility, ChemSusChem 4 (9) (2011) 1301–1310, https://doi.org/10.1002/cssc.201100220.
[8] F. Meng, Y. Meng, T. Ju, S. Han, L. Lin, J. Jiang, Research progress of aqueous amine solution for CO_2 capture: a review, Renew. Sust. Energ. Rev. 168 (2022) 112902, https://doi.org/10.1016/j.rser.2022.112902.
[9] F. Vega, F.M. Baena-Moreno, L.M. Gallego Fernández, E. Portillo, B. Navarrete, Z. Zhang, Current status of CO_2 chemical absorption research applied to CCS: towards full deployment at industrial scale, Appl. Energy 260 (2020) 114313, https://doi.org/10.1016/j.apenergy.2019.114313.
[10] O. Akeeb, L. Wang, W. Xie, R. Davis, M. Alkasrawi, S. Toan, Post-combustion CO_2 capture via a variety of temperature ranges and material adsorption process: a review, J. Environ. Manag. 313 (2022) 115026, https://doi.org/10.1016/j.jenvman.2022.115026.
[11] X. Li, Z. Wang, Z. Liu, R. Feng, S. Song, J. Huang, et al., A novel preparation of solid amine sorbents for enhancing CO_2 adsorption capacity using alumina-extracted waste, Energy 248 (2022) 123677, https://doi.org/10.1016/j.energy.2022.123677.
[12] M.-G. Jang, S. Yun, J.-K. Kim, Process design and economic analysis of membrane-integrated absorption processes for CO_2 capture, J. Clean. Prod. 368 (2022) 133180, https://doi.org/10.1016/j.jclepro.2022.133180.
[13] H. Fu, K. Xue, Z. Li, H. Zhang, D. Gao, H. Chen, Study on the performance of CO_2 capture from flue gas with ceramic and PTFE membrane contactors, Energy 263 (2023) 125677, https://doi.org/10.1016/j.energy.2022.125677.
[14] C. Song, Q. Liu, S. Deng, H. Li, Y. Kitamura, Cryogenic-based CO_2 capture technologies: state-of-the-art developments and current challenges, Renew. Sust. Energ. Rev. 101 (2019) 265–278, https://doi.org/10.1016/j.rser.2018.11.018.
[15] M. Shen, L. Tong, S. Yin, C. Liu, L. Wang, W. Feng, et al., Cryogenic technology progress for CO_2 capture under carbon neutrality goals: a review, Sep. Purif. Technol. 299 (2022) 121734, https://doi.org/10.1016/j.seppur.2022.121734.
[16] D. Wang, A. Joshi, L.-S. Fan, Chemical looping technology – a manifestation of a novel fluidization and fluid-particle system for CO_2 capture and clean energy conversions, Powder Technol. 409 (2022) 117814, https://doi.org/10.1016/j.powtec.2022.117814.
[17] T. Czakiert, J. Krzywanski, A. Zylka, W. Nowak, Chemical looping combustion: a brief overview, Energies 15 (4) (2022) 1563, https://doi.org/10.3390/en15041563.
[18] M.H. Ibrahim, M.H. El-Naas, R. Zevenhoven, S.A. Al-Sobhi, Enhanced CO_2 capture through reaction with steel-making dust in high salinity water, Int. J. Greenh. Gas. Control. 91 (2019) 102819, https://doi.org/10.1016/j.ijggc.2019.102819.
[19] B.S. Adam, B. Niels, Is carbon capture too expensive?, 2022. ⟨https://policycommons.net/artifacts/1427544/is-carbon-capture-too-expensive/⟩. (Accessed 15 February 2023).
[20] D. Kang, J. Byun, J. Han, Electrochemical production of formic acid from carbon dioxide: a life cycle assessment study, J. Environ. Chem. Eng. 9 (5) (2021) 106130, https://doi.org/10.1016/j.jece.2021.106130.
[21] A. Mustafa, B.G. Lougou, Y. Shuai, S. Razzaq, Z. Wang, E. Shagdar, et al., A Techno-economic study of commercial electrochemical CO_2 reduction into diesel fuel and formic acid, J. Electrochem. Sci. Technol. 13 (1) (2022) 148–158, https://doi.org/10.33961/jecst.2021.00584.
[22] J.S. Lee, J. Jung, K. Roh, S. Heo, U. Lee, J.H. Lee, Risk-based uncertainty assessment to identify key sustainability hurdles for emerging CO_2 utilization technologies, Green. Chem. 24 (11) (2022) 4588–4605, https://doi.org/10.1039/D2GC00514J.
[23] H. Yang, R. Masel, CO_2 and Renewable Electricity Into Chemicals: Formic Acid Production from Coal Flue Gas, Office of Scientific and Technical Information (OSTI), 2021.
[24] S.M. Jarvis, S. Samsatli, Technologies and infrastructures underpinning future CO_2 value chains: a comprehensive review and comparative analysis, Renew. Sust. Energ. Rev. 85 (2018) 46–68, https://doi.org/10.1016/j.rser.2018.01.007.
[25] X. Chen, Y. Liu, J. Wu, Sustainable production of formic acid from biomass and carbon dioxide, Mol. Catal. 483 (2020) 110716, https://doi.org/10.1016/j.mcat.2019.110716.
[26] Global Status of CCS, 2021. ⟨https://www.globalccsinstitute.com/wp-content/uploads/2021/11/Global-Status-of-CCS-2021-Global-CCS-Institute-1121.pdf⟩. (Accessed 30 October 2022).
[27] B.-j Kim, G. Piao, S. Kim, S.Y. Yang, Y. Park, D.S. Han, et al., High-efficiency solar desalination accompanying electrocatalytic conversions of desalted chloride and captured carbon dioxide, ACS Sustain. Chem. Eng. 7 (18) (2019) 15320–15328, https://doi.org/10.1021/acssuschemeng.9b02640.
[28] Ammonia production worldwide from 2010 to 2021, 2021. ⟨https://www.statista.com/statistics/1266378/global-ammonia-production/⟩. (Accessed 10 February 2023).
[29] Global Formic Acid Market (2022 - 2027) - Mordor Intelligence, 2021. ⟨https://www.mordorintelligence.com/industry-reports/formic-acid-market⟩. (Accessed 19 October 2022).
[30] N. Mardini, Y. Bicer, Direct synthesis of formic acid as hydrogen carrier from CO_2 for cleaner power generation through direct formic acid fuel cell, Int. J. Hydrog. Energy 46 (24) (2021) 13050–13060, https://doi.org/10.1016/j.ijhydene.2021.01.124.
[31] M. Iguchi, M. Chatterjee, N. Onishi, Y. Himeda, H. Kawanami, Sequential hydrogen production system from formic acid and H_2/CO_2 separation under high-pressure conditions, Sustain. Energy Fuels 2 (8) (2018) 1719–1725, https://doi.org/10.1039/C8SE00087E.
[32] Y. Liu, F. Wang, Z. Jiao, S. Bai, H. Qiu, L. Guo, Photochemical systems for solar-to-fuel production, Electrochem. Energy Rev. 5 (3) (2022), https://doi.org/10.1007/s41918-022-00132-y.
[33] R. Cauwenbergh, S. Das, Photochemical reduction of carbon dioxide to formic acid, Green. Chem. 23 (7) (2021) 2553–2574, https://doi.org/10.1039/d0gc04040a.
[34] A.S. Agarwal, E. Rode, N. Sridhar, D. Hill, Conversion of CO_2 to value added chemicals: opportunities and challenges. Handbook of Climate Change Mitigation and Adaptation, Springer International Publishing, 2022, pp. 1585–1623.
[35] Z. Kou, X. Li, T. Wang, Y. Ma, W. Zang, G. Nie, et al., Fundamentals, on-going advances and challenges of electrochemical carbon dioxide reduction, Electrochem. Energy Rev. 5 (1) (2021) 82–111, https://doi.org/10.1007/s41918-021-00096-5.
[36] O. Hakami, Thermocatalytic and solar thermochemical carbon dioxide utilization to solar fuels and chemicals: a review, Int. J. Energy Res. 46 (14) (2022) 19929–19960, https://doi.org/10.1002/er.8702.
[37] A. Badreldin, K. Elsaid, Y. Wubulikasimu, K. Youssef, Z.K. Ghouri, A. El Ghenymy, et al., Direct thermochemical CO_2 reduction to reduced graphene oxide-like nanomaterials: implications for environmental and energy storage and conversion applications, ACS Appl. Nano Mater. 5 (10) (2022) 14785–14797, https://doi.org/10.1021/acsanm.2c03083.
[38] L.N. Nguyen, M.T. Vu, H.P. Vu, M.A.H. Johir, L. Labeeuw, P.J. Ralph, et al., Microalgae-based carbon capture and utilization: a critical review on current system developments and biomass utilization, Crit. Rev. Environ. Sci. Technol. 53 (2) (2022) 216–238, https://doi.org/10.1080/10643389.2022.2047141.
[39] E. Daneshvar, R.J. Wicker, P.-L. Show, A. Bhatnagar, Biologically-mediated carbon capture and utilization by microalgae towards sustainable CO_2 biofixation and biomass valorization – a review, Chem. Eng. J. 427 (2022) 130884, https://doi.org/10.1016/j.cej.2021.130884.
[40] T. Skytt, S.N. Nielsen, B.-G. Jonsson, Global warming potential and absolute global temperature change potential from carbon dioxide and methane fluxes as indicators of regional sustainability – a case study of Jämtland, Sweden, Ecol. Indic. 110 (2020) 105831, https://doi.org/10.1016/j.ecolind.2019.105831.
[41] S.O. Rogers, J.D. Castello, Defrosting Ancient Microbes: Emerging Genomes in a Warmer World, 1st Edition ed, CRC Press, 2019.
[42] J. Shen, R. Yin, S. Zhang, T.J. Algeo, D.J. Bottjer, J. Yu, et al., Intensified continental chemical weathering and carbon-cycle perturbations linked to volcanism during the Triassic-Jurassic transition, Nat. Commun. 13 (1) (2022) 299, https://doi.org/10.1038/s41467-022-27965-x.
[43] M.R. Diaz, G.P. Eberli, E. Hiatt, Microbial contribution to early marine cementation, Sedimentology 69 (2) (2021) 798–822, https://doi.org/10.1111/sed.12926.
[44] A. Millot, N. Maïzi, From open-loop energy revolutions to closed-loop transition: What drives carbon neutrality, Technol. Forecast. Soc. Change 172 (2021) 121003, https://doi.org/10.1016/j.techfore.2021.121003.
[45] J. Wachsmuth, V. Duscha, J. Eckstein, A. Herbst, P. Plötz, K.M. Duwe, et al., The European Commission's 2050 Vision "A clean planet for all" – Implications for Sector Strategies and Climate Governance German Environment Agency, 2021.
[46] K. Dahal, S. Juhola, J. Niemelä, The role of renewable energy policies for carbon neutrality in Helsinki Metropolitan area, Sustain. Cities Soc. 40 (2018) 222–232, https://doi.org/10.1016/j.scs.2018.04.015.
[47] R.M. Pulselli, S. Broersma, C.L. Martin, G. Keeffe, S. Bastianoni, A. van den Dobbelsteen, Future city visions. The energy transition towards carbon-neutrality: lessons learned from the case of Roeselare, Belgium, Renew. Sust. Energ. Rev. 137 (2021) 110612, https://doi.org/10.1016/j.rser.2020.110612.
[48] Z. Liu, Z. Deng, G. He, H. Wang, X. Zhang, J. Lin, et al., Challenges and opportunities for carbon neutrality in China, Nat. Rev. Earth Environ. 3 (2) (2021) 141–155, https://doi.org/10.1038/s43017-021-00244-x.
[49] Z.W. Su, M. Umar, D. Kirikkaleli, T.S. Adebayo, Role of political risk to achieve carbon neutrality: evidence from Brazil, J. Environ. Manag. 298 (2021) 113463, https://doi.org/10.1016/j.jenvman.2021.113463.
[50] K.R. Gurney, J. Liang, G. Roest, Y. Song, K. Mueller, T. Lauvaux, Under-reporting of greenhouse gas emissions in U.S. cities, Nat. Commun. 12 (1) (2021) 553, https://doi.org/10.1038/s41467-020-20871-0.
[51] J. Gasparotto, K. Da Boit Martinello, Coal as an energy source and its impacts on human health, Energy Geosci. 2 (2) (2021) 113–120, https://doi.org/10.1016/j.engeos.2020.07.003.
[52] C. Zou, B. Xiong, H. Xue, D. Zheng, Z. Ge, Y. Wang, et al., The role of new energy in carbon neutral, Petrol. Explor. Dev. 48 (2) (2021) 480–491, https://doi.org/10.1016/s1876-3804(21)60039-3.
[53] Hydrogen Insights 2021, 2021. ⟨https://hydrogencouncil.com/en/hydrogen-insights-2021/⟩. (Accessed 15 January 2023).
[54] Z.Y. Dong, J. Yang, L. Yu, R. Daiyan, R. Amal, A green hydrogen credit framework for international green hydrogen trading towards a carbon neutral future, Int. J. Hydrog. Energy 47 (2) (2022) 728–734, https://doi.org/10.1016/j.ijhydene.2021.10.084.
[55] S.K. Kar, S. Harichandan, B. Roy, Bibliometric analysis of the research on hydrogen economy: an analysis of current findings and roadmap ahead, Int. J. Hydrog. Energy 47 (20) (2022) 10803–10824, https://doi.org/10.1016/j.ijhydene.2022.01.137.

[56] A. Grahame, K.-F. Aguey-Zinsou, Properties and applications of metal (M) dodecahydro-closo-dodecaborates ($M_{n=1,2}B_{12}H_{12}$) and their implications for reversible hydrogen storage in the borohydrides, Inorganics 6 (4) (2018) 106, https://doi.org/10.3390/inorganics6040106.

[57] M.M. Mohideen, B. Subramanian, J. Sun, J. Ge, H. Guo, A.V. Radhamani, et al., Techno-economic analysis of different shades of renewable and non-renewable energy-based hydrogen for fuel cell electric vehicles, Renew. Sust. Energ. Rev. 174 (2023) 113153, https://doi.org/10.1016/j.rser.2023.113153.

[58] D. Zivar, S. Kumar, J. Foroozesh, Underground hydrogen storage: a comprehensive review, Int. J. Hydrog. Energy 46 (45) (2021) 23436–23462, https://doi.org/10.1016/j.ijhydene.2020.08.138.

[59] F. Wang, J.D. Harindintwali, Z. Yuan, M. Wang, F. Wang, S. Li, et al., Technologies and perspectives for achieving carbon neutrality, Innovation 2 (4) (2021) 100180, https://doi.org/10.1016/j.xinn.2021.100180.

[60] J. Eppinger, K.W. Huang, Formic acid as a hydrogen energy carrier, ACS Energy Lett. 2 (1) (2016) 188–195, https://doi.org/10.1021/acsenergylett.6b00574.

[61] P. Preuster, C. Papp, P. Wasserscheid, Liquid organic hydrogen carriers (LOHCs): toward a hydrogen-free hydrogen economy, Acc. Chem. Res 50 (1) (2017) 74–85, https://doi.org/10.1021/acs.accounts.6b00474.

[62] M. Navlani-García, K. Mori, D. Salinas-Torres, Y. Kuwahara, H. Yamashita, New approaches toward the hydrogen production from formic acid dehydrogenation over Pd-based heterogeneous catalysts, Front. Mater. 6 (2019), https://doi.org/10.3389/fmats.2019.00044.

[63] Report of the Newfoundland and Labrador Oil and Gas Industry Recovery Task Force, 2022. ⟨https://www.gov.nl.ca⟩. (Accessed 8 August 2023).

[64] B. Ghorbani, S. Zendehboudi, M.H. Monajati Saharkhiz, Z.A. Afrouzi, O. Mohammadzadeh, A. Elkamel, Multi-objective optimization of a novel hybrid structure for co-generation of ammonium bicarbonate, formic acid, and methanol with net-zero carbon emissions, Energy Fuels 37 (16) (2023) 12474–12502, https://doi.org/10.1021/acs.energyfuels.3c01756.

[65] B. Lee, D. Lim, H. Lee, H. Lim, Which water electrolysis technology is appropriate?: Critical insights of potential water electrolysis for green ammonia production, Renew. Sust. Energ. Rev. 143 (2021) 110963, https://doi.org/10.1016/j.rser.2021.110963.

[66] F. Harber, Rl Rossignol, Production of Ammonia, in: U.S.P. Office (Ed.) B.A.S.F. SE, US, 1909.

[67] S. Ghavam, M. Vahdati, I.A.G. Wilson, P. Styring, Sustainable ammonia production processes, Front. Energy Res. 9 (2021), https://doi.org/10.3389/fenrg.2021.580808.

[68] Ammonia Market Size, Share and COVID-19 Impact Analysis, 2021. ⟨https://www.fortunebusinessinsights.com/industry-reports/ammonia-market-101716⟩. (Accessed 16 February 2023).

[69] Global Ammonia Market (2022 - 2027) - Mordor Intelligence, 2022. ⟨https://www.mordorintelligence.com/industry-reports/ammonia-market⟩. (Accessed 22 October 2022).

[70] A.G. Olabi, K. Obaideen, K. Elsaid, T. Wilberforce, E.T. Sayed, H.M. Maghrabie, et al., Assessment of the pre-combustion carbon capture contribution into sustainable development goals SDGs using novel indicators, 153 (2022) 111710, https://doi.org/10.1016/j.rser.2021.111710.

[71] M.Z. Shahid, J.-K. Kim, Design and economic evaluation of a novel amine-based CO_2 capture process for SMR-based hydrogen production plants, J. Clean. Prod. 402 (2023) 136704, https://doi.org/10.1016/j.jclepro.2023.136704.

[72] S. Cloete, M.N. Khan, S.M. Nazir, S. Amini, Cost-effective clean ammonia production using membrane-assisted autothermal reforming, Chem. Eng. J. 404 (2021) 126550, https://doi.org/10.1016/j.cej.2020.126550.

[73] S. Cloete, M.N. Khan, S. Amini, Economic assessment of membrane-assisted autothermal reforming for cost effective hydrogen production with CO_2 capture, Int. J. Hydrog. Energy 44 (7) (2019) 3492–3510, https://doi.org/10.1016/j.ijhydene.2018.12.110.

[74] R.J. Lee Pereira, P.A. Argyris, V. Spallina, A comparative study on clean ammonia production using chemical looping based technology, Appl. Energy 280 (2020) 115874, https://doi.org/10.1016/j.apenergy.2020.115874.

[75] I. Martínez, D. Armaroli, M. Gazzani, M.C. Romano, Integration of the Ca–Cu process in ammonia production plants, Ind. Eng. Chem. Res. 56 (9) (2017) 2526–2539, https://doi.org/10.1021/acs.iecr.6b04615.

[76] T. Mattisson, M. Keller, C. Linderholm, P. Moldenhauer, M. Rydén, H. Leion, et al., Chemical-looping technologies using circulating fluidized bed systems: status of development, Fuel Process. Technol. 172 (2018) 1–12, https://doi.org/10.1016/j.fuproc.2017.11.016.

[77] A. Ugwu, C. Arnaiz del Pozo, A. Zaabout, S.M. Nazir, N.U. Kalendar, S. Cloete, et al., Gas switching technology: economic attractiveness for chemical looping applications and scale up experience to 50 kWth, Int. J. Greenh. Gas. Control. 114 (2022) 103593, https://doi.org/10.1016/j.ijggc.2022.103593.

[78] V. Spallina, B. Marinello, F. Gallucci, M.C. Romano, M. Van Sint Annaland, Chemical looping reforming in packed-bed reactors: modelling, experimental validation and large-scale reactor design, Fuel Process. Technol. 156 (2017) 156–170, https://doi.org/10.1016/j.fuproc.2016.10.014.

[79] S.A. Wassie, F. Gallucci, A. Zaabout, S. Cloete, S. Amini, M. van Sint Annaland, Hydrogen production with integrated CO_2 capture in a novel gas switching reforming reactor: proof-of-concept, Int. J. Hydrog. Energy 42 (21) (2017) 14367–14379, https://doi.org/10.1016/j.ijhydene.2017.04.227.

[80] I. Adánez-Rubio, F. García-Labiano, A. Abad, L.F. de Diego, J. Adánez, Synthesis gas and H2 production by chemical looping reforming using bio-oil from fast pyrolysis of wood as raw material, Chem. Eng. J. 431 (2022), https://doi.org/10.1016/j.cej.2021.133376.

[81] N. Nemati, Y. Tsuji, T. Mattisson, M. Rydén, Chemical looping combustion in a packed fluidized bed reactor - fundamental modeling and batch experiments with random metal packings, Energy Fuels 36 (17) (2022) 9538–9550, https://doi.org/10.1021/acs.energyfuels.2c00527.

[82] B. Young, M. Krynock, D. Carlson, T.R. Hawkins, J. Marriott, B. Morelli, et al., Comparative environmental life cycle assessment of carbon capture for petroleum refining, ammonia production, and thermoelectric power generation in the United States, Int. J. Greenh. Gas. Control. 91 (2019), https://doi.org/10.1016/j.ijggc.2019.102821.

[83] J. Atchison, Decarbonising fertiliser production in Iowa via CCS. (Accessed 20 March 2023).

[84] ADNOC to Build World-Scale Blue Ammonia Project, 2022. ⟨https://www.adnoc.ae/news-and-media/press-releases/2021/adnoc-to-build-world-scale-blue-ammonia-project#:~:text=Blue%20ammonia%20is%20made%20from,hydrogen%20production%20captured%20and%20stored⟩. (Accessed 5 November 2022).

[85] Qatar Energy to build world's largest blue ammonia facility, 2022. ⟨https://www.offshore-energy.biz/qatarenergy-to-build-worlds-largest-blue-ammonia-facility/⟩. (Accessed 5 November 2022).

[86] Supporting the energy transition: Blue hydrogen and blue ammonia, 2022. ⟨https://www.aramco.com/en/sustainability/climate-change/supporting-the-energy-transition/blue-hydrogen-and-blue-ammonia⟩. (Accessed 10 November 2022).

[87] The first Russian-German low-carbon ammonia supply chain, 2022. ⟨https://www.ammoniaenergy.org/articles/the-first-russian-german-low-carbon-ammonia-supply-chain/⟩. (Accessed 12 November 2022).

[88] Top Countries in Ammonia Production, 2022. ⟨https://www.nationmaster.com/nmx/ranking/ammonia-production⟩. (Accessed 15 November 2022).

[89] R. Wainwright, India's ammonia capacity is expected to witness double digit growth over the next six years, says Global Data, 2019. ⟨https://www.worldfertilizer.com/project-news/29012019/indias-ammonia-capacity-is-expected-to-witness-double-digit-growth-over-the-next-six-years-says-globaldata/⟩. (Accessed 22 October 2022).

[90] R. Brelsford, Russian operator starts up country's largest ammonia plant, 2019. ⟨https://www.ogj.com/refining-processing/petrochemicals/article/14038968/russian-operator-starts-up-countrys-largest-ammonia-plant⟩. (Accessed 15 March 2023).

[91] L. Fernández, Ammonia plant production capacity in the United States in 2021, by facility, 2022. ⟨https://www.statista.com/statistics/1266392/ammonia-plant-capacities-united-states/⟩. (Accessed 15 March 2023).

[92] Trinidad's Ammonia Industry, 2021. ⟨https://www.energy.gov.tt/our-business/lng-petrochemicals/petrochemicals/ammonia/#:~:text=Grace%20and%20acquired%20by%20Norsk,plants%20and%20one%20urea%20plant⟩. (Accessed 15 February 2023).

[93] Ammonia plant in Indonesia tops own world mark, 2022. ⟨https://www.ogj.com/home/article/17211207/ammonia-plant-in-indonesia-tops-own-world-mark⟩. (Accessed 22 October 2022).

[94] UNIAN: Ukraine's largest chemical plant in Odesa resumes ammonia, carbamide production, 2022. ⟨https://www.kyivpost.com/ukraine-politics/unian-ukraines-largest-chemical-plant-odesa-resumes-ammonia-carbamide-production.html⟩. (Accessed 30 October 2022).

[95] The largest commercial application of KBR KAAP™ technology, 2022. ⟨https://www.kbr.com/en/experience/ebic-ammonia-plant⟩. (Accessed 30 October 2022).

[96] Less ammonia - less fertiliser - less food: BASF considers production cuts, 2022. ⟨https://tvpworld.com/61511186/less-ammonia-less-fertiliser-less-food-basf-considers-production-cuts⟩. (Accessed 5 November 2022).

[97] J. Ikäheimo, J. Kiviluoma, R. Weiss, H. Holttinen, Power-to-ammonia in future North European 100% renewable power and heat system, Int. J. Hydrog. Energy 43 (36) (2018) 17295–17308, https://doi.org/10.1016/j.ijhydene.2018.06.121.

[98] R. Nayak-Luke, R. Bañares-Alcántara, I. Wilkinson, Green" ammonia: impact of renewable energy intermittency on plant sizing and levelized cost of ammonia, Ind. Eng. Chem. Res. 57 (43) (2018) 14607–14616, https://doi.org/10.1021/acs.iecr.8b02447.

[99] J.R. Gomez, J. Baca, F. Garzon, Techno-economic analysis and life cycle assessment for electrochemical ammonia production using proton conducting membrane, Int. J. Hydrog. Energy 45 (1) (2019) 721–737, https://doi.org/10.1016/j.ijhydene.2019.10.174.

[100] J. Armijo, C. Philibert, Flexible production of green hydrogen and ammonia from variable solar and wind energy: case study of Chile and Argentina, Int. J. Hydrog. Energy 45 (3) (2020) 1541–1558, https://doi.org/10.1016/j.ijhydene.2019.11.028.

[101] Y. Bicer, F. Khalid, A.M.O. Mohamed, M. Al-Breiki, M.M. Ali, Electrochemical modelling of ammonia synthesis in molten salt medium for renewable fuel production using wind power, Int. J. Hydrog. Energy 45 (60) (2020) 34938–34948, https://doi.org/10.1016/j.ijhydene.2020.03.085.

[102] H. Zhang, L. Wang, J. Van herle, F. Maréchal, U. Desideri, Techno-economic comparison of green ammonia production processes, Appl. Energy 259 (2020), https://doi.org/10.1016/j.apenergy.2019.114135.

[103] H. Ishaq, I. Dincer, Dynamic analysis of a new solar-wind energy- based cascaded system for hydrogen to ammonia, Int. J. Hydrog. Energy 45 (38) (2020) 18895–18911, https://doi.org/10.1016/j.ijhydene.2020.04.149.

[104] H. Ishaq, I. Dincer, Dynamic modelling of a solar hydrogen system for power and ammonia production, Int. J. Hydrog. Energy 46 (27) (2021) 13985–14004, https://doi.org/10.1016/j.ijhydene.2021.01.201.

[105] S.A. Nosherwani, R.C. Neto, Techno-economic assessment of commercial ammonia synthesis methods in coastal areas of Germany, J. Energy Storage 34 (2021) 102201, https://doi.org/10.1016/j.est.2020.102201.

[106] M. Ozturk, I. Dincer, An integrated system for ammonia production from renewable hydrogen: a case study, Int. J. Hydrog. Energy 46 (8) (2021) 5918–5925, https://doi.org/10.1016/j.ijhydene.2019.12.127.

[107] N. Tukenmez, M. Koc, M. Ozturk, A novel combined biomass and solar energy conversion-based multigeneration system with hydrogen and ammonia generation, Int. J. Hydrog. Energy 46 (30) (2021) 16319–16343, https://doi.org/10.1016/j.ijhydene.2021.02.215.

[108] J.S. Cardoso, V. Silva, J.A.M. Chavando, D. Eusébio, M.J. Hall, M. Costa, Small-Scale Biomass Gasification for Green Ammonia Production in Portugal: A Techno-Economic Study, Energy Fuels 35 (17) (2021) 13847–13862, https://doi.org/10.1021/acs.energyfuels.1c01928.

[109] N.D. Pawar, H.U. Heinrichs, C. Winkler, P.-M. Heuser, S.D. Ryberg, M. Robinius, et al., Potential of green ammonia production in India, Int. J. Hydrog. Energy 46 (54) (2021) 27247–27267, https://doi.org/10.1016/j.ijhydene.2021.05.203.

[110] Enova funding for three ammonia players: Yara, Horisont & Viridis, 2022. ⟨https://www.ammoniaenergy.org/articles/enova-funding-for-three-ammonia-players-yara-horisont-viridis/⟩. (Accessed 12 November 2022).

[111] REDDAP: The world's first dynamic green ammonia plant, 2022. ⟨https://stateofgreen.com/en/solutions/reddap-the-worlds-first-dynamic-green-ammonia-plant/⟩. (Accessed 15 January 223).

[112] J.A. Faria, Renaissance of ammonia synthesis for sustainable production of energy and fertilizers, Curr. Opin. Green. Sustain. Chem. 29 (2021) 100466, https://doi.org/10.1016/j.cogsc.2021.100466.

[113] S. Chatterjee, I. Dutta, K.-W. Huang, 8 - Power to formic acid, in: G. Spazzafumo (Ed.), Power to Fuel, Academic Press, 2021, pp. 169–210.

[114] S. Chavez, B. Werghi, K.M. Sanroman Gutierrez, R. Chen, S. Lall, M. Cargnello, Studying, promoting, exploiting, and predicting catalyst dynamics: the next frontier in heterogeneous catalysis, J. Phys. Chem. C. 127 (5) (2023) 2127–2146, https://doi.org/10.1021/acs.jpcc.2c06519.

[115] J.C. Scaiano, A beginners guide to understanding the mechanisms of photochemical reactions: things you should know if light is one of your reagents, Chem. Soc. Rev. 52 (18) (2023) 6330–6343, https://doi.org/10.1039/D3CS00453H.

[116] S.D.A. Zondag, D. Mazzarella, T. Noël, Scale-up of photochemical reactions: transitioning from lab scale to industrial production, Annu. Rev. Chem. Biomol. Eng. 14 (1) (2023) 283–300, https://doi.org/10.1146/annurev-chembioeng-101121-074313.

[117] F. Proietto, R. Rinicella, A. Galia, O. Scialdone, Electrochemical conversion of CO_2 to formic acid using a Sn based cathode: combined effect of temperature and pressure, J. CO_2 Util. 67 (2023), https://doi.org/10.1016/j.jcou.2022.102338.

[118] K. Fernández-Caso, G. Díaz-Sainz, M. Alvarez-Guerra, A. Irabien, Electroreduction of CO_2: advances in the continuous production of formic acid and formate, ACS Energy Lett. 8 (4) (2023) 1992–2024, https://doi.org/10.1021/acsenergylett.3c00489.

[119] P.R. Yaashikaa, P. Senthil Kumar, S.J. Varjani, A. Saravanan, A review on photochemical, biochemical and electrochemical transformation of CO_2 into value-added products, J. CO_2 Util. 33 (2019) 131–147, https://doi.org/10.1016/j.jcou.2019.05.017.

[120] T.P. Nguyen, D.L.T. Nguyen, V.-H. Nguyen, T.-H. Le, D.-V.N. Vo, Q.T. Trinh, et al., Recent advances in TiO_2-based photocatalysts for reduction of CO_2 to fuels, Nanomaterials 10 (2) (2020) 337, https://doi.org/10.3390/nano10020337.

[121] S. Yu, N. Yang, S. Liu, X. Jiang, Electrochemical and photochemical CO_2 reduction using diamond, Carbon 175 (2021) 440–453, https://doi.org/10.1016/j.carbon.2021.01.116.

[122] L. Zhang, J. Zhang, Metal-organic frameworks for CO_2 photoreduction, Front. Energy 13 (2) (2019) 221–250, https://doi.org/10.1007/s11708-019-0629-8.

[123] Y. Kamakura, S. Yasuda, N. Hosokawa, S. Nishioka, S. Hongo, T. Yokoi, et al., Selective CO_2-to-formate conversion driven by visible light over a precious-metal-free nonporous coordination polymer, ACS Catal. 12 (16) (2022) 10172–10178, https://doi.org/10.1021/acscatal.2c02177.

[124] Y. Benseghir, A. Solé-Daura, D.R. Cairnie, A.L. Robinson, M. Duguet, P. Mialane, et al., Unveiling the mechanism of the photocatalytic reduction of CO_2 to formate promoted by porphyrinic Zr-based metal–organic frameworks, J. Mater. Chem. A 10 (35) (2022) 18103–18115, https://doi.org/10.1039/D2TA04164B.

[125] L. Liu, J. Zhang, X. Cheng, M. Xu, X. Kang, Q. Wan, et al., Amorphous NH_2-MIL-68 as an efficient electro- and photo-catalyst for CO_2 conversion reactions, Nano Res (2022) 181–188, https://doi.org/10.1007/s12274-022-4664-0.

[126] S.K. Lee, M. Kondo, M. Okamura, T. Enomoto, G. Nakamura, S. Masaoka, Function-integrated Ru catalyst for photochemical CO_2 reduction, J. Am. Chem. Soc. 140 (49) (2018) 16899–16903, https://doi.org/10.1021/jacs.8b09933.

[127] T. Fogeron, P. Retailleau, L.M. Chamoreau, Y. Li, M. Fontecave, Pyranopterin related dithiolene molybdenum complexes as homogeneous catalysts for CO_2 photoreduction, Angew. Chem. 57 (52) (2018) 17033–17037, https://doi.org/10.1002/anie.201809084.

[128] S. Sato, T. Morikawa, [Ir(tpy)(bpy)Cl] as a photocatalyst for CO_2 reduction under visible-light irradiation, ChemPhotoChem 2 (3) (2018) 207–212, https://doi.org/10.1002/cptc.201700133.

[129] K. Maeda, D. An, R. Kuriki, D. Lu, O. Ishitani, Graphitic carbon nitride prepared from urea as a photocatalyst for visible-light carbon dioxide reduction with the aid of a mononuclear ruthenium(II) complex, Beilstein J. Org. Chem. 14 (2018) 1806–1812, https://doi.org/10.3762/bjoc.14.153.

[130] T. Oshima, T. Ichibha, K.S. Qin, K. Muraoka, J.J.M. Vequizo, K. Hibino, et al., Undoped layered perovskite oxynitride $Li_2LaTa_2O_6N$ for photocatalytic CO_2 reduction with visible light, Angew. Chem. Int. Ed. 57 (27) (2018) 8154–8158, https://doi.org/10.1002/anie.201803931.

[131] Y. Hameed, G.K. Rao, J.S. Ovens, B. Gabidullin, D. Richeson, Visible-light photocatalytic reduction of CO_2 to formic acid with a Ru catalyst supported by N, N′-Bis(diphenylphosphino)-2,6-diaminopyridine ligands, ChemSusChem 12 (15) (2019) 3453–3457, https://doi.org/10.1002/cssc.201901326.

[132] K. Muraoka, T. Uchiyama, D. Lu, Y. Uchimoto, O. Ishitani, K. Maeda, A Visible-Light-Driven Z-Scheme CO_2 Reduction System Using Ta_3N_5 and a Ru(II) Binuclear Complex, Bull. Chem. Soc. Jpn. 92 (1) (2019) 124–126, https://doi.org/10.1246/bcsj.20180239.

[133] Z. Guo, G. Chen, C. Cometto, B. Ma, H. Zhao, T. Groizard, et al., Selectivity control of CO versus HCOO− production in the visible-light-driven catalytic reduction of CO_2 with two cooperative metal sites, Nat. Catal. 2 (9) (2019) 801–808, https://doi.org/10.1038/s41929-019-0331-6.

[134] Y. Hameed, P. Berro, B. Gabidullin, D. Richeson, An integrated Re(i) photocatalyst/sensitizer that activates the formation of formic acid from reduction of CO_2, Chem. Commun. 55 (74) (2019) 11041–11044, https://doi.org/10.1039/C9CC03943K.

[135] Y. Arikawa, I. Tabata, Y. Miura, H. Tajiri, Y. Seto, S. Horiuchi, et al., Photocatalytic CO_2 reduction under visible-light irradiation by ruthenium CNC pincer complexes, Chem. Eur. J. 26 (25) (2020) 5603–5606, https://doi.org/10.1002/chem.201905840.

[136] K. Kamada, J. Jung, T. Wakabayashi, K. Sekizawa, S. Sato, T. Morikawa, et al., Photocatalytic CO_2 reduction using a robust multifunctional iridium complex toward the selective formation of formic acid, J. Am. Chem. Soc. 142 (23) (2020) 10261–10266, https://doi.org/10.1021/jacs.0c03097.

[137] S.E. Lee, A. Nasirian, Y.E. Kim, P.T. Fard, Y. Kim, B. Jeong, et al., Visible-light photocatalytic conversion of carbon dioxide by Ni(II) complexes with N4S2 coordination: highly efficient and selective production of formate, J. Am. Chem. Soc. 142 (45) (2020) 19142–19149, https://doi.org/10.1021/jacs.0c08145.

[138] D. Lee, S. Choi, M.S. Choe, S.-Y. Kim, K. Park, C.H. Kim, et al., Photochemical CO_2-to-formate/CO conversion catalyzed by half-metallocene Ir(III) catalyst and its mechanistic investigation, Organometallics 40 (15) (2021) 2430–2442, https://doi.org/10.1021/acs.organomet.1c00180.

[139] C. Back, Y. Seo, S. Choi, M.S. Choe, D. Lee, J.-O. Baeg, et al., Secondary coordination effect on monobipyridyl Ru(II) catalysts in photochemical CO_2 reduction: effective proton shuttle of pendant brønsted acid/base sites (OH and N$(CH_3)_2$) and its mechanistic investigation, Inorg. Chem. 60 (18) (2021) 14151–14164, https://doi.org/10.1021/acs.inorgchem.1c01559.

[140] A. Nakada, H. Kumagai, M. Robert, O. Ishitani, K. Maeda, Molecule/semiconductor hybrid materials for visible-light CO_2 reduction: design principles and interfacial engineering, Acc. Mater. Res. 2 (6) (2021) 458–470, https://doi.org/10.1021/accountsmr.1c00060.

[141] T. Akai, M. Kondo, Y. Saga, S. Masaoka, Photochemical hydrogen production based on the HCOOH/CO_2 cycle promoted by a pentanuclear cobalt complex, ChemComm 58 (23) (2022) 3755–3758, https://doi.org/10.1039/D1CC06445B.

[142] Y. Gao, W. Li, X. Sun, Y. Zhao, H. Ji, H. Luo, et al., Boosting the performance of formate dehydrogenase by silver nanoclusters for photoreduction of CO_2 to formate, ACS Sustain. Chem. Eng. 10 (45) (2022) 14888–14896, https://doi.org/10.1021/acssuschemeng.2c04801.

[143] V.M. Badiani, C. Casadevall, M. Miller, S.J. Cobb, R.R. Manuel, I.A.C. Pereira, et al., Engineering electro- and photocatalytic carbon materials for CO_2 reduction by formate dehydrogenase, J. Am. Chem. Soc. 144 (31) (2022) 14207–14216, https://doi.org/10.1021/jacs.2c04529.

[144] P. Singh, R.K. Yadav, C. Singh, S. Chaubey, S. Singh, A.P. Singh, et al., Photocatalytic activity of ultrathin 2DPNs for enzymatically generating formic acid from CO_2 and C–S/C–N bond formation, Sustain. Energy Fuels 6 (9) (2022) 2223–2232, https://doi.org/10.1039/D1SE01103K.

[145] R.N. Sampaio, D.C. Grills, D.E. Polyansky, D.J. Szalda, E. Fujita, Unexpected roles of triethanolamine in the photochemical reduction of CO_2 to formate by ruthenium complexes, J. Am. Chem. Soc. 142 (5) (2020) 2413–2428, https://doi.org/10.1021/jacs.9b11897.

[146] F. Schneck, J. Ahrens, M. Finger, A.C. Stuckl, C. Wurtele, D. Schwarzer, et al., The elusive abnormal CO_2 insertion enabled by metal-ligand cooperative photochemical selectivity inversion, Nat. Commun. 9 (1) (2018) 1161, https://doi.org/10.1038/s41467-018-03239-3.

[147] E. Fujita, D.C. Grills, G.F. Manbeck, D.E. Polyansky, Understanding the role of inter- and intramolecular promoters in electro- and photochemical CO_2 reduction using Mn, Re, and Ru catalysts, Acc. Chem. Res. 55 (5) (2022) 616–628, https://doi.org/10.1021/acs.accounts.1c00616.

[148] Y. Wang, X. Shang, J. Shen, Z. Zhang, D. Wang, J. Lin, et al., Direct and indirect Z-scheme heterostructure-coupled photosystem enabling cooperation of CO_2 reduction and H_2O oxidation, Nat. Commun. 11 (1) (2020) 3043, https://doi.org/10.1038/s41467-020-16742-3.

[149] A. Kumar, V. Hasija, A. Sudhaik, P. Raizada, Q. Van Le, P. Singh, et al., Artificial leaf for light-driven CO_2 reduction: basic concepts, advanced structures and selective solar-to-chemical products, Chem. Eng. J. 430 (2022) 133031, https://doi.org/10.1016/j.cej.2021.133031.

[150] M. Ding, Z. Chen, C. Liu, Y. Wang, C. Li, X. Li, et al., Electrochemical CO_2 reduction: progress and opportunity with alloying copper, Mater. Rep. Energy (2023) 100175, https://doi.org/10.1016/j.matre.2023.100175.

[151] S. Zhao, S. Li, T. Guo, S. Zhang, J. Wang, Y. Wu, et al., Advances in Sn-based catalysts for electrochemical CO_2 reduction, Nano. Micro Lett. 11 (1) (2019) 62, https://doi.org/10.1007/s40820-019-0293-x.

[152] X. Wang, Y. Zou, Y. Zhang, B. Marchetti, Y. Liu, J. Yi, et al., Tin-based metal organic framework catalysts for high-efficiency electrocatalytic CO_2 conversion

into formate, J. Colloid Interface Sci. 626 (2022) 836–847, https://doi.org/10.1016/j.jcis.2022.07.008.
[153] D. Xia, H. Yu, H. Xie, P. Huang, R. Menzel, M.M. Titirici, et al., Recent progress of Bi-based electrocatalysts for electrocatalytic CO_2 reduction, Nanoscale 14 (22) (2022) 7957–7973, https://doi.org/10.1039/d2nr01900k.
[154] H. Yang, J.J. Kaczur, S.D. Sajjad, R.I. Masel, Electrochemical conversion of CO_2 to formic acid utilizing Sustainion™ membranes, J. CO_2 Util. 20 (2017) 208–217, https://doi.org/10.1016/j.jcou.2017.04.011.
[155] C. Xia, P. Zhu, Q. Jiang, Y. Pan, W. Liang, E. Stavitski, et al., Continuous production of pure liquid fuel solutions via electrocatalytic CO_2 reduction using solid-electrolyte devices, Nat. Energy 4 (9) (2019) 776–785, https://doi.org/10.1038/s41560-019-0451-x.
[156] N. Han, Y. Wang, H. Yang, J. Deng, J. Wu, Y. Li, et al., Ultrathin bismuth nanosheets from in situ topotactic transformation for selective electrocatalytic CO_2 reduction to formate, Nat. Commun. 9 (1) (2018) 1320, https://doi.org/10.1038/s41467-018-03712-z.
[157] W. Choi, M. Kim, B.-j Kim, Y. Park, D.S. Han, M.R. Hoffmann, et al., Electrocatalytic arsenite oxidation in bicarbonate solutions combined with CO_2 reduction to formate, Appl. Catal. B 265 (2020) 118607, https://doi.org/10.1016/j.apcatb.2020.118607.
[158] J. Li, Y. Kuang, Y. Meng, X. Tian, W.H. Hung, X. Zhang, et al., Electroreduction of CO_2 to formate on a copper-based electrocatalyst at high pressures with high energy conversion efficiency, J. Am. Chem. Soc. 142 (16) (2020) 7276–7282, https://doi.org/10.1021/jacs.0c00122.
[159] Y. Chen, A. Vise, W.E. Klein, F.C. Cetinbas, D.J. Myers, W.A. Smith, et al., A robust, scalable platform for the electrochemical conversion of CO_2 to formate: identifying pathways to higher energy efficiencies, ACS Energy Lett. 5 (6) (2020) 1825–1833, https://doi.org/10.1021/acsenergylett.0c00860.
[160] Q. Lai, W. Yuan, W. Huang, G. Yuan, Sn/SnO_x electrode catalyst with mesoporous structure for efficient electroreduction of CO_2 to formate, Appl. Surf. Sci. 508 (2020) 145221, https://doi.org/10.1016/j.apsusc.2019.145221.
[161] M. Fan, S. Prabhudev, S. Garbarino, J. Qiao, G.A. Botton, D.A. Harrington, et al., Uncovering the nature of electroactive sites in nano architectured dendritic Bi for highly efficient CO_2 electroreduction to formate, Appl. Catal. B 274 (2020) 119031, https://doi.org/10.1016/j.apcatb.2020.119031.
[162] Y. Liang, W. Zhou, Y. Shi, C. Liu, B. Zhang, Unveiling in situ evolved In/In_2O_3–heterostructure as the active phase of In_2O_3 toward efficient electroreduction of CO_2 to formate, Sci. Bull. 65 (18) (2020) 1547–1554, https://doi.org/10.1016/j.scib.2020.04.022.
[163] D. Zhang, Z. Tao, F. Feng, B. He, W. Zhou, J. Sun, et al., High efficiency and selectivity from synergy: Bi nanoparticles embedded in nitrogen doped porous carbon for electrochemical reduction of CO_2 to formate, Electrochim. Acta 334 (2020), https://doi.org/10.1016/j.electacta.2019.135563.
[164] L. Fan, C. Xia, P. Zhu, Y. Lu, H. Wang, Electrochemical CO_2 reduction to high-concentration pure formic acid solutions in an all-solid-state reactor, Nat. Commun. 11 (1) (2020) 3633, https://doi.org/10.1038/s41467-020-17403-1.
[165] G. Piao, S.H. Yoon, D.S. Han, H. Park, Ion-enhanced conversion of CO_2 into formate on porous dendritic bismuth electrodes with high efficiency and durability, ChemSusChem 13 (4) (2020) 698–706, https://doi.org/10.1002/cssc.201902581.
[166] H. Yang, J.J. Kaczur, S.D. Sajjad, R.I. Masel, Performance and long-term stability of CO_2 conversion to formic acid using a three-compartment electrolyzer design, J. CO_2 Util. 42 (2020) 101349.
[167] T. Zheng, C. Liu, C. Guo, M. Zhang, X. Li, Q. Jiang, et al., Copper-catalysed exclusive CO_2 to pure formic acid conversion via single-atom alloying, Nat. Nanotechnol. 16 (12) (2021) 1386–1393, https://doi.org/10.1038/s41565-021-00974-5.
[168] M. Zhang, W. Wei, S. Zhou, D.-D. Ma, A. Cao, X.-T. Wu, et al., Engineering a conductive network of atomically thin bismuthene with rich defects enables CO_2 reduction to formate with industry-compatible current densities and stability, Energy Environ. Sci. 14 (9) (2021) 4998–5008, https://doi.org/10.1039/D1EE01495A.
[169] M. Park, W. Shin, Long-term stable and selective conversion of carbon dioxide to formate using dental amalgam electrode, J. CO_2 Util. 45 (2021) 101435, https://doi.org/10.1016/j.jcou.2021.101435.
[170] X.-H. Zhao, Q.-S. Chen, D.-H. Zhuo, J. Lu, Z.-N. Xu, C.-M. Wang, et al., Oxygen vacancies enriched Bi based catalysts for enhancing electrocatalytic CO_2 reduction to formate, Electrochim. Acta 367 (2021) 137478, https://doi.org/10.1016/j.electacta.2020.137478.
[171] L. Li, A. Ozden, S. Guo, Ad.A.F.P. Garci, C. Wang, M. Zhang, et al., Stable, active CO_2 reduction to formate via redox-modulated stabilization of active sites, Nat. Commun. 12 (1) (2021) 5223, https://doi.org/10.1038/s41467-021-25573-9.
[172] J. Zhang, T. Fan, P. Huang, X. Lian, Y. Guo, Z. Chen, et al., Electro-reconstruction-induced strain regulation and synergism of Ag-In-S toward highly efficient CO_2 electrolysis to formate, Adv. Funct. Mater. 32 (25) (2022) 2113075, https://doi.org/10.1002/adfm.202113075.
[173] J. Xu, S. Yang, L. Ji, J. Mao, W. Zhang, X. Zheng, et al., High current CO_2 reduction realized by edge/defect-rich bismuth nanosheets, Nano Res. 16 (1) (2022) 53–61, https://doi.org/10.1007/s12274-022-4770-z.
[174] D. Wang, T. Sun, L. Xu, L. Gong, B. Chen, P. Zhang, et al., Interfacial engineering of SnO_2/$Bi_2O_2CO_3$ heterojunction on heteroatoms-doped carbon for high-performance CO_2 electroreduction to formate, Nano Res. 16 (2) (2022) 2278–2285, https://doi.org/10.1007/s12274-022-5058-z.
[175] Q. Yang, Y. Zhao, L. Meng, Z. Liu, J. Lan, Y. Zhang, et al., Nanoporous intermetallic snte enables efficient electrochemical CO_2 reduction into formate via promoting the fracture of metal-oxygen bonding, Small 18 (17) (2022) e2107968, https://doi.org/10.1002/smll.202107968.
[176] J. Lee, H. Liu, Y. Chen, W. Li, Bismuth nanosheets derived by in situ morphology transformation of bismuth oxides for selective electrochemical CO_2 reduction to formate, ACS Appl. Mater. Interfaces 14 (12) (2022) 14210–14217, https://doi.org/10.1021/acsami.1c25217.
[177] Z. Li, Y. Feng, Y. Li, X. Chen, N. Li, W. He, et al., Fabrication of Bi/Sn bimetallic electrode for high-performance electrochemical reduction of carbon dioxide to formate, Chem. Eng. J. 428 (2022) 130901, https://doi.org/10.1016/j.cej.2021.130901.
[178] T. Shi, D. Liu, N. Liu, Y. Zhang, H. Feng, Q. Li, Triple-phase interface engineered hierarchical porous electrode for CO_2 electroreduction to formate, Adv. Sci. 9 (30) (2022) 2204472, https://doi.org/10.1002/advs.202204472.
[179] B. Ávila-Bolívar, R. Cepitis, M. Alam, J.-M. Assafrei, K. Ping, J. Aruväli, et al., CO_2 reduction to formate on an affordable bismuth metal-organic framework based catalyst, J. CO_2 Util. 59 (2022) 101937, https://doi.org/10.1016/j.jcou.2022.101937.
[180] H. Lv, F. Lv, H. Qin, X. Min, L. Sun, N. Han, et al., Single-crystalline mesoporous palladium and palladium-copper nanocubes for highly efficient electrochemical CO_2 reduction, CCS Chem. 4 (4) (2022) 1376–1385, https://doi.org/10.31635/ccschem.021.202100958.
[181] M. Wu, Y. Xiong, B. Hu, Z. Zhang, B. Wei, L. Li, et al., Indium doped bismuth subcarbonate nanosheets for efficient electrochemical reduction of carbon dioxide to formate in a wide potential window, J. Colloid Interface Sci. 624 (2022) 261–269, https://doi.org/10.1016/j.jcis.2022.05.054.
[182] M.-N. Zhu, B.-W. Zhang, M.-R. Gao, P.-F. Sui, C. Xu, L. Gong, et al., Electrochemically reconstructed perovskite with cooperative catalytic sites for CO_2-to-formate conversion, Appl. Catal. B 306 (2022) 121101, https://doi.org/10.1016/j.apcatb.2022.121101.
[183] S. Liu, Y. Fan, Y. Wang, S. Jin, M. Hou, W. Zeng, et al., Surface-oxygen-rich Bi@C nanoparticles for high-efficiency electroreduction of CO_2 to formate, Nano Lett. (2022) 9107–9114, https://doi.org/10.1021/acs.nanolett.2c03573.
[184] B. Jia, Z. Chen, C. Li, Z. Li, X. Zhou, T. Wang, et al., Indium cyanamide for industrial-grade CO(2) electroreduction to formic acid, J. Am. Chem. Soc. 145 (25) (2023) 14101–14111, https://doi.org/10.1021/jacs.3c04288.
[185] G. Díaz-Sainz, K. Fernández-Caso, T. Lagarteira, S. Delgado, M. Alvarez-Guerra, A. Mendes, et al., Coupling continuous CO_2 electroreduction to formate with efficient Ni-based anodes, J. Environ. Chem. Eng. 11 (1) (2023) 109171, https://doi.org/10.1016/j.jece.2022.109171.
[186] X. An, S. Li, X. Hao, Z. Xie, X. Du, Z. Wang, et al., Common strategies for improving the performances of tin and bismuth-based catalysts in the electrocatalytic reduction of CO_2 to formic acid/formate, Renew. Sust. Energ. Rev. 143 (2021) 110952, https://doi.org/10.1016/j.rser.2021.110952.
[187] S. Yang, Y. Sun, C. Wang, L. Lv, M. Hu, J. Jin, et al., One-step co-electrodeposition of SnBi for efficient electrochemical reduction of carbon dioxide to formic acid, Catal. Sci. Technol. 13 (3) (2023) 758–766, https://doi.org/10.1039/D2CY00859A.
[188] M. Zhang, X. Xuan, J. Zhang, J. Sun, M. Wang, Y. Wu, et al., Mass transport enhancement effect induced by superstructure catalyst for carbon dioxide reduction to formic acid, Int. J. Hydrog. Energy 48 (91) (2023) 35572–35583, https://doi.org/10.1016/j.ijhydene.2023.05.285.
[189] M. Zheng, X. Zhou, Y. Wang, G. Chen, M. Li, Theoretical study on the reduction mechanism of CO_2 to HCOOH on Pd_3Au: an explicit solvent model is essential, J. Mater. Chem. A 11 (12) (2023) 6591–6602, https://doi.org/10.1039/D2TA08552F.
[190] L. Legrand, Q. Shu, M. Tedesco, J.E. Dykstra, H.V.M. Hamelers, Role of ion exchange membranes and capacitive electrodes in membrane capacitive deionization (MCDI) for CO_2 capture, J. Colloid Interface Sci. 564 (2020) 478–490, https://doi.org/10.1016/j.jcis.2019.12.039.
[191] M. Rahimi, A. Khurram, T.A. Hatton, B. Gallant, Electrochemical carbon capture processes for mitigation of CO_2 emissions, Chem. Soc. Rev. 51 (20) (2022) 8676–8695, https://doi.org/10.1039/d2cs00443g.
[192] M. Sassenburg, M. Kelly, S. Subramanian, W.A. Smith, T. Burdyny, Zero-Gap Electrochemical CO_2 reduction cells: challenges and operational strategies for prevention of salt precipitation, ACS Energy Lett. 8 (1) (2023) 321–331, https://doi.org/10.1021/acsenergylett.2c01885.
[193] G.-T. Jeong, S.-K. Kim, Statistical optimization of levulinic acid and formic acid production from lipid-extracted residue of Chlorella vulgaris, J. Environ. Chem. Eng. 9 (2) (2021) 105142, https://doi.org/10.1016/j.jece.2021.105142.
[194] M.-R. Park, H.S. Kim, S.-K. Kim, G.-T. Jeong, Thermo-chemical conversion for production of levulinic and formic acids from glucosamine, Fuel Process. Technol. 172 (2018) 115–124, https://doi.org/10.1016/j.fuproc.2017.12.016.
[195] G.-T. Jeong, S.-K. Kim, Thermochemical conversion of defatted microalgae Scenedesmus obliquus into levulinic and formic acids, Fuel 283 (2021) 118907, https://doi.org/10.1016/j.fuel.2020.118907.
[196] Y. Yang, H. Zhong, R. He, X. Wang, J. Cheng, G. Yao, et al., Synergetic conversion of microalgae and CO_2 into value-added chemicals under hydrothermal conditions, Green. Chem. 21 (6) (2019) 1247–1252, https://doi.org/10.1039/C8GC03645D.
[197] M. Andérez-Fernández, E. Pérez, S. Ferrero, C.M. Álvarez, J. Gumiel, Á. Martín, et al., Simultaneous formic acid production by hydrothermal CO_2 reduction and biomass derivatives conversion in a continuous reactor, Chem. Eng. J. 453 (2023) 139741, https://doi.org/10.1016/j.cej.2022.139741.
[198] R.E. Siegel, S. Pattanayak, L.A. Berben, Reactive capture of CO_2: opportunities and challenges, ACS Catal. 13 (1) (2022) 766–784, https://doi.org/10.1021/acscatal.2c05019.

[199] P.H. Pandey, H.S. Pawar, Cu dispersed TiO_2 catalyst for direct hydrogenation of carbon dioxide into formic acid, J. CO_2 Util. 41 (2020) 101267, https://doi.org/10.1016/j.jcou.2020.101267.
[200] G. Bharath, K. Rambabu, P.P. Morajkar, R. Jayaraman, J. Theerthagiri, S.J. Lee, et al., Surface functionalized highly porous date seed derived activated carbon and MoS_2 nanocomposites for hydrogenation of CO_2 into formic acid, J. Hazard. Mater. 409 (2021) 124980, https://doi.org/10.1016/j.jhazmat.2020.124980.
[201] M.I. Chinchilla, F.A. Mato, A. Martin, M.D. Bermejo, Hydrothermal CO_2 Reduction by glucose as reducing agent and metals and metal oxides as catalysts, Molecules 27 (5) (2022), https://doi.org/10.3390/molecules27051652.
[202] A. Cherevotan, B. Ray, A. Yadav, D. Bagchi, A.K. Singh, M. Riyaz, et al., Tuning the hybridization and charge polarization in metal nanoparticles dispersed over Schiff base functionalized SBA-15 enhances CO_2 capture and conversion to formic acid, J. Mater. Chem. A 10 (35) (2022) 18354–18362, https://doi.org/10.1039/D2TA03690H.
[203] K. Park, K.R. Lee, S. Ahn, S.-H. Kim, A. Haider, S. Choung, et al., Structural effects of nitrogen-doped titanium oxide supports on stabilization of ruthenium active species in carbon dioxide hydrogenation to formate, Appl. Catal. B: Environ. 335 (2023), https://doi.org/10.1016/j.apcatb.2023.122873.
[204] T. Sengupta, S.N. Khanna, Converting CO_2 to formic acid by tuning quantum states in metal chalcogenide clusters, Commun. Chem. 6 (1) (2023) 53, https://doi.org/10.1038/s42004-023-00851-3.
[205] J.C. Wood, Z. Yuan, B. Virdis, Towards carbon neutral chemicals production: opportunities for combining fermentation with electrochemical processes, Curr. Opin. Electrochem. 37 (2023), https://doi.org/10.1016/j.coelec.2022.101177.
[206] A. Singh, U. Alam, P. Chakraborty, B. Sundararaju, N. Verma, A sustainable approach for the production of formate from CO_2 using microalgae as a clean biomass and improvement using potassium-doped g-C3N4, Chem. Eng. J. 454 (2023) 140303, https://doi.org/10.1016/j.cej.2022.140303.
[207] Y. Pei, W. Gu, S. Cheng, S. Xiao, C. Wang, Y. Yang, et al., Thermo-electrochemically induced dynamic Snδ+/Sn interface for direct bicarbonate reduction to formate, ACS Catal. 13 (18) (2023) 12082–12091, https://doi.org/10.1021/acscatal.3c02630.
[208] F.M. Schwarz, J. Moon, F. Oswald, V. Müller, Biological hydrogen storage and release through multiple cycles of bi-directional hydrogenation of CO_2 to formic acid in a single process unit, Joule 6 (6) (2022) 1304–1319, https://doi.org/10.1016/j.joule.2022.04.020.
[209] E.P. Komarala, A.A. Alkhoori, X. Zhang, H.-M. Cheng, K. Polychronopoulou, Design and synthesis of thermally stable single atom catalysts for thermochemical CO_2 reduction, J. Energy Chem. 86 (2023) 246–262, https://doi.org/10.1016/j.jechem.2023.07.032.
[210] M. Aziz, A.T. Wijayanta, A.B.D. Nandiyanto, Ammonia as effective hydrogen storage: a review on production, storage and utilization, Energies 13 (12) (2020) 3062, https://doi.org/10.3390/en13123062.
[211] National Center for Biotechnology Information. PubChem Compound Summary for CID 222, Ammonia., 2023. ⟨https://pubchem.ncbi.nlm.nih.gov/compound/ammonia⟩. (Accessed 17 October 2022).
[212] National Center for Biotechnology Information. PubChem Compound Summary for CID 283, Formate., 2022. ⟨https://pubchem.ncbi.nlm.nih.gov/compound/283⟩. (Accessed 17 october 2021).
[213] K.N. Osipova, S.M. Sarathy, O.P. Korobeinichev, A.G. Shmakov, Laminar burning velocities of formic acid and formic acid/hydrogen flames: an experimental and modeling study, Energy Fuels 35 (2) (2021) 1760–1767, https://doi.org/10.1021/acs.energyfuels.0c03818.
[214] T. Winkler, F. Baccot, K. Eränen, J. Wärnå, G. Hilpmann, R. Lange, et al., Catalytic decomposition of formic acid in a fixed bed reactor – an experimental and modelling study, Catal. Today 387 (2022) 128–139, https://doi.org/10.1016/j.cattod.2021.10.022.
[215] S.M. Sarathy, P. Brequigny, A. Katoch, A.M. Elbaz, W.L. Roberts, R.W. Dibble, et al., Laminar burning velocities and kinetic modeling of a renewable E-fuel: formic acid and its mixtures with H_2 and CO_2, Energy Fuels 34 (6) (2020) 7564–7572, https://doi.org/10.1021/acs.energyfuels.0c00944.
[216] S. Hinokuma, K. Sato, Ammonia combustion catalysts, Chem. Lett. 50 (4) (2021) 752–759, https://doi.org/10.1246/cl.200843.
[217] Q. Yao, Y. Ding, Z.-H. Lu, Noble-metal-free nanocatalysts for hydrogen generation from boron- and nitrogen-based hydrides, Inorg. Chem. Front. 7 (20) (2020) 3837–3874, https://doi.org/10.1039/d0qi00766h.
[218] S. Mukherjee, S.V. Devaguptapu, A. Sviripa, C.R.F. Lund, G. Wu, Low-temperature ammonia decomposition catalysts for hydrogen generation, Appl. Catal. B: Environ. 226 (2018) 162–181, https://doi.org/10.1016/j.apcatb.2017.12.039.
[219] S.-F. Yin, B.-Q. Xu, C.-F. Ng, C.-T. Au, Nano Ru/CNTs: a highly active and stable catalyst for the generation of CO_x-free hydrogen in ammonia decomposition, Appl. Catal. B: Environ. 48 (4) (2004) 237–241, https://doi.org/10.1016/j.apcatb.2003.10.013.
[220] T.E. Bell, L. Torrente-Murciano, H_2 production via ammonia decomposition using non-noble metal catalysts: a review, Top. Cata 59 (15-16) (2016) 1438–1457, https://doi.org/10.1007/s11244-016-0653-4.
[221] W.U. Khan, H.S. Alasiri, S.A. Ali, M.M. Hossain, Recent advances in bimetallic catalysts for hydrogen production from ammonia, Chem. Rec. 22 (7) (2022) e202200030, https://doi.org/10.1002/tcr.202200030.
[222] W. Zheng, T.P. Cotter, P. Kaghazchi, T. Jacob, B. Frank, K. Schlichte, et al., Experimental and theoretical investigation of molybdenum carbide and nitride as catalysts for ammonia decomposition, J. Am. Chem. Soc. 135 (9) (2013) 3458–3464, https://doi.org/10.1021/ja309734u.
[223] R.-B. Zhang, Z.-A. Tu, S. Meng, G. Feng, Z.-H. Lu, Y.-Z. Yu, et al., Engineering morphologies of yttrium oxide supported nickel catalysts for hydrogen production, Rare Met 42 (1) (2023) 176–188, https://doi.org/10.1007/s12598-022-02136-5.
[224] Z. Zhang, Y. Luo, S. Liu, Q. Yao, S. Qing, Z.-H. Lu, A PdAg-CeO_2 nanocomposite anchored on mesoporous carbon: a highly efficient catalyst for hydrogen production from formic acid at room temperature, J. Mater. Chem. A 7 (37) (2019) 21438–21446, https://doi.org/10.1039/C9TA06987A.
[225] F. Hu, R. Ye, Z.-H. Lu, R. Zhang, G. Feng, Structure–activity relationship of ni-based catalysts toward CO2 methanation: recent advances and future perspectives, Energy Fuels 36 (1) (2022) 156–169, https://doi.org/10.1021/acs.energyfuels.1c03645.
[226] Y. Luo, Q. Yang, W. Nie, Q. Yao, Z. Zhang, Z.-H. Lu, Anchoring IrPdAu nanoparticles on NH_2-SBA-15 for fast hydrogen production from formic acid at room temperature, ACS Appl. Mater. Interfaces 12 (7) (2020) 8082–8090, https://doi.org/10.1021/acsami.9b16981.
[227] X. Li, Q. Wang, S. Wu, Z. Hu, J. Bai, Critical upstream technologies for hydrogen energy industry: research progress on ammonia decomposition catalysts, Sustain Chem. Pharm. 38 (2024) 101492, https://doi.org/10.1016/j.scp.2024.101492.
[228] D. Gaffen, How the Russia-Ukraine war accelerated a global energy crisis, 2022. ⟨https://www.reuters.com/business/energy/year-russia-turbocharged-global-energy-crisis-2022-12-13/⟩. (Accessed 13 December 2022).
[229] L. Burger, BASF readies more ammonia production cuts in gas supply crunch, 2022. ⟨https://www.reuters.com/business/energy/basf-considers-more-ammonia-production-cuts-gas-supply-crunch-sources-2022-07-27/⟩. (Accessed 15 March 2023).
[230] Curtailed ammonia production in Antwerp and Ludwigshafen, 2021. ⟨https://www.basf.com/global/en/media/news-releases/2021/09/p-21-327.html⟩. (Accessed 30 January 2023).
[231] R. van Putten, T. Wissink, T. Swinkels, E.A. Pidko, Fuelling the hydrogen economy: scale-up of an integrated formic acid-to-power system, Int. J. Hydrog. Energy 44 (53) (2019) 28533–28541, https://doi.org/10.1016/j.ijhydene.2019.01.153.
[232] M. Rumayor, A. Dominguez-Ramos, P. Perez, A. Irabien, A techno-economic evaluation approach to the electrochemical reduction of CO_2 for formic acid manufacture, J. CO_2 Util. 34 (2019) 490–499, https://doi.org/10.1016/j.jcou.2019.07.024.
[233] F. Proietto, A. Galia, O. Scialdone, Towards the electrochemical conversion of CO_2 to formic acid at an applicative scale: technical and economic analysis of most promising routes, ChemElectroChem 8 (12) (2021) 2169–2179, https://doi.org/10.1002/celc.202100213.
[234] N. Norouzi, M. Hosseinpour, S. Talebi, M. Fani, A 4E analysis of renewable formic acid synthesis from the electrochemical reduction of carbon dioxide and water: studying impacts of the anolyte material on the performance of the process, J. Clean. Prod. 293 (2021), https://doi.org/10.1016/j.jclepro.2021.126149.
[235] D. Yang, S. Li, S. He, Y. Zheng, Can conversion of CO_2 into fuels via electrochemical or thermochemical reduction be energy efficient and reduce emissions, Energy Convers. Manag. 273 (2022), https://doi.org/10.1016/j.enconman.2022.116425.
[236] L. Ai, S.F. Ng, W.J. Ong, A prospective life cycle assessment of electrochemical CO_2 reduction to selective formic acid and ethylene, ChemSusChem 15 (19) (2022) e202200857, https://doi.org/10.1002/cssc.202200857.
[237] C. Kim, Y. Lee, K. Kim, U. Lee, Implementation of formic acid as a liquid organic hydrogen carrier (LOHC): techno-economic analysis and life cycle assessment of formic acid produced via CO_2 utilization, Catalysts 12 (10) (2022) 1113, https://doi.org/10.3390/catal12101113.
[238] C. Kim, Y. Lee, H. Lee, U. Lee, K. Kim, Economic and environmental potential of green hydrogen carriers (GHCs) produced via reduction of amine-captured CO_2, Energy Convers. Manag. 291 (2023) 117302, https://doi.org/10.1016/j.enconman.2023.117302.